No. 2/2016

HIDRAULICA

HYDRAULICS-PNEUMATICS-TRIBOLOGY-ECOLOGY-SENSORICS-MECHATRONICS

http://hidraulica.fluidas.ro

ISSN 1453 - 7303
ISSN-L 1453 - 7303

CONTENTS

Published by:
Hydraulics and Pneumatics Research Institute, Bucharest-Romania
Address: 14 Cuţitul de Argint, district 4, Bucharest, 040558, Romania
Phone: +40 21 336 39 91; Fax:+40 21 337 30 40; e-Mail: ihp@fluidas.ro; Web: www.ihp.ro
with support from:
National Professional Association of Hydraulics and Pneumatics in Romania - FLUIDAS
e-Mail: fluidas@fluidas.ro; Web: www.fluidas.ro

HIDRAULICA Magazine is indexed by international databases:

ISSN 1453 – 7303; ISSN – L 1453 – 7303

EDITORIAL

The outburst of research programmes

Ph.D.Eng. Petrin DRUMEA
DIRECTOR OF PUBLICATION

In the past two months, about the same time, there have been restarted several research subprogrammes, either by launching the competition, or by moving forward to concluding financial agreements for projects gained in a different competition last year. After all, this is ok, too, and it's also good that something moves. Now, when things have settled down, I started to think over the problems that we had to face when elaborating project proposals and concluding contracts.

It should be said from the very beginning that, although all project information packs have been subjected to public debate, the ending was pretty weird, at least for me. For instance, in the subprogramme 2.1 Competitiveness through research, development and innovation - knowledge transfer to the economic unit (Bridge Grant), from the beginning abnormal restrictions have been applied, thus deciding to transfer directly only the expertise of universities, but not the one of research institutes. Consequently, projects submitted jointly by a university and an institute show that the institutes, and also other research centers, have been forced to take an intermediate so that they could be able to collaborate with an economic unit under this research subprogramme. It is a praiseworthy fact that for this subprogramme work with students, Master's and PhD students is core activity, but the issue is forcibly set down, so that ultimately the involvement itself of young people -potential specialists- in research projects becomes counterproductive, turning into internship arrangement.

In the same subprogramme 2.1 there took place the competition for experimental demonstration projects (PED), in which the elaboration guidelines were quite loosely formulated, at the discretion of participants, thereby leaving a very wide margin of subjectivity in project assessment. The large number of competitors proves that our experts have ideas, but many of them are only theoretical, with little chance to penetrate the real economy sphere.

Under the subprogramme 2.1 there have been also launched the projects for transfer to the economic operator, which manage to establish a serious connection between research and real economy. The only problem was related to the limited number of pages allowed for a project proposal, given the size and importance of more accurate assessment precisely by providing a large amount of information.

There are some general conclusions to be drawn, in addition to all the above.
It's a great thing that the authorities have restarted the activity of launching research programmes and concluding financial agreements for the projects already approved.
It's a great thing that the information packs have been condensed in length, but it's a shame that they have not found a solution for reducing requirements in elaborating proposals as well, at an equivalent level.
It's a great thing that in order to determine the expertise of a specialist there are taken into account first and foremost the project topic-related elements, still it is wrong that the ground is represented only by theoretical papers, and not practical previous achievements.
In the end, let me wish success to all the participants in these competitions.

Simulation of Turbulent Axisymmetric Waterjet Using Computational Fluid Dynamics (CFD)

PhD. Eng. **Nicolae MEDAN**[1]

[1]Technical University Cluj-Napoca, North University Center Baia Mare, Nicolae.Medan@cunbm.utcluj.ro

Abstract: *This paper presents numerical simulation of axisymmetric turbulent free waterjet developed in water using RANS method with k-ε model. GAMBIT and FLUENT software has been used. There are presented graphs and contours for axial and radial velocities of waterjet, contours for the turbulence kinetic energy (TKE) and graphs representing the turbulence intensity (IT). There is briefly presented also the concept of computational fluid dynamics and methods developed for numerical simulation of fluid flow.*

Keywords: *turbulent axisymmetric jet, CFD, FLUENT*

1. Introduction

Computational Fluid Dynamics (CFD) is a branch of fluid mechanics that uses numerical methods and algorithms to analyze work processes and phenomena involving fluid flow [1], [9]. Computational fluid dynamics is an interdisciplinary and practical approach linking disciplines: fluid dynamics, mathematics and computing. In terms of fluid dynamics, computational fluid dynamics (CFD) is dedicated to studying fluid motion and fluid flow affects how processes are involved. In terms of mathematical equations are required to describe the state of the process fluid to be investigated. In order to solve these mathematical equations that describe fluid are converted by computer programs software packages. In the last years, the usage of CFD in the studies of fluids has increased, due to the advantages that it presents [6], [8].

1.1 Developed methods for numerical simulation of fluid flow

Using the Reynolds decomposition representation of turbulent motion, the movement is divided into an average component and a pulsating and using mathematics to describe the movement system Navier-Stokes equations, are reported in the literature several methods developed for numerical simulation: **DNS** (Direct Numerical Simulation), **LES** (Large Eddy Simulation), **DES** (Detached Eddy Simulations), **RANS** (Reynolds Averaged Navier-Stokes equation).
RANS method is the oldest and also the most used method. It consists in mediating temporal Navier-Stokes equations based on the representation Reynolds turbulent motion. Following this operation, there are a number of additional terms due to turbulent pulsations temporal mediation with tensions apparent significance (Reynolds stresses). The method uses different models which explains these tensions and can close the system of equations. Turbulence models used in RANS method can be grouped into two categories:

1) Models using Boussinesq's hypothesis. In this group are included: models based on mixing length theory (Prandtl), models with "zero equation" and models with "two equations", k-ω or k-ε. The standard k-ε model proposed by Spalding is the most used.

2) Models for Reynolds stresses. These models introduce one transport equation for each Reynolds stress resulting from mediation Navier-Stokes equations. Number of unknowns increases considerably and therefore the calculation effort is high. These models are seldom used.

RANS method with k-ε model is the professional software package CFD (Computational Fluid Dynamics) for simulating turbulent flows.

1.2 Mathematical description of RANS method for turbulent axisymmetric fluid flows

The mathematical model used to describe the movement of axisymmetric turbulent jets feature, use the pressure and velocity coupling Cartesian coordinate system. To solve the system of equations is using standard k-ε turbulence model [5], [7]. Forming equations describing turbulent flow system can be written in the following general form [5]:

$$\underbrace{\frac{\partial}{\partial x_j}\left(\rho\overline{u_j}\overline{\phi}\right)}_{convection} = \underbrace{\frac{\partial}{\partial x_j}\left(\Gamma_\phi \frac{\partial\overline{\phi}}{\partial x_j}\right)}_{diffusion} + \underbrace{S\phi}_{source} \quad (1)$$

2. Numerical Simulation of Axisymmetric Turbulent Jet Using CFD

CFD software package contains three modules, namely [4]:
1) Pre-processor,
2) Solver (governing equations solve on a mesh),
3) Post-processor.
In the present study is performed 2D axisymmetric simulation of turbulent jets using the Fluent 6.3 [2]. For definition and scope of work meshing program Gambit [3] was used.

2.1 Field work

Consider a cylindrical nozzle through which fluid effluent, which in this case is water. Jet is formed in the ambient fluid that is all water.
In figure 1 is presented the schematic diagram of the computational domain with dimensions.

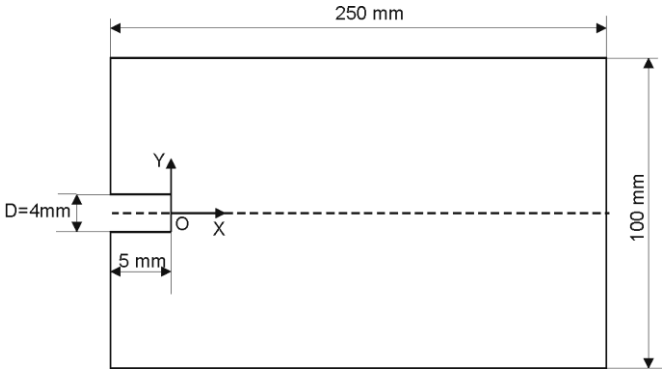

Fig. 1. Schematic diagram of the computational domain

Is studied the evolution of axisymmetric turbulent jets for different speeds effluent fluid out of the nozzle. We deal with free jets drowned (ambient fluid is at rest). It is known that the main property of turbulence is given by the Reynolds number. In most cases if the Reynolds number exceeds 2300, flow becomes turbulent. In this case we want to study the axisymmetric turbulent jets and therefore the lowest value of Reynolds number which will be modelled is Re = 3,636.
Table 1 presents the input parameters for conducting experiments.

TABLE 1: Input parameters for conducting experiments.

Speed / Parameters	v=1 m/s	v=3 m/s	v=5 m/s	v=7.76 m/s
Reynolds Re	3,636	10,908	18,180	28,200
Turbulence Intensity T.I.	0.44	0.51	0.54	0.57

2.2 Initial conditions (pre-processor)

To define the initial conditions using Gambit software [3] and includes the following steps:
1) Creating geometry, based on field work schedule (figure 1).
2) Meshing method. There are used rectangular cells with dimensions 0.33mmx0.5mm in area next to the entrance and rectangular cells with dimensions 0.5mmx0.5mm in rest.
3) Boundary conditions. How is define the types of boundaries is shown in figure 2.

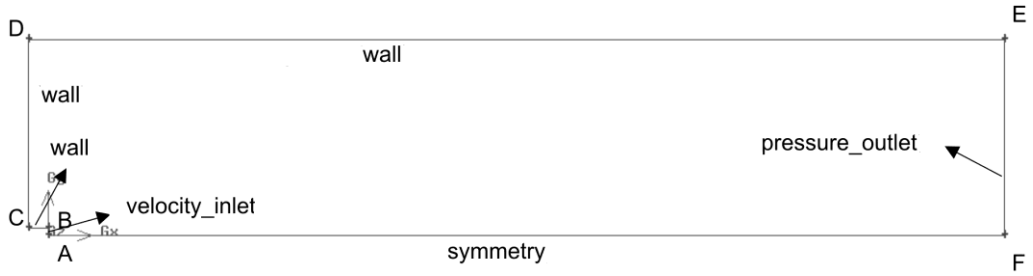

Fig. 2. Computational domain and boundary conditions

2.3 Perform simulation (solver)

After defining the domain and meshing, the simulation was performed using FLUENT 6.3 software. It defines the turbulent motion model solved. To define the turbulent flow model that solves movement RANS method was chosen to model 2 equation k-ε standard. Table 2 presents discretization scheme used for turbulent jet flow equation. It used the pressure-velocity coupling (SIMPLE method).

TABLE 2: Discretization schemes for jet flow

Variable	Discretization scheme
Pressure	Presto
Momentum	Second Order Upwind
Turbulent kinetic energy	Second Order Upwind
Turbulent dissipation rate	Second Order Upwind

3. Results

Still present some results obtained from simulations with FLUENT software [2].

3.1 Graphs representing the heart jet axial velocity and radial velocity

For graphical representation of flow velocity, I present results for all four cases considered velocity. In figure 3 is represented the numerical simulation of variation of axial velocity in the centre jet speed for all cases considered and for a distance of 100 mm from the jet origin.

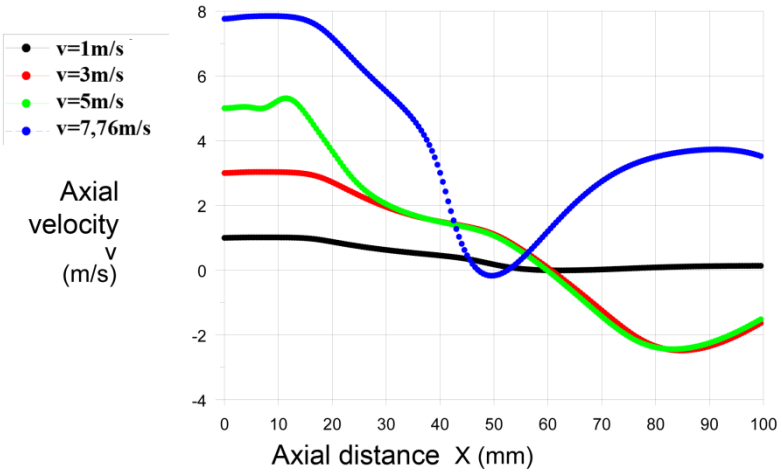

Fig. 3. Variation of axial velocity in the centre of jet for x=0÷100 mm

In figure 4 is represented the numerical simulation of radial flow velocity variation for different distances from the jet origin x = 1 mm, x = 2mm and x =4mm and fluid velocity at the nozzle exit is for all cases considered.

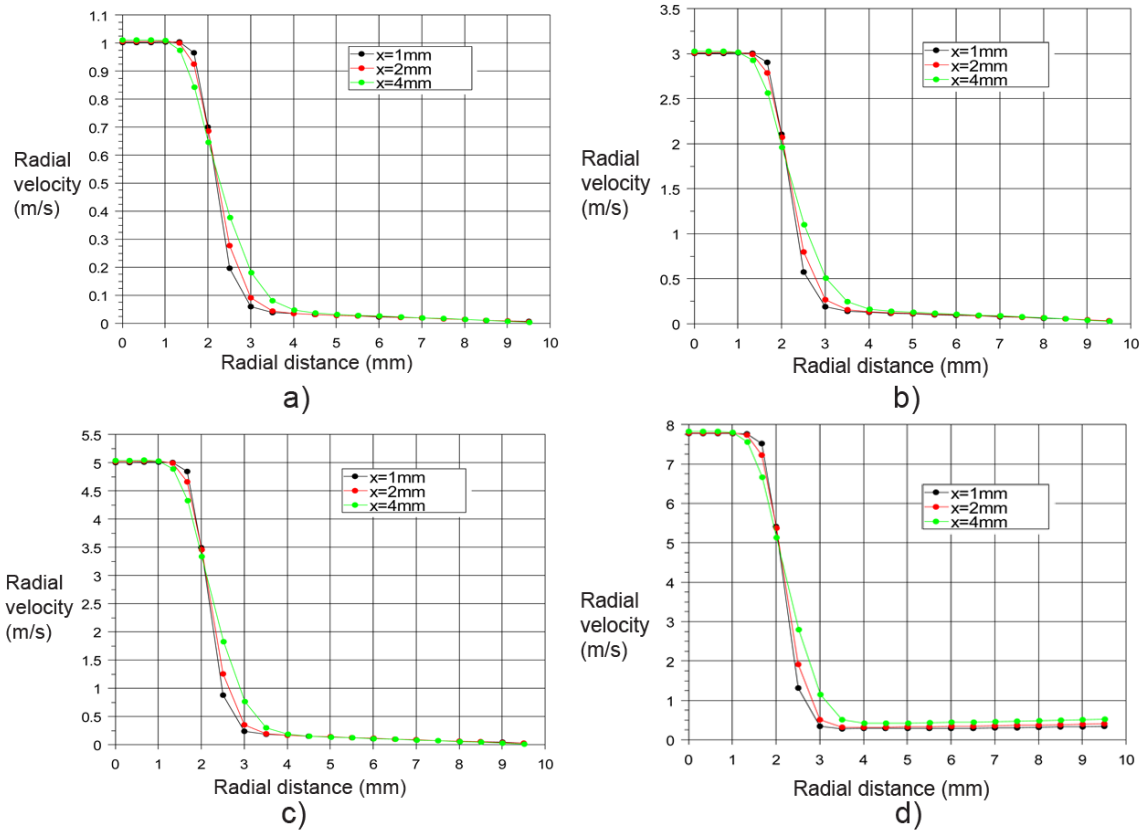

Fig. 4. Variation of radial velocity for a) v=1 m/s, b) v=3 m/s, c) v=5 m/s, d) v=7.76 m/s

3.2 Contours represent the axial and radial velocities of jet

In figure 5 are the axial flow velocity contours for all 4 values of the speed, for the entire area define.

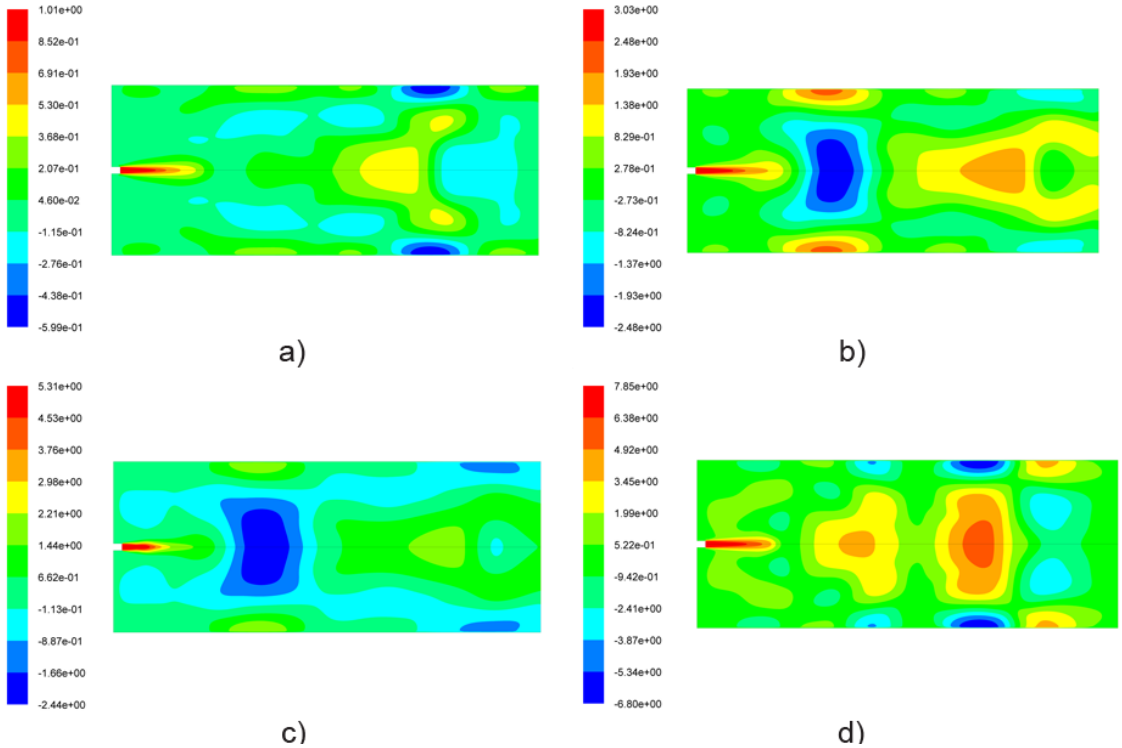

Fig. 5. Contours of axial velocity for a) v=1 m/s, b) v=3 m/s, c) v=5 m/s, d) v=7.76 m/s

In figure 6 are the radial flow velocity contours for all 4 values of the speed.

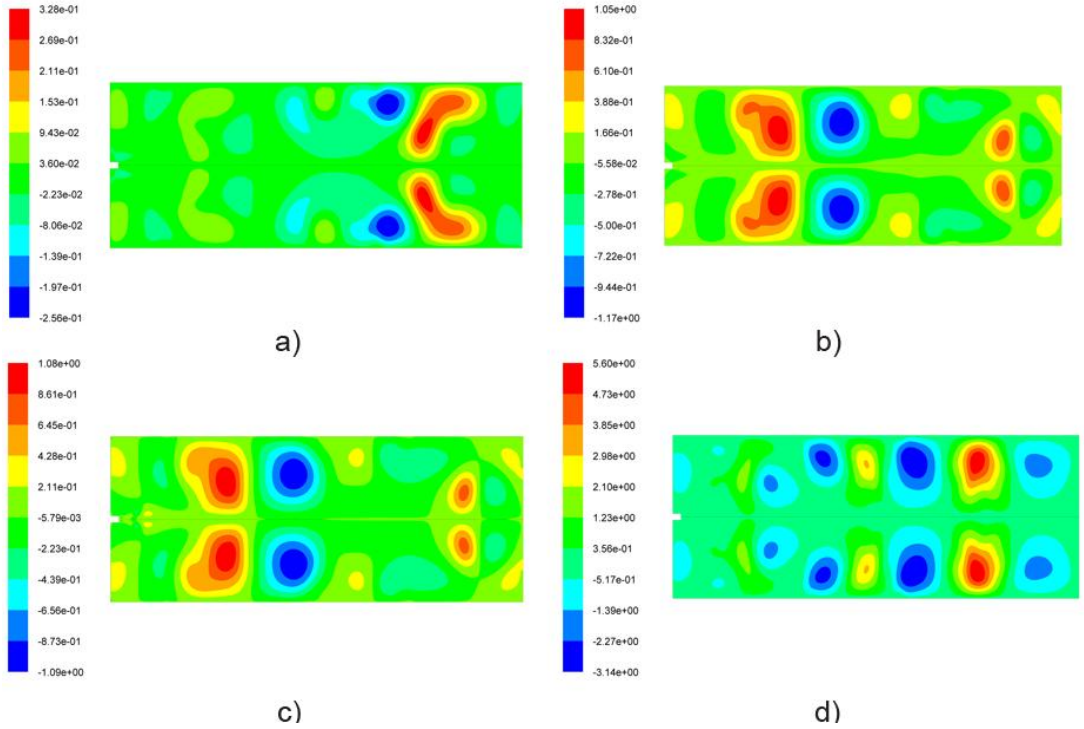

Fig. 6. Contours of radial velocity for a) v=1 m/s, b) v=3 m/s, c) v=5 m/s, d) v=7.76 m/s

3.3 Contours represent the turbulence kinetic energy (TKE)

In figure 7 are represented the turbulence kinetic energy (TKE) for all 4 values of the speed, for the entire area define. TKE is the kinetic energy per unit mass of the turbulent fluctuations in a turbulent flow.

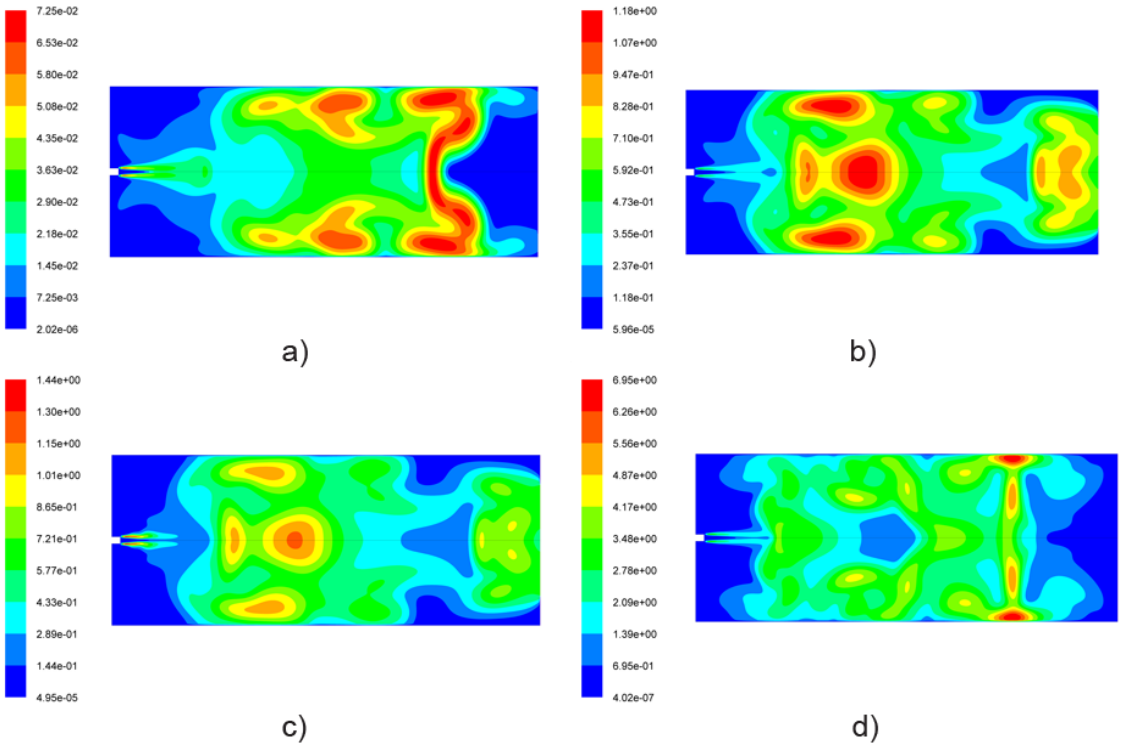

Fig. 7. Contours of turbulence kinetic energy (TKE) for a) v=1 m/s, b) v=3 m/s, c) v=5 m/s, d) v=7.76 m/s

3.4 Graphs representing the turbulence intensity (IT)

In figure 8 are represented the turbulence intensity (IT) for all 4 values of the speed, for the entire area define along the axial distance.

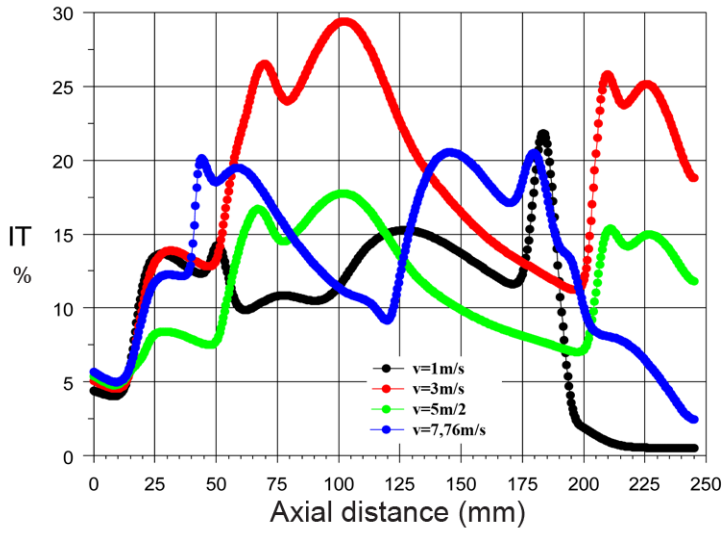

Fig. 8. Variations of turbulence intensity (IT) for v=1 m/s, v=3 m/s, v=5 m/s, v=7.76 m/s

4. Conclusions

In this study was performed CFD simulation of axisymmetric turbulent flow for waterjets using the RANS method with model 2 equations k-ε standard. For this application was used Gambit and Fluent.

To define the initial conditions was used Gambit software and includes the following steps: creating geometry, based on field work schedule, defining the mesh and the boundary conditions.

The numerical simulation was performed for different values of axial velocity at the exit of jet: v =1m/s, v =3 m/s, v =5 m/s and v =7.76 m/s. To generate the mesh area was used rectangular cells with dimensions 0.33mmx0.5mm in area next to the entrance and rectangular cells with dimensions 0.5mmx0.5mm in rest.

For axial velocities along the center of the jet can be seen that they decrease as moving away from the origin of the jet.

Representing the radial velocities of flow was made at distances equal to 1 mm, 2 mm and 4 mm from the jet origin for v = 7.76 m/s. It can be seen that the radial velocity decreases with increasing radial distance from the origin.

Through the representation of the contours of the axial and radial speed of the waterjet can be noticed the way of develop the waterjet. With increasing velocity of a jet at the outlet saw an increase of the area in which develop the jet.

By viewing the contours of the turbulence kinetic energy it can view the way that develops the turbulence kinetic energy (TKE) in the field work. The turbulence kinetic energy (TKE) increases with increasing the speed at the outlet from the hole.

For the graphs representing the turbulence intensity (IT), it should be observed that with increasing velocity of the waterjet at the outlet, increases in direct proportion the turbulence intensity of the fluid in the jet. With increasing distance from the origin of the jet appear variations of the turbulence intensity due to the influence of the working area. Thus for v = 1m/s the turbulence intensity is almost 0 at a distance of 200 mm, which means that the jet is fully developed in the working area. In the other 3 cases considered appear variations of the turbulence intensity due to the limits of the working area.

Numerical simulation of fluid flow is an alternative that can replace the implementation of experiments, in the sense that it can reproduce the conditions of experiments and can be viewed

and further processed results. Numerical simulation can successfully replace experiments often involve high costs.

References

[1] T.J. Chung, "Computational Fluid Dynamics", Cambridge University Press, ISBN: 978-0-521-76969-3, 2002;
[2] FLUENT 6.3.26: User manual;
[3] GAMBIT 2.3.16: User manual;
[4] T. Jiyuan, H.Y. Guan, L. Chaogun, "Computational Fluid Dynamics A Practical Approach", Elsevier Press, ISBN: 978-0-7506-8563-4, 2008;
[5] B.E. Lauder, D.B. Spalding, "Lectures in Mathematical Modeling of Turbulence", Academic Press, London, England, ISBN-10: 0124380506, 1972;
[6] P. Opriţoiu, RANS Simulation of Combined Flow and Heat Transfer Through Open-cell Aluminium Foam Heat Sink, "Hidraulica" (No. 3/2013) Magazine of Hydraulics, Pneumatics, Tribology, Ecology, Sensorics, Mechatronics, ISSN 1453 – 7303, pp. 15-25;
[7] D.B. Spalding, "Basic Equations of Fluid Mechanics and Heat and Mass Transfer and Procedures for Their Solutions", Heat Transfer Section, Report HTS/77/9, Imperial College London, 1976;
[8] K. Stračár, J. Krchnár, K. Prikkel, CFD Model of Flow in the Outlet Channel of Floating Chamber "Hidraulica" (No. 1/2014) Magazine of Hydraulics, Pneumatics, Tribology, Ecology, Sensorics, Mechatronics, ISSN 1453 – 7303, pp. 7-23;
[9] D.C. Wilcox, "Turbulence Modeling for CFD", DWC Industries Inc., La Canada California, ISBN: 0-9636051-0-0, 1994.

Tribological Effectiveness of Graphene Oxide and Ionic Liquids in PAG Oil: Could Absorbed Water Play Beneficial Role?

Prof. **Vincenzo D'AGOSTINO,** Dr. **Mario PISATURO,** Dr. **Claudia CIRILLO**,
Prof. Dr. **Maria SARNO,** Prof. Dr. **Adolfo SENATORE**

Department of Industrial Engineering, NANO_MATES Research Centre, University of Salerno, Fisciano, Italy, {dagostino, mpisaturo, clcirillo, msarno, a.senatore}@unisa.it

Abstract: *The polyalkylene glycol (PAG) lubricants are widely used as gear, bearing and compressor oils. Indeed, the base PAG oil can be used as additive in engine oil or transmission oil as well as compressor lubricant in refrigerant systems. They are designed to provide outstanding benefits in terms of efficiency, long oil life, and equipment protection. These fully synthetic lubricants were developed for use under operating conditions beyond the capabilities of other synthetic lubricants and mineral oils. Their low pour points ensure excellent low-temperature fluidity. On the other hand the main disadvantage of the PAG oils is the marked hygroscopicity, i.e. they absorb and bind moisture from the ambient air. In this paper the results from tribological testing of PAG oil featuring 46 cSt at 40°C with solid (graphene oxide) and liquid (ionic liquids) additives are proposed. Moreover, in this study the influence of the absorbed moisture from ambient air has been taken into account. Preliminary experiments with ball-on-flat setup by using reciprocatory tribometer have been carried out on the base oil PAG 46 blended with 1-Ethyl-3-methylimidazolium acetate or graphene oxide, alternatively. In this way the influence of each additive has been investigated. Based on this information the aim of this research is to test the hybrid formulations and to verify potential improvements on anti-friction and anti-wear PAG 46 behaviour in broad range of lubrication regimes. The experimental tests have been carried out by using rotational disc tribometer in ball-on-disc configuration. Additional experiments after samples exposure to ambient air and ensuing moisture absorption were executed. The results highlight that in most cases the absorbed moisture do not introduce detrimental effects on the tribological performances of the tested oil samples. Rather, water content reduces wear of the sliding steel surfaces in the whole testing spectrum and in many cases the frictional dissipation.*

Keywords: *Nanosized friction modifiers, tribological testing, graphene oxide, ionic liquid, water absorption, Stribeck graphs.*

1. Introduction

Friction and wear are the two major causes for energy and material losses in tribological conjunctions of mechanical systems. Lubrication is principal focus to improve energy efficiency and mechanical durability. In addition, in order to minimize wear not only the lubricant film needs to be kept thick enough to prevent any contact between the surfaces, but also friction has to be reduced so as to obtain an efficiency as high as possible; pressure peaks must be not large to avoid sub-surface stresses and, thus, pitting fatigue [1].
The properties of Ionic Liquids (ILs) at room-temperature make them excellent lubricants [2-4]. Their pertinent physico-chemical characteristics [5-7] include their negligible volatility, nonflammability, high thermal stability and high thermal conductivity, low melting point, and broad liquid range. In addition, ionic liquids are highly polar and miscible with water and with number of organic solvents (aromatic, heterocyclic compounds, etc.) [1]. The ILs' viscosity can be modified by selecting different lengths of the nonpolar alkyl side chain of the cation or different type of anion [8]. Indeed, the intrinsic properties of ILs could likely avoid the use of some additives [9], such as: (1) detergents because ILs act as solvents, (2) anti-oxidants due to ILs' high thermal stability, (3) several anti-wear additives such as zinc butyl and octyl dithiophosphate (ZDDP) due to the formability of surface boundary films, although for several cases due to the corrosion, additives could be needed [10-11]. Moreover literature results, [4,5,12,13], proved that pure ionic liquids even without any additives deliver low friction coefficients and wear. Ionic liquids exhibit superior tribological behaviour because of their polar structure. They can be easily adsorbed on the sliding surfaces of frictional pairs. Consequently, an effective boundary film can reduce friction and wear. Ionic liquids have comparable heat characteristics to current thermal fluids [1].

Finally, in [14,15], the Authors analysed the connection between the voltage effect on the structure of the IL layers and their lubricating properties.

On the other hand, in the field of tribological applications, nanoparticles as additives in base oil have been extensively investigated. These studies refer to synthesis and preparation of nanoscale particles and their tribological properties and friction reduction mechanisms. It has been generally found that when the nanoparticles were added to base oil, the extreme pressure property and load-carrying capacity were improved and friction coefficient was decreased.
Nanocarbon materials have received great attention by tribology researchers in the last three decades, due to high load-bearing capacity, low surface energy, high chemical stability, weak intermolecular, and strong intramolecular bonding [16-18]. The lubrication mechanism of the carbon nanoparticles has not been yet completely understood, but their properties as frictional media are definitely based on structural modification. They present the same main advantage that nanoparticles made on metal dichalcogenides: they are efficient even at room temperature. The comprehension of their action at the interfaces of frictional conjunction and the tailored functionalization will certainly aim at improving their excellent performance in this field.
As well known, graphene has recently enjoyed extensive attention because of its excellent properties, such as high thermal conductivity, high Young's modulus, large specific surface area, electromagnetic interference shielding, electrical conductivity. Recent studies focused on mechanical features of joints underline considerable increase in tensile strength with favourable effect probably due to the cumulative effects of intermolecular interactions between the graphene and resin networks [19]. From the tribological point of view, Huang et al. [20] investigated the properties of graphite nanosheets obtained by ball milling of natural flake graphite, in oil. They found that the frictional behaviour and anti-wear ability of the lubricating oil were improved when graphite nanosheets and dispersant were added to the paraffin oil at the optimal concentration. Lin et al. [21] suggested that functionalizing the graphene platelets with proper modifier is an effective way to enhance the additive dispersion.
This paper aims at investigating the tribological performance of Graphene Oxide (GO) and ionic liquid as friction modifiers in polyalkylene glycol (PAG) base oil. As well known, the base PAG oil can be used as additive in engine or transmission lubricants whereas it's the preferred compressor lubricant in refrigerant systems [22-24]. The behaviour of PAG oil with additives in the latter field is one of the targets of this research, as some reference reports of generally adverse effects [25]. Although refrigerant systems are categorized as closed systems, the absorption of moisture/humidity is inevitable due to permeation through barrier hoses [22]. For this reason additional test campaigns on the influence of water content in oil should be carried out. In the present analysis, tribological tests have been performed through ball-on-disc tribometer. The Wear Scar Diameter (WSD) after steady-state tests has been selected as wear parameter for samples comparison.
The results provide useful data about the influence of graphene oxide, ionic liquid and water on the friction coefficient and wear parameter.

2. Lubricant samples and methods

2.1 Materials

The experimental tests were carried out by using both the pure PAG 46 and the PAG 46 with IL and GO as friction modifiers. In particular, the GO nanosheets were prepared by modified Hummer method [26]. The oxidation of graphite particles were obtained from Lonza [26,27] to graphitic oxide accomplished with water-free mixture of concentrated sulfuric acid, sodium nitrate and potassium permanganate. The entire process requires less than two hours for completion at temperatures below 45°C. With the aid of further sonication step, the oxidized graphite layers were exfoliated from each other. Then 30% H_2O_2 was added to the suspension to eliminate the excess MnO^-_4. The desired products were rinsed with deionized water. The remaining salt impurities were eliminated with resinous anion and cation exchangers. The dry form of graphitic oxide was obtained by centrifugation followed by dehydration at 40°C [28]. Such synthesis process was entirely developed at Laboratories of Dept. of Industrial Engineering/Nano_Mates Research Centre at University of Salerno. The ionic liquid used as additive for the PAG base oil is the 1-Ethyl-3-

methylimidazolium acetate. Such halogen-free ionic liquids turned out as potential alternatives to fluorinated ionic liquids for lubrication and proved their liquid/metal surface interactions mainly dominated by the anion with formation of layers as tribochemical reaction mechanism with friction benefits [29].
For each oil sample sonication (Hielsher UP 400s) of 30 min followed by mixing with Silverson L5M homogenizer for 30 min has been carried out. Moreover, before each tribological test stirring of 30 min at 13.000 rpm with IKA T25 digital ULTRA-TURRAX® has been performed.
No dispersant agent has been blended with base oil and additives of the lubricant formulations under test. In this analysis three 350 ml oil samples have been tested; Tab. 1 reports the concentration of the additives for each sample.

TABLE 1: Tested oil samples

OIL SAMPLE	BASE OIL	IL [w.t.%]	GO [w.t.%]
1	PAG 46	-	-
2		2.0	0.1
3		2.0	0.5

2.2 Friction test – Stribeck curve

The experimental tests were carried out by using rotational disc WAZAU TRM100 tribometer in ball-on-disc configuration. This tribometer setup allows applying different tribopair parameters, which is desirable in order to study the different regimes in the Stribeck curve, i.e., boundary, mixed and elastohydrodynamic lubrication conditions. The normal force was applied on the mating surfaces by lever system and could be varied in the range of 0–100 N. The spinning shaft was driven by brushless motor with speed variable up to 3000 rpm. The measurement of the normal force was performed through force sensor arranged between the load lever and the lower specimen holder. The lubricant average temperature has been controlled through NiCr-Ni-thermocouple in the oil reservoir and an electric resistance. The investigated contact type was composed of an upper rotating X155CrVMo12-1 steel disc of hardness 60 HRC, roughness of Ra=0.5 μm and 105 mm in diameter. lower X39Cr13 steel ball, 57±3 HRC, grade 100, 8 mm diameter was completely immersed in temperature-controlled 350 ml lubricant bath. An average contact pressure of 1.50 GPa, corresponding to normal load of 70 N, was applied at the ball/disc interface.
A speed-sweep test at constant load on wide speed range has been designed to cover broad operating conditions with the purpose of minimizing the modification of the tribopair steel surfaces in order to get frictional results in comparable surface topography conditions. For this reason, the time extension of the tests was limited to 24 min. The disc speed rose up to 2.0 m/s in the first 4 min and dropped to zero in the following 4 min. This speed pattern was repeated three times. The tests were performed for two different temperatures, i.e., 25°C and 80°C. These two temperatures have been chosen to get useful results both for engine and gearbox applications as well as for compressor in refrigerant plants.
The current design of this experiment allowed to cover slow-to-high speed range and to obtain complete Stribeck frictional graph. Another advantage of this setting was the high reproducibility of the friction coefficient (CoF) in several ramps and the good averaging-out of the noise-level. Also, since the sliding acceleration was very low along each speed ramp there was no relevant fluid inertial phenomena and transducers dynamic effects, i.e., each ''CoF vs. speed'' curve was obtained in quasi-steady state condition.
The measured data are presented according to the Stribeck curves representation, i.e., friction coefficient vs. sliding speed. The friction coefficient is the average value calculated by considering each ramp as single test. Standard deviation calculations are also depicted on the plots in the form of error bar.

2.3 Friction and wear in steady-state tests

Long running frictional tests of 1-hour have been performed to analyse the influence of the nanoparticles on wear behaviour of the steel ball/disc pair. For this test, constant values for average contact pressure, temperature and speed were 1.50 GPa, 25°C and 80°C, 5.0 mm/s and 0.50 m/s, respectively, resulting in four combinations. After each test the wear scar diameter has been measured with Sensofar PLu-neox 3D optical profiler.

3. Results

3.1 Screening tests

Preliminary experiments were carried out on the same base oil PAG 46 blended with 1-Ethyl-3-methylimidazolium acetate or graphene oxide, alternatively. The selected lubrication regime was boundary. The tests have been performed with ball-on-flat setup on Ducom TR-BIO-282 reciprocatory tribometer: the stroke of 3 mm and the frequency of 5 Hz led to maximum sliding speed equal to 94 mm/s. According to the Figure 1, the friction measurement in 1-hour sliding test by testing the four samples displayed in the graph label exhibited similar results. Hence, no sensible gain achievable through addition of ILs or GO dispersion appeared in such testing conditions.

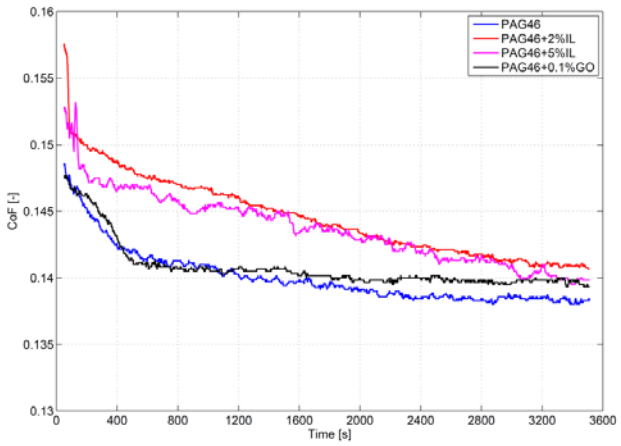

Fig. 1. Friction coefficient vs. time

Nevertheless, the analysis of the in-line values of the electric contact resistance (ECR) could lead at least to partial understanding of the concurrent phenomena taking place at sliding interfaces, Figure 2.

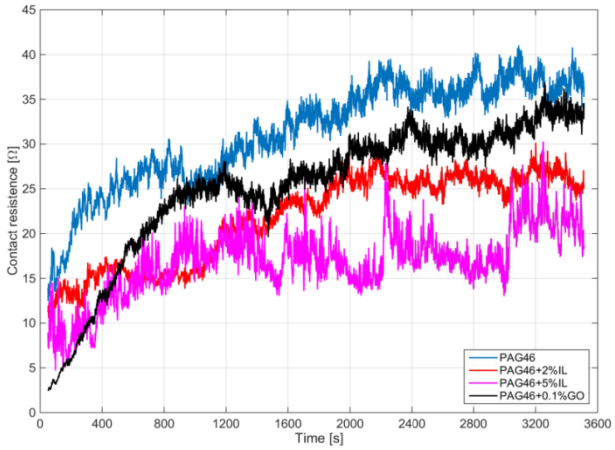

Fig. 2. Electric contact resistance (ECR) vs. time

As observed in previous papers, e.g. [30], the formation of tribolayer due to material transfer from lubricant carbon based nanoadditive to metal surface yields out rapid increment of ECR along with CoF reducing. The result is even marked by increasing the nanoparticles concentration. Hence, an inverse correlation between CoF and ECR could be stated when nanocarbon materials are used as friction modifiers. The Figure 2 shows trend inversion in the case of ILs blending with base oil, as the lower the CoF, the lower the ECR. This result would confirm the different lubrication mechanism at the metal sliding interface. By assuming as common target the lowering of frictional loss at sliding interface, the material transfer from solid nanoadditive dispersed in the lubricant and ensuing lower shear stress and prevention of direct contact between metal interfaces [28] is replaced by the lubricity property of ILs in the pure-liquid blending formulation [14].
These same four samples exhibited in steady sliding speed conditions at 5.0 mm/s and 100 mm/s: optimal anti-wear behaviour by adding 0.1 w.t.% GO with decrease of wear parameter equal to 14% and 18%, respectively; reduced CoF by ILs blending at 5 w.t.% up to 11% and 22%, respectively.
Based on the above discussion, in this research the Authors aimed at testing the hybrid formulations to verify potential improvements from both the concurrent interfacial effects to improve anti-friction and anti-wear PAG 46 behaviour in broad range of lubrication regimes.

3.2 Influence of graphene oxide and ionic liquid additives

3.2.1 Friction test – Stribeck curve

The Figure 3 shows the Stribeck curves for all oil samples at 25°C (a) and 80°C (b) before that they have been exposed to the ambient air. It is worth noting that at lower temperature for all graphs it is possible recognize well-developed minimum, that is considered the transition from mixed lubrication regime to EHL regime for increasing speed [31]. This frontier divides the region with concurrent phenomena of solid-to-solid contacts, adhesion and interaction between friction modifier additives and steel surface (mixed lubrication) from the other with predominant viscous stress and elastic deformation of the tribopair surfaces (EHL). The oil sample 2, i.e. PAG 46 with 2.0% w.t. IL and GO at 0.1% w.t. (red line), shows the lower friction coefficient. Moreover, it exhibits minimum at sliding speed of 1 m/s. In all cases the minimum falls in the sliding speed range 0.67 – 1 m/s. The reduction of the friction coefficient for the sample 2 as compared to the other samples is on average of 14%.

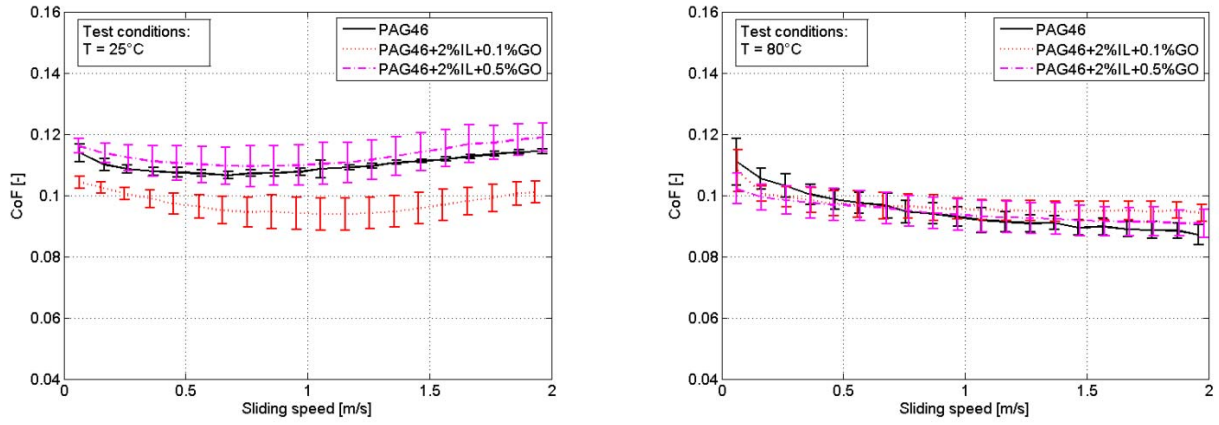

(a) (b)

Fig. 3. Stribeck curves at 25°C (a) and 80°C (b).

The lower oil viscosity at higher temperature results in transition between mixed and EHL regime at higher sliding speed. Indeed, only the boundary and the mixed lubrication regimes are prevailing in Figure 3 (b). In contrast to the results at 25°C, at higher temperature the pure PAG 46 oil exhibits friction coefficient slightly higher than other samples for sliding speeds lower than 0.7 m/s. Beyond this value the oil samples 2 and 3 display friction coefficient slightly higher than the pure base oil.

3.2.2 Friction in steady-state tests

In this section the friction coefficients measured in steady-state condition are reported. At 25°C and 5 mm/s, Figure 4 (a), the base oil PAG 46 displays higher friction coefficient than samples with solid and liquid additives; average data +17%. Moreover, for all oil samples with ILs/GO additives the measured friction coefficient is confined in more narrow range. It is worth noting that under these test conditions the best results were exhibited by the oil sample 2. In Figure 4 (c) the results with oil bath at 80°C and sliding speed of 5 mm/s are plotted. The measured friction coefficient for the base PAG 46 exhibits stable and constant behaviour. On the other hand, the oil samples with additives show variable friction coefficient which tends to stable value. This value is approximately the same of the pristine PAG 46. In any case the lower friction coefficient was measured for the oil sample with the higher concentration of graphene oxide (magenta line). Figure 4 (b) and (d) show the results at 25°C and 80°C in mixed lubrication regime, i.e. sliding speed of 0.5 m/s. In such a lubrication regime at low temperature, the oil sample 1 exhibits friction coefficient which slightly increases during the first 400 s and it attains to stable value. Instead, for the oil samples with additives the measured friction coefficients decrease in the first part of the test, reaching stable value. The lower friction coefficient was observed for the oil sample 2 which has the higher loading of graphene oxide (red line). Moreover, by comparing the Figures 4 (b) and (d) it is worth noting that the measured friction coefficients at 80°C are higher than values measured at 25°C.

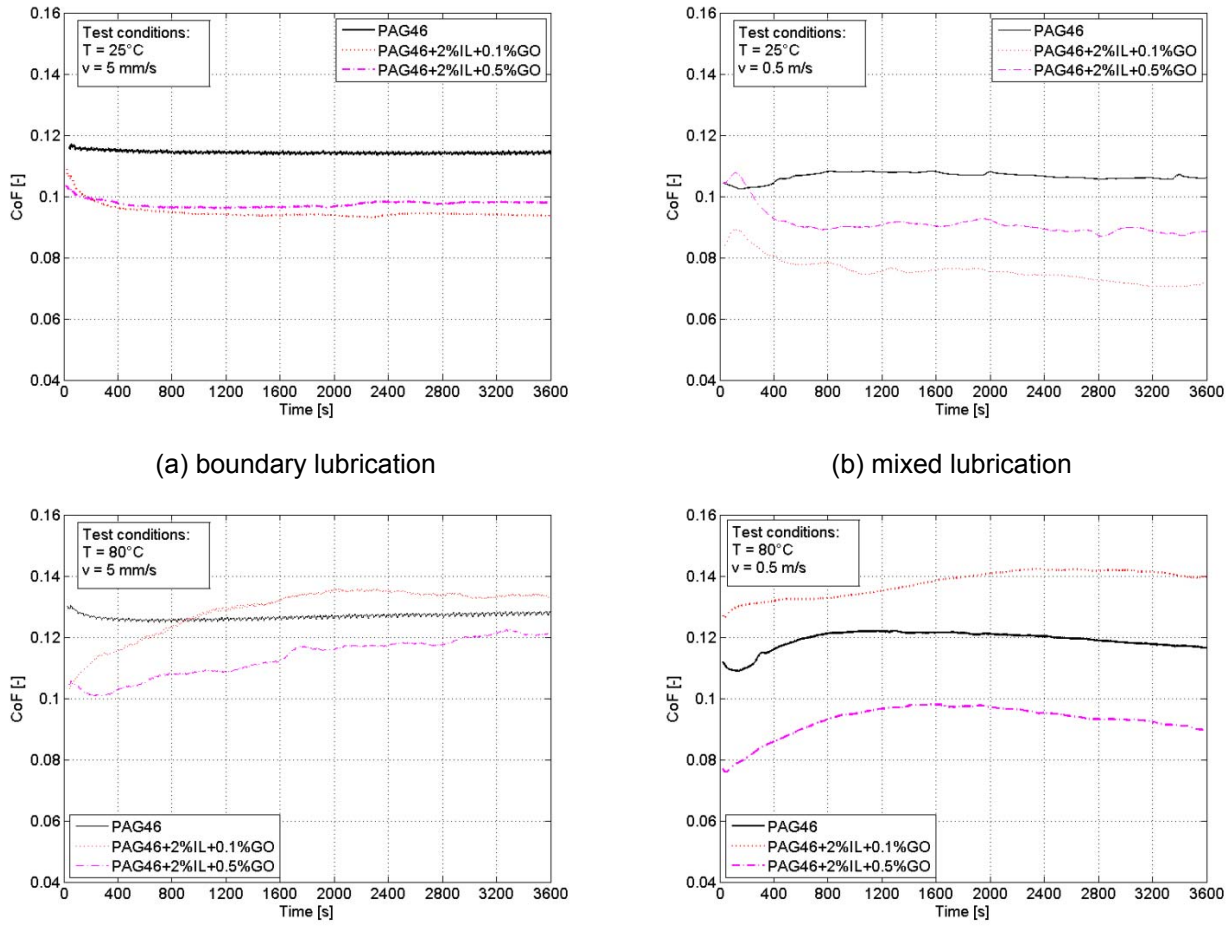

(a) boundary lubrication (b) mixed lubrication

(c) boundary lubrication (d) mixed lubrication

Fig. 4. Steady-state tests at 25°C (a)-(b) and 80°C (c)-(d).

3.3 Influence of water content

As explained in the introduction section, each sample has been exposed for two months in open air in protected from light ambient. In this way, the influence of the moisture absorption could be investigated from the tribological point of view. Such analysis has twofold purpose: the proof of

lubricant performance through lifetime without changing it, as in car or industrial refrigerator systems; the investigation about water capability to promote surface chemical reactions beneficial to friction reduction [32]. After two months weight increment of about 0.2% has been observed for each oil sample. The tab. 2 reports the water content and the labels of the samples after water absorption. The "B" label refers to the same samples of the tab. 1 ("A" labelled) after the ambient air exposure. The fifth column provides the water content in ppm. Even though the sample have been for long time in ambient air, all the samples exhibited weak hygroscopicity by comparing the present data with literature ones [22]. This behaviour can be mainly addressed to the double end capped chemical structure of the tested PAG 46 oil.

TABLE 2: Oil samples after ambient air exposure

OIL SAMPLE	BASE OIL	IL [w.t.%]	GO [w.t.%]	WATER CONTENT [ppm]
1 A	PAG 46	-	-	-
1 B		-	-	2060
2 A		2.0	0.1	-
2 B		2.0	0.1	1885
3 A		2.0	0.5	-
3 B		2.0	0.5	1833

3.3.1 Friction test – Stribeck curve

The Figures 5 show the hygroscopicity effect on friction coefficient displayed by the Stribeck curves at 25°C and 80°C. In particular, at 25°C the PAG 46 which absorbed moisture from the ambient air (case B) doesn't exhibit minimum in the analysed speed range. Indeed, the friction coefficient significantly decreases with the sliding speed. On the other hand, the same figure highlights that at sliding speed lower than 0.40 m/s the friction coefficient is lower for PAG 46 case A. Also at 80°C the water contained in PAG oil results in lower friction coefficient at higher sliding speed. However, in this case at lower sliding speed the friction coefficient exhibits the same behaviour in both cases.

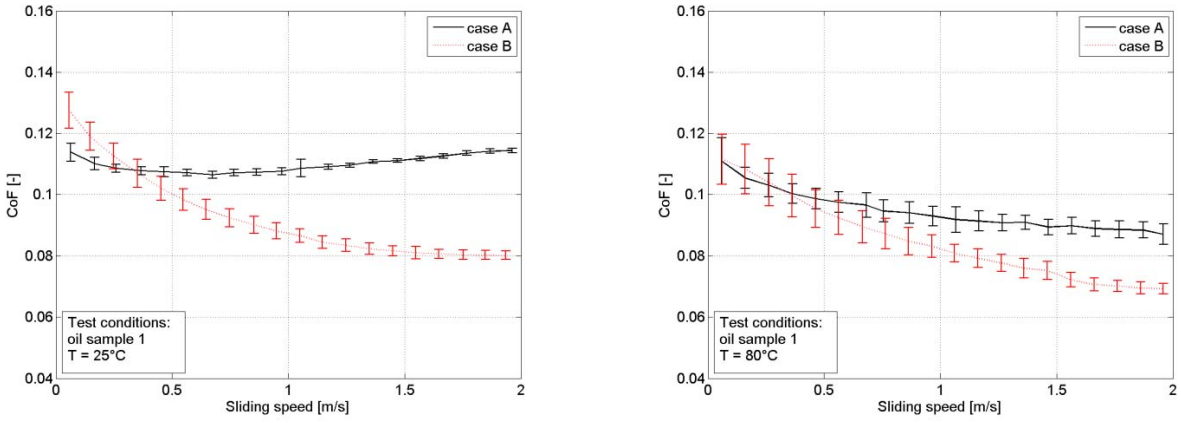

(a) (b)

Fig. 5. Stribeck curves at 25°C (a) and 80°C (b) – oil sample 1: case A (before water absorption), case B (after water absorption).

In Figure 6, the results obtained by testing the oil sample 2 are presented. As for the previous sample, at 25°C the oil which absorbed moisture from ambient air (case B) doesn't exhibit minimum in the whole speed range. At 80°C the water absorbed by the sample results in lower

friction coefficient at higher sliding speed, whereas at lower sliding speed the friction coefficient exhibits the same behaviour in both cases.

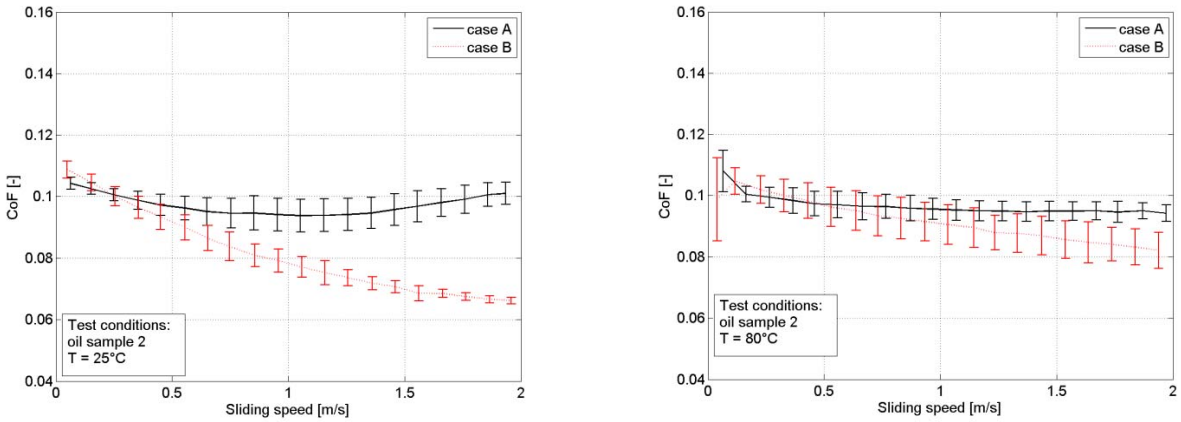

(a) (b)

Fig. 6. Stribeck curves at 25°C (a) and 80°C (b) – oil sample 2:
case A (before water absorption), case B (after water absorption).

Finally, in Figure 7 the results for the oil sample 3 are presented. In this case, at 25°C the oil sample which absorbed moisture from ambient air (case B) exhibits minimum around 1.40 m/s. Moreover, both at 25°C and at 80°C the water bound in oil results in reduction of the friction coefficient in the whole analysed speed range.

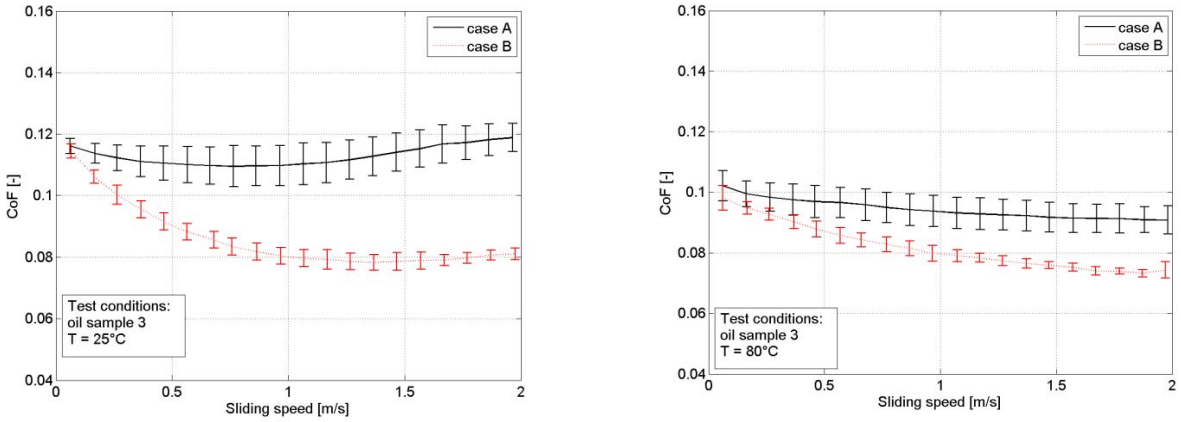

(a) (b)

Fig. 7. Stribeck curves at 25°C (a) and 80°C (b) – oil sample 3:
case A (before water absorption), case B (after water absorption).

3.3.2 Friction in steady-state tests

In this section the friction coefficients measured in steady-state condition are described. In Figure 8 the friction coefficient vs. time both at 25°C, sliding speed 5 mm/s (a) and 0.5 m/s (b) and 80°C, sliding speed 5 mm/s (c) and 0.5 m/s (d), for the pure PAG 46 is showed. It is worth noting that only at 25°C and sliding speed 5 mm/s, i.e. graph (a), an increment of the friction coefficient, on average of 8%, in the oil which has absorbed moisture (case B) has been observed. Instead, in all others tests carried out on pure PAG 46 have highlighted reduction of the friction coefficient, on average from 8 to 25%.

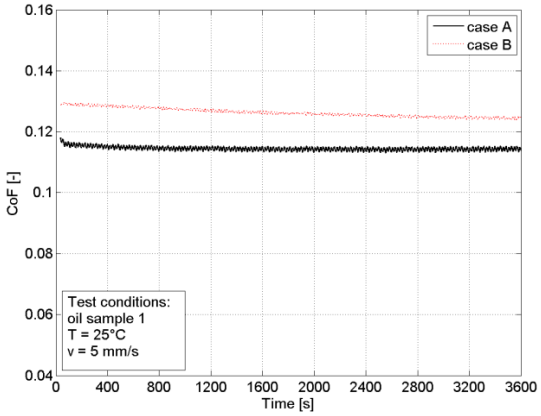

(a) boundary lubrication

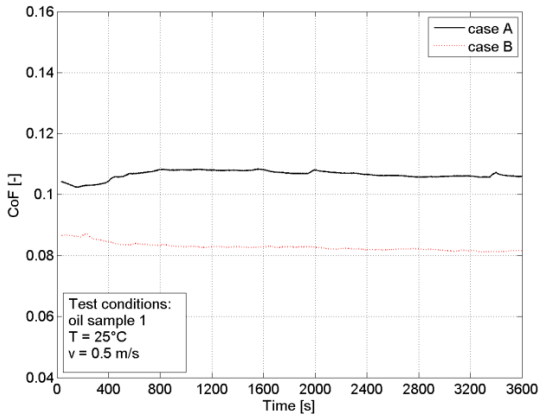

(b) mixed lubrication

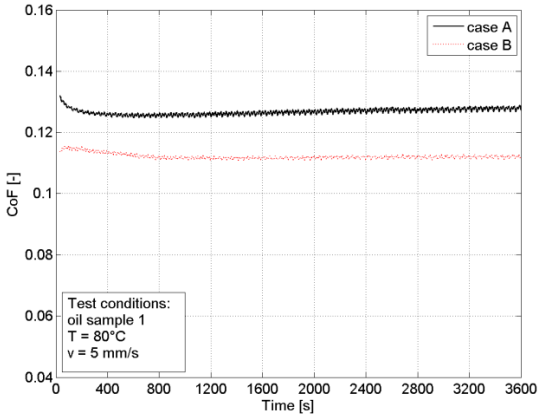

(c) boundary lubrication

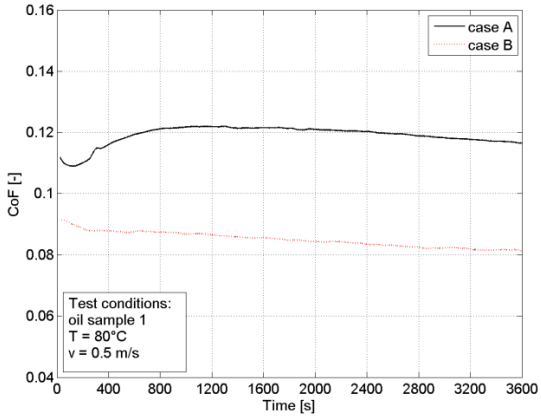

(d) mixed lubrication

Fig. 8. Steady-state tests at 25°C (a)-(b) and 80°C (c)-(d) – oil sample 1: case A (before water absorption), case B (after water absorption).

In Figure 9, the friction coefficient vs. time both at 25°C, sliding speed 5 mm/s (a) and 0.5 m/s (b) and 80°C, sliding speed 5 mm/s (c) and 0.5 m/s (d), for the PAG46 with 2.0w.t.% IL and GO at 0.1w.t.% is shown. For this oil sample the results are conflicting. In fact, at lower temperature both in boundary lubrication regime and mixed lubrication regime the water absorption results in higher friction coefficient, + 35% and +10%, respectively. On the other hand, at 80°C in both lubrication regimes lower friction coefficient has been observed in the oil sample with water content. In particular, in boundary regime the average reduction is about 10% whereas in mixed regime it attains 40%.

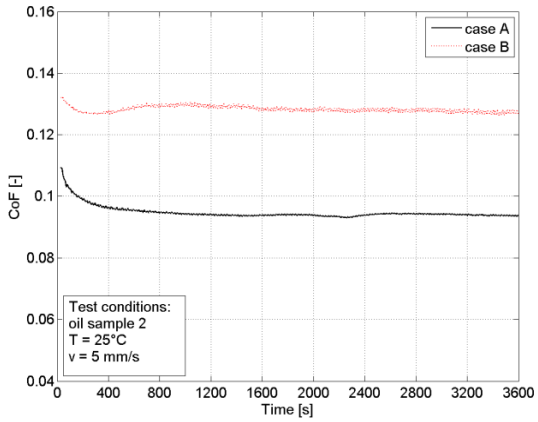

(a) boundary lubrication

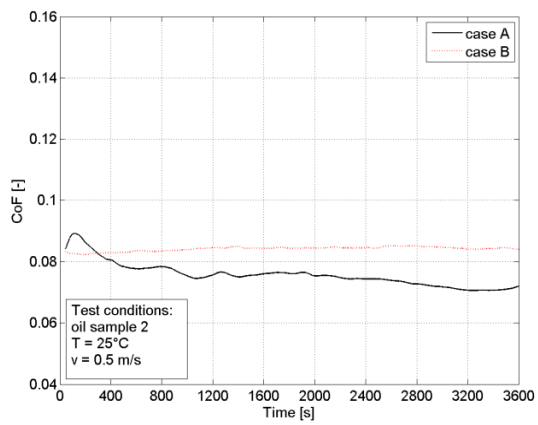

(b) mixed lubrication

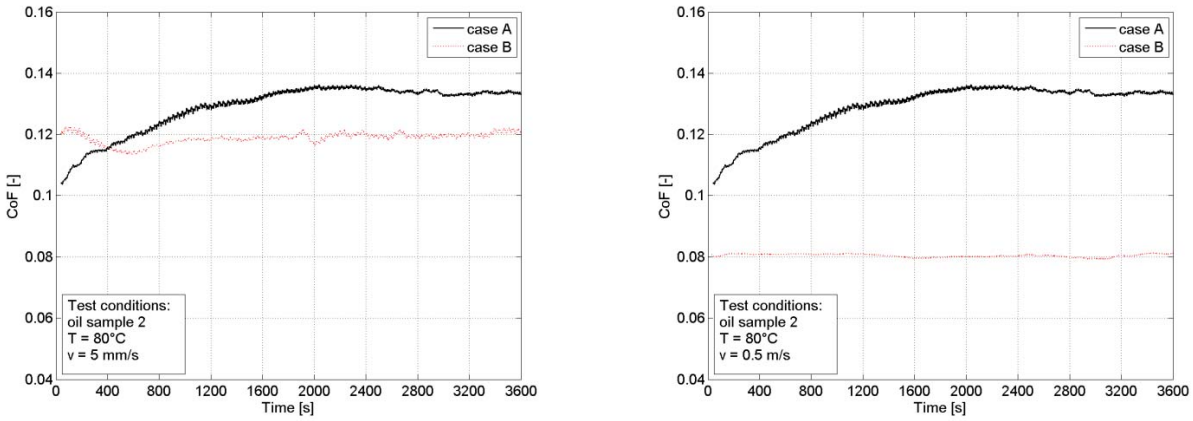

(c) boundary lubrication (d) mixed lubrication

Fig. 9. Steady-state tests at 25°C (a)-(b) and 80°C (c)-(d) – oil sample 2: case A (before water absorption), case B (after water absorption).

Finally, in Figure 10 the friction coefficient vs. time both at 25°C, sliding speed 5 mm/s (a) and 0.5 m/s (b) and 80°C, sliding speed 5 mm/s (c) and 0.5 m/s (d), for the PAG46 with 2.0w.t.% IL and GO at 0.5w.t.% is showed. For this oil sample the differences between the two cases, A and B, are more evident in boundary lubrication regime. Conversely, in mixed lubrication regime only small differences could be noticed.

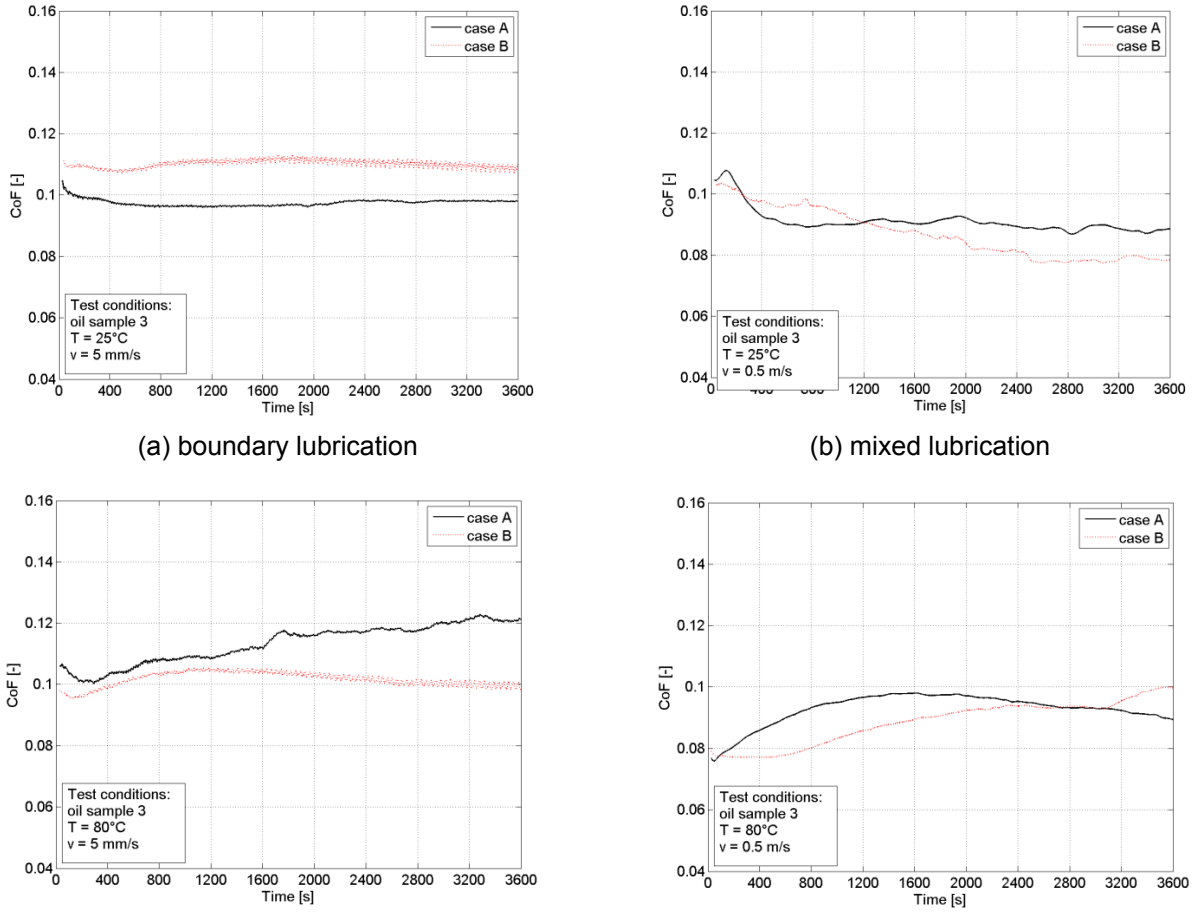

(a) boundary lubrication (b) mixed lubrication

(c) boundary lubrication (d) mixed lubrication

Fig. 10. Steady-state tests at 25°C (a)-(b) and 80°C (c)-(d) – oil sample 3: case A (before water absorption), case B (after water absorption).

3.4 Wear parameter in steady-state tests

As explained before, at the end of 1-hour steady state tests, the worn surface of the steel ball has been measured with Sensofar PLu-neox 3D optical profiler to acquire the wear scar diameter (WSD). In Figure 11 typical 3D surface image is reported.

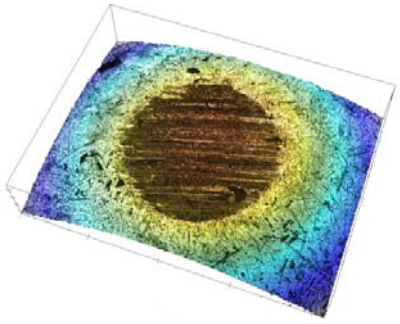

Fig. 11. Steel ball specimen and wear scar on its top side.

Smaller wear scar diameters have been observed at the end of steady tests carried out with lubricant samples whit water content, table 3, both in boundary regime, sliding speed of 5 10^{-3} m/s and mixed regime, sliding speed of 5 10^{-1} m/s. These results confirms the analysis in [32], whose Authors explain that in boundary lubrication condition the presence of air and water in polar lubricants promote surface chemical reactions with ensuing friction and wear reduction.

TABLE 3: Wear Scar Diameter (WSD)

SAMPLE	v [m/s]	WSD at 25°C [μm]	WSD At 80°C [μm]
1 A	5 10^{-3}	340	290
1 B		270	280
1 A	5 10^{-1}	590	470
1 B		300	280
2 A	5 10^{-3}	320	470
2 B		270	330
2 A	5 10^{-1}	630	450
2 B		310	320
3 A	5 10^{-3}	350	500
3 B		276	285
3 A	5 10^{-1}	650	530
3 B		400	450

4. Discussion

Previous studies about the reduction of frictional losses obtained by nanoparticles as friction modifiers additive finds several physical explanations: rolling-sliding motions coupled to flexibility behaviour, nanoadditive exfoliation and material transfer to metal surface to form the so called "tribofilm" or "tribolayer", electronic effects in tribological interfaces, surface roughness reduction or "mending", sliding on lower shear stress layers with reduced direct contact between metal surfaces [28,33,34]. The results of the present research confirm the sensible reduction of friction coefficient in boundary and mixed lubrication regime in the region of high contact pressure provided by the dispersion of GO. However, low stability of GO dispersion was observed at the end of tests at 80°C; i.e. settlement tendency due to low viscosity of the base oil. Hence, the concentration of GO at inlet side of lubricated wedge is actually lower than the expected theoretical data. Unfortunately, the inclusion of ionic liquid in the lubricant formulations under test did not provide an improvement of GO dispersion stability, as possible side-effect benefit.

The anti-wear action performed by the tested formulations was generally weak. Apart from couple of outliers, the selected wear parameter generally fell for both GO/ILs based formulations in the uncertainty range of the PAG 46 data with weak tendency to increase with the additives loading, regardless their nature, solid or liquid one. On the other hand, the water absorption results in clear improvement of the anti-wear action, as confirmed from wear parameter measurements. The water content enables friction coefficient reduction in the whole range of sliding speed of the tests, as displayed by the Stribeck graphs. Nevertheless, steady state tests provided less straight results with detrimental role of adsorbed water in some test at 25°C. The latter point needs deepening in future researches.

5. Conclusions

The tribological performance of graphene oxide (GO) and ionic liquids (ILs) as friction modifiers in polyalkylene glycol (PAG) base oil have been measured in the region of high contact pressure, 1.50 GPa, in boundary lubrication regime and mixed regime as well. Lubricant samples with different concentration of ILs and GO have been tested by way of tribometer setups. The experiments were carried out through sweep-speed tests to achieve the Stribeck curves for each sample as well as in steady-state condition to capture the friction coefficient evolution resultant from tribopair surfaces modification. The results confirm the reduction of friction coefficient provided by GO dispersion, although certain settlement tendency of such solid additive appeared, especially at higher lubricant temperature. The inclusion of ionic liquid allows enhancing of frictional behaviour at higher temperature by compensating the reduced GO action in such operating conditions. About anti-wear properties the tested formulations before moisture exposure showed weak protection. On the other hand, experimental tests on the influence of water content in oil have highlighted improvements of the anti-wear action in the entire testing spectrum and reduction of the friction coefficient in many cases.
Forthcoming experimental analysis will focus on the stability improvement of the colloidal suspension through tailored dispersant agent as well as the role of water content at different temperature levels.

Acknowledgement

This research was partially funded by the program "Legge Regionale 28/03/2002 N. 5 - Regione Campania, Bando 2007"- Research project name: "Indagini sperimentali su accoppiamenti meccanici in presenza di lubrificanti innovativi additivati con nanoparticelle basso impatto ambientale/Experimental investigations on mechanical pairs with innovative lubricant based on environment-friendly nanoparticles additives".

References

[1] A. S. Pensado, M. J. P. Comuñas, and J. Fernández, 'The Pressure–Viscosity Coefficient of Several Ionic Liquids', Tribol. Lett., vol. 31, no. 2, pp. 107–118, Aug. 2008.
[2] W. Liu, C. Ye, Q. Gong, H. Wang, and P. Wang, 'Tribological performance of room-temperature ionic liquids as lubricant', Tribol. Lett., vol. 13, no. 2, pp. 81–85, 2002.
[3] Q. Lu, H. Wang, C. Ye, W. Liu, and Q. Xue, 'Room temperature ionic liquid 1-ethyl-3-hexylimidazolium- bis(trifluoromethylsulfonyl)-imide as lubricant for steel-steel contact', Tribol. Int., vol. 37, no. 7, pp. 547–552, 2004.
[4] C. Ye, W. Liu, Y. Chen, and L. Yu, 'Room-temperature ionic liquids novel versatile lubricant', Chem. Commun., no. 21, pp. 2244–2245, Oct. 2001.
[5] A.-E. Jiménez and M.-D. Bermúdez, 'Ionic liquids as lubricants for steel–aluminum contacts at low and elevated temperatures', Tribol. Lett., vol. 26, no. 1, pp. 53–60, Feb. 2007.
[6] A. E. Jiménez, M. D. Bermúdez, F. J. Carrión, and G. Martínez-Nicolás, 'Room temperature ionic liquids as lubricant additives in steel–aluminium contacts: Influence of sliding velocity, normal load and temperature', Wear, vol. 261, no. 3–4, pp. 347–359, Aug. 2006.
[7] H. Kamimura, T. Kubo, I. Minami, and S. Mori, 'Effect and mechanism of additives for ionic liquids as new lubricants', Tribol. Int., vol. 40, no. 4, pp. 620–625, 2007.
[8] J. N. A. Canongia Lopes and A. A. H. Pádua, 'Nanostructural Organization in Ionic Liquids', J. Phys. Chem. B, vol. 110, no. 7, pp. 3330–3335, Feb. 2006.
[9] J. Qu, J. J. Truhan, S. Dai, H. Luo, and P. J. Blau, 'Ionic liquids with ammonium cations as lubricants

or additives', Tribol. Lett., vol. 22, no. 3, pp. 207–214, 2006.
[10] I. Minami, N. Watanabe, H. Nanao, S. Mori, K. Fukumoto, and H. Ohno, 'Improvement in the tribological properties of imidazolium-derived ionic liquids by additive technology', J. Synth. Lubr., vol. 25, no. 2, pp. 45–55, Apr. 2008.
[11] M. Uerdingen, C. Treber, M. Balser, G. Schmitt, and C. Werner, 'Corrosion behaviour of ionic liquids', Green Chem., vol. 7, no. 5, p. 321, 2005.
[12] H. Wang, Q. Lu, C. Ye, W. Liu, and Z. Cui, 'Friction and wear behaviors of ionic liquid of alkylimidazolium hexafluorophosphates as lubricants for steel/steel contact', Wear, vol. 256, no. 1–2, pp. 44–48, Jan. 2004.
[13] L. J. Weng, X. Q. Liu, Y. M. Liang, and Q. J. Xue, 'Effect of tetraalkylphosphonium based ionic liquids as lubricants on the tribological performance of steel-on-steel system', Tribol. Lett., vol. 26, no. 1, pp. 11–17, 2007.
[14] O. Y. Fajardo, F. Bresme, A. A. Kornyshev, and M. Urbakh, 'Electrotunable lubricity with ionic liquid nanoscale films.', Sci. Rep., vol. 5, p. 7698, 2015.
[15] O. Y. Fajardo, F. Bresme, A. A. Kornyshev, and M. Urbakh, 'Electrotunable Friction with Ionic Liquid Lubricants: How Important Is the Molecular Structure of the Ions?', J. Phys. Chem. Lett., vol. 6, no. 20, pp. 3998–4004, 2015.
[16] H. W. Kroto, J. R. Heath, S. C. O'Brien, R. F. Curl, and R. E. Smalley, 'C60: Buckminsterfullerene', Nature, vol. 318, no. 6042, pp. 162–163, Nov. 1985.
[17] K. Lee, Y. Hwang, S. Cheong, L. Kwon, S. Kim, and J. Lee, 'Performance evaluation of nano-lubricants of fullerene nanoparticles in refrigeration mineral oil', Curr. Appl. Phys., vol. 9, no. 2 SUPPL., pp. e128–e131, 2009.
[18] V. Chauveau, D. Mazuyer, F. Dassenoy, and J. Cayer-Barrioz, 'In Situ Film-Forming and Friction-Reduction Mechanisms for Carbon-Nanotube Dispersions in Lubrication', Tribol. Lett., vol. 47, no. 3, pp. 467–480, Sep. 2012.
[19] L. Guadagno, M. Sarno, U. Vietri, M. Raimondo, C. Cirillo, and P. Ciambelli 'Graphene-based structural adhesive to enhance adhesion performance', RSC Adv., vol. 5, 27874-27886, 2015.
[20] H. D. Huang, J. P. Tu, L. P. Gan, and C. Z. Li, 'An investigation on tribological properties of graphite nanosheets as oil additive', Wear, vol. 261, no. 2, pp. 140–144, Jul. 2006.
[21] J. Lin, L. Wang, and G. Chen, 'Modification of Graphene Platelets and their Tribological Properties as Lubricant Additive', Tribol. Lett., vol. 41, no. 1, pp. 209–215, Jan. 2011.
[22] Y. Kawaguchi, M. Kaneko, and M. Takagi, 'The Performance of End Capped PAG as Refrigeration Oil for HFC134a', in International Compressor Engineering Conference, 1998, pp. 267–273.
[23] M. Woydt, I.-S. Rhee, and S. W. Dean, 'Polyalkylene Glycols as Next Generation Engine Oils', J. ASTM Int., vol. 8, no. 6, p. 103368, 2011.
[24] J. Thoen, D. Zweifel, and M. Woydt, 'Potential for polyalkylene glycols in automotive engine oil applications', in Engine oil circulation system of internal combustion engines, 2009.
[25] P. N. Ananthanarayanan, Refrigeration and Air Conditioning, Third. Tata McGraw-Hill Education, 2005.
[26] J. William S. Hummers and R. E. Offeman, 'Preparation of Graphitic Oxide', J. Am. Chem. Soc, vol. 80, no. 1937, p. 1339, 1958.
[27] -, 'The history of Lonza's graphite powders', Ind. Lubr. Tribol., vol. 27, no. 2, pp. 59–59, 1948.
[28] M. Sarno, A. Senatore, C. Cirillo, V. Petrone, and P. Ciambelli, 'Oil Lubricant Tribological Behaviour Improvement Through Dispersion of Few Layer Graphene Oxide', J. Nanosci. Nanotechnol., vol. 14, no. 7, pp. 4960–4968, 2014.
[29] MINILUBES Report Summary, available at URL: http://cordis.europa.eu/result/rcn/47466_en.html accessed on Sept. 17th, 2015.
[30] V. Zin, F. Agresti, S. Barison, L. Colla, C. Pagura, and M. Fabrizio, 'Investigation on tribological properties of nanolubricants with carbon nano-horns as additives at different temperatures', in Proceedings of World Tribology Congress 2013, 2013, pp. 1–4.
[31] M. Kalin, I. Velkavrh, and J. Vižintin, 'The Stribeck curve and lubrication design for non-fully wetted surfaces', Wear, vol. 267, no. 5–8, pp. 1232–1240, Jun. 2009.
[32] W. H. Van Glabbeek, T. K. Sheiretov, and C. Cusano, 'The Effect of Dissolved Water on the Tribological Properties of Polyalkylene Glycol and Polyolester Oils', Report of ACRC Project 04 Compressor--Lubrication, Friction, and Wear, 1994.
[33] L. Yadgarov, V. Petrone, R. Rosentsveig, Y. Feldman, R. Tenne, and A. Senatore, 'Tribological studies of rhenium doped fullerene-like MoS_2 nanoparticles in boundary, mixed and elasto-hydrodynamic lubrication conditions', Wear, vol. 297, no. 1–2, pp. 1103–1110, 2013.
[34] C. Altavilla, M. Sarno, P. Ciambelli, A. Senatore, and V. Petrone, 'New "Chimie Douce" approach to the synthesis of hybrid nanosheets of MoS_2 on CNT and their anti-friction and anti-wear properties', Nanotechnology, vol. 24, no. 12, 2013.

Aerodynamic Protection of Wind Turbines

Prof. Em. PhD. Eng. **Mircea BĂRGLĂZAN**[1], Assoc. Prof. PhD. Eng. **Teodor MILOŞ**[2]

[1] "Politehnica" University of Timişoara, e-mail: mbarglazan@yahoo.com

[2] e-mail: Teodor.Milos@gmail.com

Abstract: *In this work are presented the problems of aerodynamic protection of rapid axial wind turbines, with horizontal aggregate's shaft. There are investigated in detail the interaction phenomena of wind (fluid flow) with aerodynamic shaped blades of the turbine runner. It is calculated for the realized wind power plants (designed by "Politehnica" University of Timişoara) the attack angles of fluid flow on the blade airfoils at different runner radiuses. Also it is determined the operation reserve without separation of the flow from the blade in function of the wind velocity and / or the maximum angle of rotation of the runner blades in respect of blade shaft.*

Keywords: *horizontal axis wind turbines, flow separation from the blades, dynamic stall, three-dimensional flow in the runner, wind power aggregate protection.*

1. Introduction

Wind turbines are usually erected for maximum power production at around 15 m / s wind velocities. It is not economic to design and realize the turbines to withstand for much greater wind velocities. This is the reason why to limit the turbine's power in high wind conditions. If it is not made this protection, there are produced high runner speeds of rotation, overloading all mechanical ensemble and electric generator and sometimes producing catastrophic accidents.
In this article we focus on rapid axial horizontal axis wind turbine (HAWT) realized in two variant: with fixed runner blades and with mobile runner blades. In both cases the aerodynamic protection is realized limiting the absorbed power form the wind turbine, when the airflow separates from the runner blades. By wind turbines with the fixed blades the separation occurs when the wind velocity exceeds a definite value. Mobile blades wind turbine protection is assured through synchronous rotation of these blades around their axis at an external command and consequently producing the flow separation from the blades.

2. Fluid flow separation by rapid axial wind turbines

The aerodynamic protection of wind power plant is realized through a complex phenomenon of interaction of fluid flow (wind) with a solid aerodynamic shaped body in a rotation motion (wind turbine runner blade) by the separation regime of the fluid from the solid. The complexity is produced once by the character of the fluid flow (wind with direction and intensity variable in space and time, turbulence and gust) with three –dimensional structure in the boundary layer and second by the blade geometry (composed of aerodynamic profiles by different radiuses connected and twisted in space) and with its rotation motion. Wind turbine power control [2] through passive separation of the flow from the blade by stall - in a two-dimensional interpretation – takes place when the attack (incidence) angle of the blade constitutive profiles surpasses the stall critical angle and the lift decreases and shows fluctuating values. The advantage of this control system is that it didn't introduced solid mobile parts through the protection device. The disadvantage consists through the possibility of blade vibrations through the phenomenon of flutter. The majority of wind power plants, in operation nowadays, are using this type of control and protection. Wind turbine power control [3] through active separation of the flow is realized through the synchronous rotation of the wind turbine blades. By little wind velocities the wind turbine blades are put in the position of optimal power. When it is attaint the nominal (maximum) power and the tendency is to raise the power then the control device change action direction and induces a separation of the flow from the blades (stall). The advantage consists of the possibility to control the power especially by start

and by gusts. Also at high wind velocities it is maintained the nominal power different from passive control, where the power decreases because of increase separation of the flow Fig. 1.

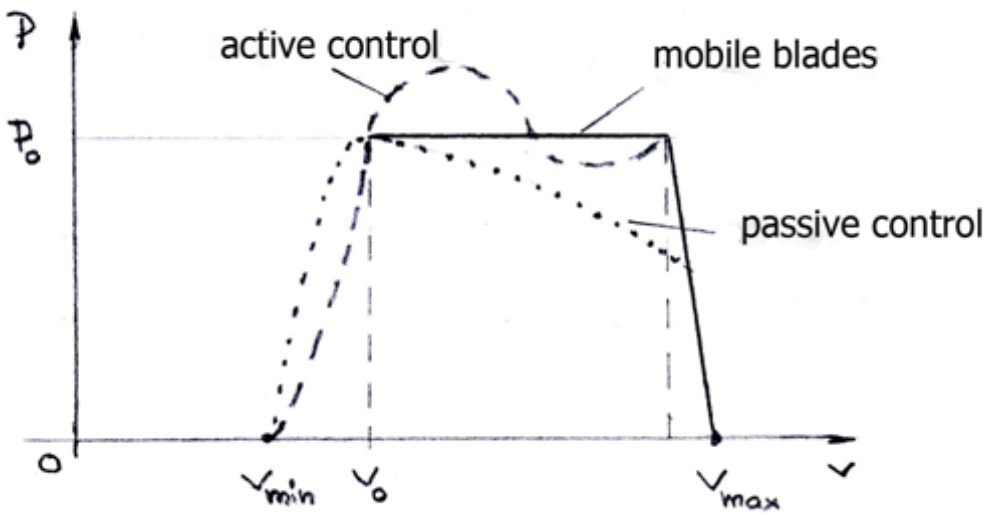

Fig. 1. Passive and active control of separation and control through blade rotation.
P_0 – nominal power; v_0 – nominal velocity

The 3D character of the flow structure in the wind turbine runner blade boundary layer of HAWT [4], is visualized in Fig. 2.

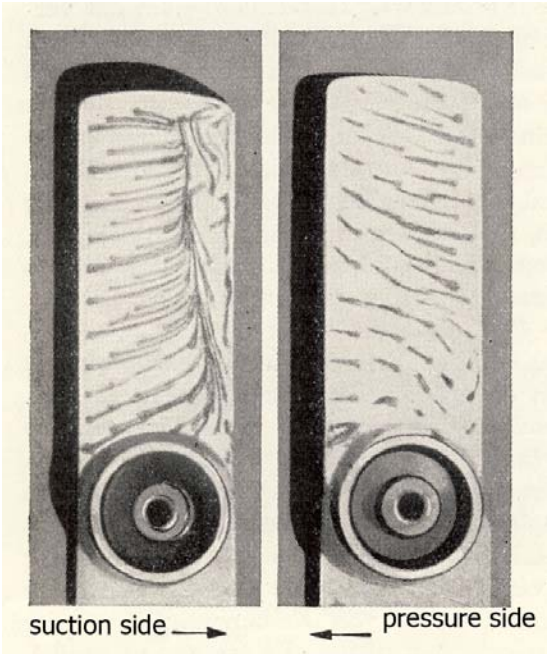

Fig. 2. Flow visualization in blade boundary layer of a turbo-machine [7].

From Fig.2 it is obvious that the fluid flow velocity has axial, tangential and radial components. So the separation investigations need to pass from a 2D analysis to a 3D analysis. Instead of a separation point it occur a separation line on the solid surface Fig. 3 [13].

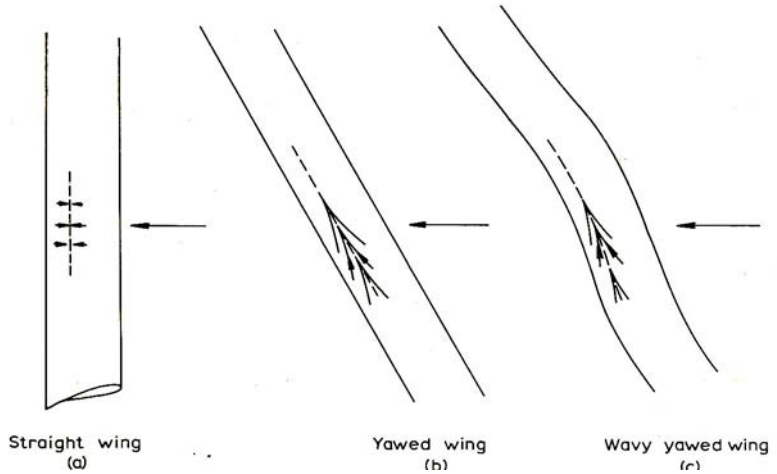

Fig. 3. Flow separation from a blade with different relative positions

Inclined separation comparative with transversal separation of the flow is postponed and occurs by higher wind velocities as it is seen in Fig. 3 qualitatively and this is the case by wind turbines. This kind separation is not so much investigated [13] as the 2D separation of a fluid flow from an airfoil Fig. 4 [5].

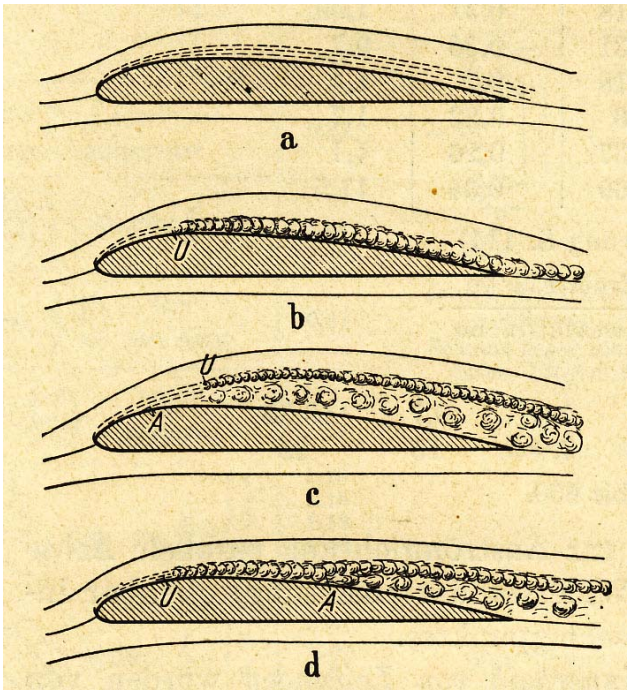

Fig. 4. Development of the boundary layer and the flow separation from a blade:
a – laminar boundary layer; b – laminar – turbulent transition; c – separation in the laminar zone;
d – separation in the turbulent zone; A – separation point ; U – transition point.

Separation from one or two points of the suction side of the airfoil depends from a lot of factors. So the geometry of the profile (and thickness, camber, roughness), fluid characteristics (pressure, temperature) and wind parameters (velocity, direction, turbulence, gust) are important. If the profile is a part from the blade it are added the variability of the profile shape with the radius, blade twist, variation of the attack angle with the radius, Reynolds and Mach numbers. All this elements made a difficult task to establish unique functional dependence of the conditions and power developed by the wind turbine at the stall limit in function of the wind.
The correlation is more like a zone with a definite degree of uncertainty Fig. 5.

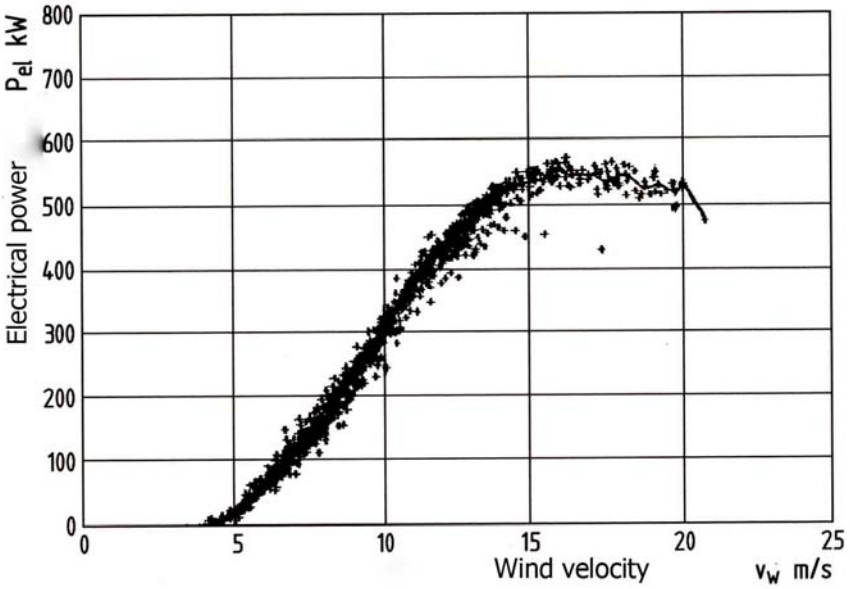

Fig. 5. Mean measurements, with 10 minutes rate, power in function of wind velocity at a wind turbine with fixed blades and with the limiting power through flow separation of the flow from the blade (stall).

Other modalities to protect the wind turbines may be realized through ailerons, aggregate rotation or mechanical and electrical brakes.
Experimentally investigations about the 2 D stall on an airfoil, put in evidence in [7], is analytically studied on the base of Beddoes-Leishman , ONERA and MEXICO models in [8],[9],[10],[11],and [12]. Non-stationary character of the phenomena, measured from apparatus with high dynamic qualities, recorded in Fig. 6 showed the flutter of the airfoil.

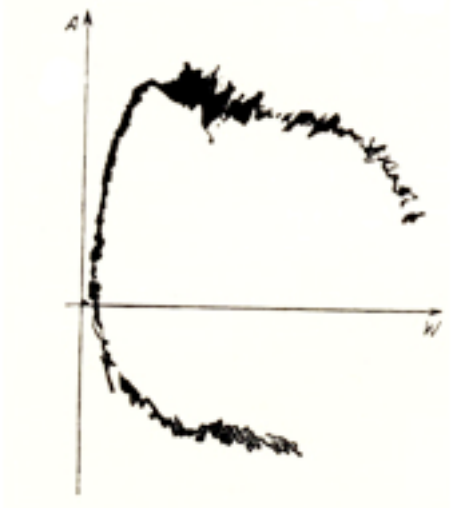

Fig. 6. Polar curve of an airfoil recorded with high dynamic qualities.

The comparison between static and dynamic characteristics with hysteresis of an airfoil is represented in fig. 7.

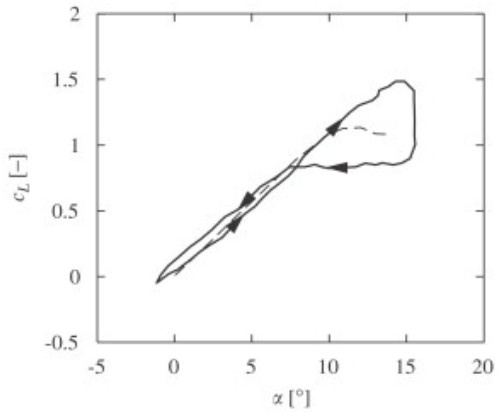

Fig. 7. Static and dynamic with hysteresis lift coefficient in function of attack angle by an airfoil.

The dynamic characteristics with hysteresis showed different aspect in function of the position of the profile along the radius of the blade and frequency of oscillation. Only one example with the hysteresis zone presented in detail is in Fig. 8.

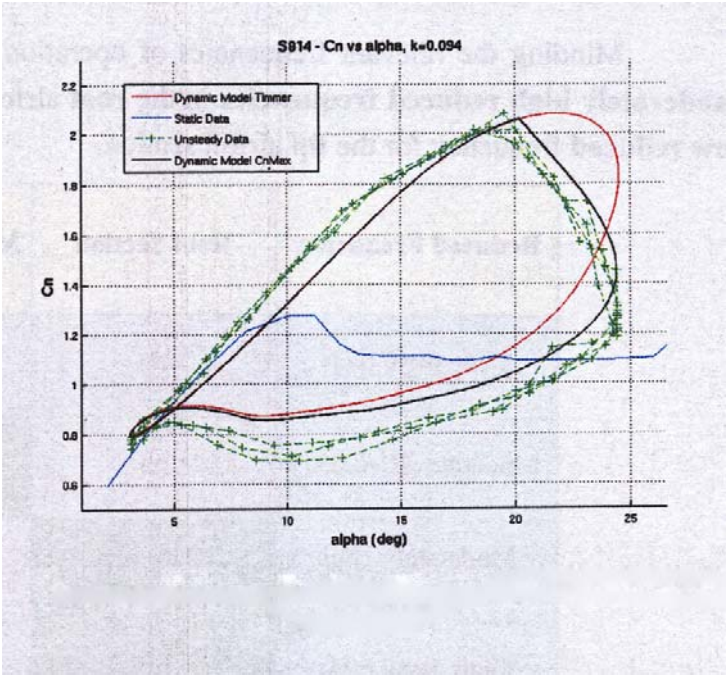

Fig. 8. Static and dynamic lift coefficient in function of attack angle at the root of the blade and with high frequency airfoil oscillation.

3. Protection calculus of the wind turbine from Ciugud

Aerodynamic protection of wind power plant from Marga and Ciugud were verified on the base of flow separation of the flow from the horizontal wind turbine blades through stall. Wind aggregates of 5 kW power in accord with the design [1] and rated wind velocity of v_0 = 8,5 m / s, and rated rotation speed of n_0 = 120 rev / min, for the constant speed of rotation and an interval of Δn_0 = 60 – 120 rev / min for the variable speed of rotation. Knowing the blades geometry through the coordinate of the aerodynamic airfoils at different runner radiuses and grid angles it is calculated the tangential velocity " u ", flow angle " β " and attack angle " i " of the airfoils with the formulas:

$$u = \omega \cdot r = \frac{\pi \cdot n}{30} \cdot r \qquad (1)$$

$$\beta = arc\,tg\left(\frac{v}{u}\right) \tag{2}$$

$$i = \beta - \varphi \tag{3}$$

From the 28 known sections of the wind runner blades there are chosen three representative sections for the hub, middle and outside zones. Data are extracted from [1] referring to breath of the blade (profile's chord) "b" and the complementary stagger angle of the profiles "φ". Results are given in Table 1.

TABLE 1

Rated values v = v_o = 8,5 m / s ; n_o = 120 rev / min.						
r [m]	**b [m]**	**φ [^{0}]**	**Profile NACA**	**u [m /s]**	**β [^{0}]**	**i [^{0}]**
3.5	0.355	4.2857	654415	43.982	10.938	6.6523
2.5	0.525	7.6000	654418	31.416	15.140	7.5401
1.5	0.695	15.3333	654421	18.850	24.272	8.9387

Analytic connection between profile's attack angle and blade radius is :

$$i = 11.99488 - 2.4207 \cdot r + 0.2555 \cdot r^2 \tag{4}$$

$$\text{with the mean error : } \varepsilon_m = 4.6259 \cdot 10^{-18} \tag{5}$$

For the wind turbines with variable speed it is considered the minimum speed in Table 2:

TABLE 2

Minimum speed values v = v_o = 8,5 m / s ; n_o = 60 rev / min.						
r [m]	**b [m]**	**φ [^{0}]**	**Profile NACA**	**u [m /s]**	**β [^{0}]**	**i [^{0}]**
3.5	0.355	4.2857	654415	21.990	21.1335	16.8478
2.5	0.525	7.6000	654418	15.7075	28.4197	20.8197
1.5	0.695	15.3333	654421	9.425	42.0459	26.7126

In this case the analytic connection between profile's attack angle and blade radius is:

$$i = 39.15383 - 9.7349 \cdot r + 0.9605 \cdot r^2 \tag{6}$$

$$\text{with the mean error : } \varepsilon_m = 8.0954 \cdot 10^{-18} \tag{7}$$

Comparative analysis of the results about the attack angles form Table 1 and Table 2 shows that runner speed decreasing produce the flow separation at the runner blade hub. Considering the accepted model for fluid flow structure in the runner wind turbines zone given by [2] and [3] it is possible to introduce the axial velocity correction a = 1/3:

$$v_a = v_o \cdot (1\text{-}a) \tag{8}$$

The vortex influence which occurs after the runner on the tangential velocity is introduced through the coefficient "a' ". It depends on the axial correction "a" and rapidity „λ":

$$a' \cdot \left(1 + a'\right) = \frac{a \cdot \left(1 + a\right)}{\lambda^2} \tag{9}$$

$$\lambda = \frac{u\left(R\right)}{v} \tag{10}$$

$$u' = u\,(1 + a') \tag{11}$$

TABLE 3

Rated value n_0 = =120 rev / /min							
a **-**	**v_0** **[m/s]**	**u(R)** **[m/s]**	**λ** **-**	**a'** **-**	**v_a** **[m/s]**	**u'(R)** **[m/s]**	**λ'** **-**
1 / 3	8.5	43.982	5.174	0.0412	5.667	45.794	8.081

From Table 3 it is observed that the rapidity of the wind turbine is in the best operation interval of such type machine. Also the value of correction coefficient for axial velocity is considerable but the correction coefficient for tangential velocity is negligible.
Data from catalog NACA [6] gives characteristic curves of the profiles used in Fig. 9, Fig. 10 and Fig. 11.

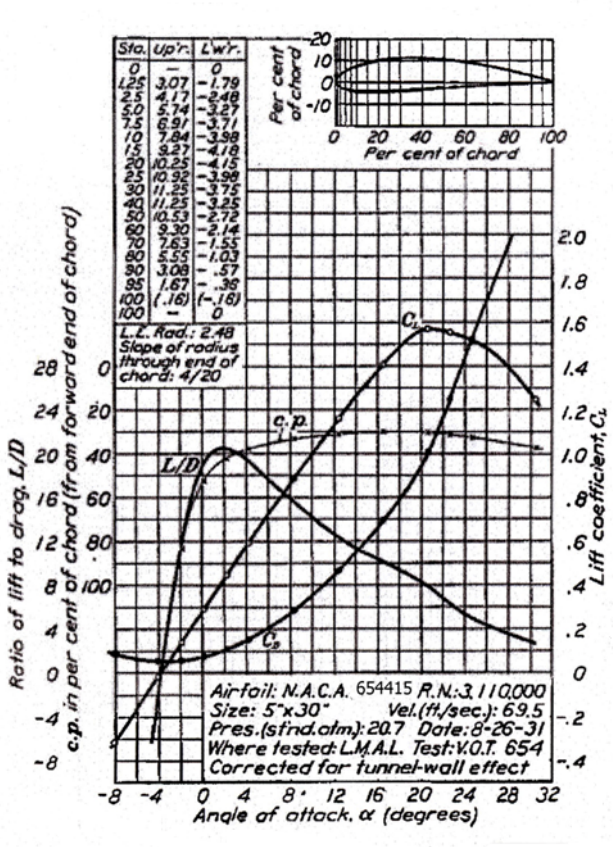

Fig. 9. Characteristic curves of the NACA 654415 profile

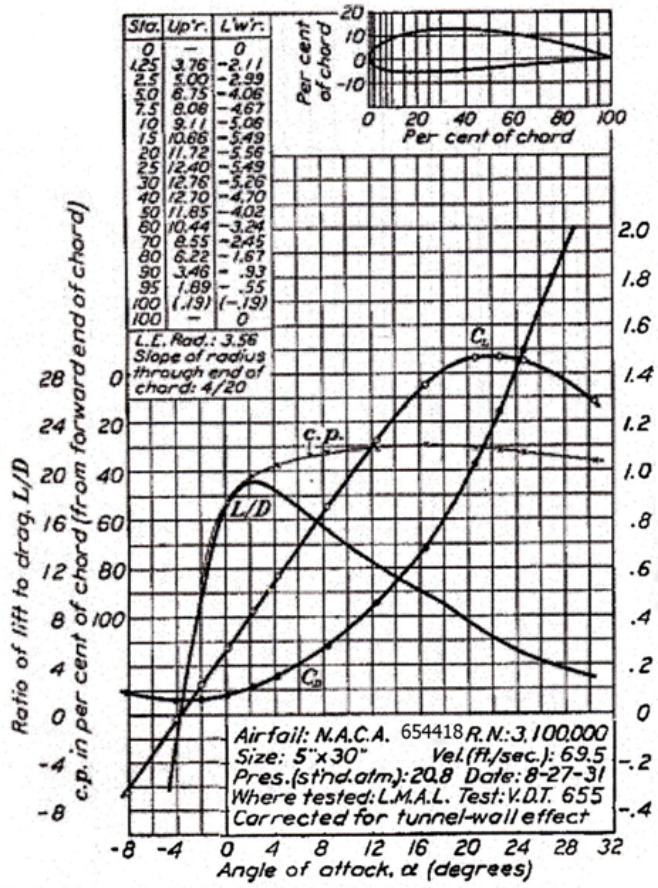

Fig. 10. Characteristic curves of the NACA 654418 profile

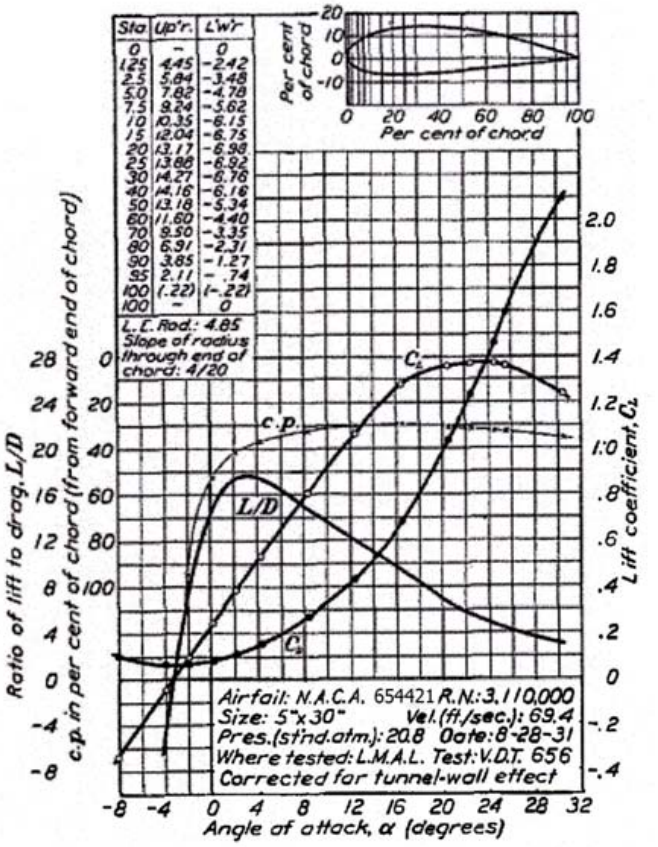

Fig. 11. Characteristic curves of the NACA 654421 profile

From these curves it is deduced the lift coefficient "C_L" corresponding to the attack angle "i" by different operation regimes, Also it is possible to determine critical attack angle values "i_{cr}" for maximum lift coefficient " C_{Lmax}" which assures the operation of the profile respectively the turbines blades without separation. See Table 4.

TABLE 4

Rated values v_o = 8,5 m / s ; n_o = 120 rot / min.				
Profile	**i [°]**	**C_L -**	**i_{cr} [°]**	**$C_{L\,max}$ -**
NACA 654415	6.6523	0.6	20.8	1.57
NACA 654418	7.54	0.8	22	1.47
NACA 654421	8.9387	0.85	24	1.38

Now it is possible to determine the blade axis rotation and the corresponding wind velocity by which the separation of the flow will occur based on the flow structure accepted model namely the interaction of the wind with the blades constitutive profiles.
The blade axis rotation angle Δφ, equal with attack angle modification Δi :

$$\Delta\varphi = \Delta i = i_{cr} - i \tag{12}$$

The angle between the flow relative velocity with the opposite angle of the tangential velocity of the runner, β, is equal with:

$$\beta_{cr} = i_{cr} + \varphi \tag{13}$$

and the maximum wind velocity, v_{max} , at the limit of flow separation from the blade surface :

$$v_{max} = u \cdot tg\beta_{cr} \tag{14}$$

Results are given in Table 5:

TABLE 5

Rated values v_o = 8,5 m / s ; n_o = 120 rot / min.				
Profile	**u** [m / s]	**Δi** [°]	**β_{cr}** [°]	**v_{max}** [m / s]
NACA 654415	43.98	14.1477	25.0857	20.588
NACA 654418	31.415	14.46	29.6	17.846
NACA 654421	18.849	15.0613	39.333	15.446

This table shows the safety of the wind turbine against air flow separation from the runner blades. Namely approximately 14 degrees of blade axis rotation at wind aggregates with mobile blades and for wind velocities approximately of 15 m / s both cases in the situation of zero azimuth angle. After the 14 degrees rotation the separation begins at the out side of the blade (Profile NACA 654415) and the hub zone (NACA 654421) at wind velocities 1.76 times greater than the rated 8.5 m / s velocity.

4. Conclusions

a) Air flow separation from the rapid axial wind turbines blades is complex. The complexity consists on the interaction from three-dimensional fluid flow with a profiled solid body in a rotation movement. Restrictions refers to dynamic stall phenomena namely the aerodynamic separation of the air flow, viscous fluid, two – or three – dimensional, incompressible, stationary and subsonic. Separation from the blades occurs in constant speed of rotation and zero azimuth angles.
b) Analytic and numerical models which describe the separation of the fluid through the interaction of the flow with runner blade surface are perfectible.
c) The three-dimensional structure of the fluid flow occurs because the air velocity has on the vicinity of the blades an axial, a tangential and a radial component and this delays the separation of the fluid from the blade.
d) Wind power plants protection against flutter calculated through two-dimensional model is secure.
e) The proposed method applied to power plants Ciugud and Marga demonstrates its validity and utility.

References

[1] Project RO 0018/2009, "Improvement of the structures and efficiency of small horizontal axis wind generators", EEA Grants Norway, 2009 – 2012;
[2] E. Hau, Windkraftanlagen. Springer Verlag, Berlin, 2014;
[3] T. Burton,.., Wind Energy Handbook, John Wiley ed., Chichester, 1997;
[4] M. Bărglăzan, Turbine hidraulice şi transmisii hidrodinamice, Ed. Politehnica, Timişoara, 2000;
[5] P. K. Chang, Control of Flow Separation, Hemisphere Publ. Washington, 1978;
[6] N. Eastman,…, The characteristics of 78 Related Profiles Sections from Tests in the variable wind-tunnel, Report 460, NACA 1993;
[7] B. Eck, Technische Strömungslehre, Springer-Verlag, Berlin, 1954;
[8] B. F. Xu,.., Development and application of a dynamic stall model for rotating wind turbine blades, Journal of Physics, Conf. Series 524, NASA 2014;
[9] R. Pereira,.., Validation of the Beddoes – Leishman dynamic stall model for horizontal axis wind turbines using MEXICO data, Wind Energy Journal, AIAA, Wiley, 2012;
[10] T. C. Corke,.., Dynamic stall model for wind turbine airfoils, Univ. Notre Dame, Indiana USA, 2015;
[11] J. W. Larsen,.., Dynamic stall model for wind turbine airfoils, Journal of Fluid Structures, Elsevier, Amsterdam, Oct. 2007;
[12] R. Balbina,.., Validation the Beddoes – Leishman Dynamic Stall Model in HAWT Environment, Master Thesis, 2009;
[13] E. S. Taylor, Some Problems of Recognizing and Defining Separation of the Skewed Boundary Layer, Fluid Mechanics of Internal Flows, Elsevier, Amsterdam, 1967;
[14] G. B. Mc Coullough, Examples of three representative types of airfoil section stall at low speed, NACA TN 2502 / 1951;
[15] M. Ragheb, Modern wind generators, Talbot Lab. USA, 2014;
[16] E. Potocar,.., Control of Separation Flow over a Wind Turbine Blade with Plasma Actuators, Journal of Mechanical Engineering, Slovenia, 2011;
[17] D. Kaminski, Active Control of Flow Separation, New York SERDA, 2010;
[18] I. Curiac, .., Doubly feed induction generator for biomass combined heat and power systems, Hidraulica no. 1/ 2013, pp. 61-64;
[19] G. Matache, C. Cristescu, C. Dumitrescu, V. Miroiu, Pregătirea specialiştilor în vederea adaptabilităţii şi creşterii competitivităţii, Hidraulica no. 3-4/ 2012, pp. 7-14;
[20] T. Miloş,…, The 3D blade surface generation for Kaplan turbines using analytical methods and CAD techniques, Hidraulica no. 2 / 2013.

Water Supply Operating Rules in Parallel Dams by Means of Genetic Algorithms

Maritza L. ARGANIS[1], Rosalva MENDOZA[1], Ramón DOMÍNGUEZ[1], Gerardo ACUÑA[1]

[1] Engineering Institute, National Autonomous University of Mexico

marganisj@iingen.unam.mx, rmr@pumas.iingen.unam.mx, rdm@pumas.iingen.unam.mx, gacuna00@gmail.com

Abstract: *The Cutzamala system is the work of urban water infrastructure most important of Mexico since 1974, because it supplies drinking water to the Metropolitan Area of Mexico City with a flow rate of approximately 16 m^3/s. The main dams of the Cutzamala system are: El Bosque, located in MIchoacan State; Valle de Bravo and Villa Victoria in the State of Mexico. In this analysis it was considered a parallel operation of these dams, i.e. independently feeding the water treatment plant Los Berros. A historical review was carried out considering, at each year, constant monthly extractions for each storage dam, genetic algorithms were then used to evaluate an objective function which maximize the extractions and minimize, by means of penalty coefficients, the presence of spills and deficits in the system. Finally, the obtained operating rules where simulated, using the historical record of input volumes by basin in the period 1994-2011. The use of genetic algorithms, engaging a simulation program of the operation of a system of three parallel dams, led to the identification of optimal policies of removal, for purposes of potable water for human consumption in the Cutzamala River system. The optimal operating rule successfully allowed reconciling the objectives.*

Keywords: *Cutzamala System, Genetic Algorithms, Operating Rules, Drinking water.*

1. Introduction

Countries suffering moderate water stress have less than 1700 cubic meters of water per person per year. This means that water is not often available at certain times of the year in certain places, which produces a hard choice to make between personal consumption, agriculture or industry. [1]
Nowadays the water of reservoirs created by dams provide a pool of water that guarantees reliable supply to the population, this promotes better human conditions. Actually, it has become a key priority find a way to optimize the work performance of a system in terms of energy efficiency and a good water supply network. [2]
The decision to bring water from basins located outside the Valley of Mexico was due to the impacts caused by the sinking of the city by the extraction of groundwater. The excessive growth of population during the thirties, became apparent that groundwater sources are insufficient to meet the demand of thousands of new residents. It should be mentioned that the basin where the Mexico City and its metropolitan area is located, it is surrounded by five basins, being Lerma and Cutzamala nearby basins. The other three are Amacuzac, Libres Oriental and Tecolutla River. Of these, the first two were more appropriate to become the first contributors of water to the Mexico City. [3]
The Cutzamala system is the most important work of urban water infrastructure of the country's central portion since 1974, due to it supplies of potable water to Mexico City Metropolitan Area (MCMA) with a flow of approximately 16 m^3/s [4]. The dams of the Cutzamala system are Tuxpan and El Bosque located in the state of Michoacan, Ixtapan Del Oro, Colorines, Valle de Bravo, Chilesdo and Villa Victoria in the State of Mexico [5], as shown in the diagram of Figure 1. [6]
The drinking water supply was recognized as one of the major challenges that will determine the sustainability in Mexico City [7]. Currently It shows obvious signs of degradation, lack of investment, and reduction in the capacity of the system. The effects of climate change need to be evaluated in order to determine its impact and promote strategies that enable us to deal with this challenge.

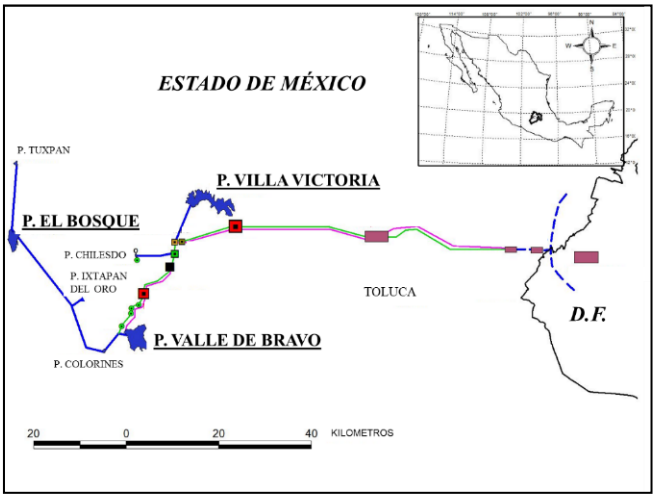

Fig. 1. Cutzamala System Diagram

The system deliveries water with an estimated efficiency of 60 %, the flow which doesn't get to be delivered is attributed to the leak along the pipelines [7], would be proposed to revise the losses caused by the system in order to achieve the required performance, there is a need not only adequate static and dynamic parameters, but also a modern concept diagram of a hydrostatic transmission work [8]; it is believed that part of the problem can also be due to the policies of operation of the dams in the system. If such policies will be modified the operation of the whole system, it could be improved and thus to achieve better extractions, avoiding deficits or decrease them as much as possible, while ensuring that spills do not occur in these dams, by all those reasons the operation of the system is complex.
Currently the estimated supply for the Metropolitan Area is an average flow of 59.9 m^3/s divided between various sources that are shown in Table 1.

TABLE 1: Water supply to the MCMA

Infrastructure	Supply (m^3/s)	% to input
Aquifer MCMA	39.00	65 %
Cutzamala System	**14.70**	**25 %**
Lerma System	4.80	8 %
Madín Dam	1.40	2 %

With the historical review of the system operation it is intended to investigate the possible lack of operating rules. It is important to notice that, in the analysis, it was assumed that the system works in parallel, that means that the dams: El Bosque, Valle de Bravo and Villa Victoria will catch their own inflow and their outputs or extractions will arrive directly to the Water Treatment Plant Los Berros. [9].
As mentioned, there is no complete data of the four diversion dams: Tuxpan, Ixtapan del Oro, Colorines and Chilesdo; so it only took into account the three major dams and were considered to be able to take one hundred percent of the delivered volume to the Metropolitan Area of Mexico's Valley (MCMA).
Another hypothesis considered in the operation of the reservoirs was to assume a constant monthly extraction at each year for the three dams.

2. Background

Nowadays, drinking water supply represents one of the most important priorities, so it is important to attend the new demands and gradually reduce the over- exploitation to which has been

subjected the aquifer of the Mexico's Valley in recent years. The Cutzamala system was composed of three stages of construction, and they were originally designed to export into the Valley of Mexico a maximum flow rate of 19 m^3/s (599 hm^3/year), however, the system has stabilized itself at 16 m^3/s (505 hm^3/year).

Valle de Bravo Dam

Valle de Bravo dam covers a surface of 2900 hectare and it has an altitude of 1768 meters above sea level. The maximum storage capacity was initially 457 hm^3, reduced by blockage to 394.66 hm^3. Nevertheless, the artificial lake was the promoter of the tourist activity and currently must keep a certain minimum level due to socio-economic activities seated around the reservoir [10]. The average extraction is 6.8 m^3/s, which represents approximately 43 % of the total of the three dams. Typically, the highest levels of storage are reached in September, as a result of the accumulation of the runoff and they were kept until the month of March, when begin the decreases, reaching levels of minimum storage in the month of June. [10]

Villa Victoria Dam

Villa Victoria dam is located at an altitude of 2544 meters above sea level; it has a total capacity of 254 hm^3 and a useful storage capacity of 185.73 hm^3. The dam provides 18 % of the drinking water for the MCMA. Its main contribution is La Compañia River, in addition to other runoff of minor importance. Its storage is reduced during the period from April to August, and then it grows as a result of the runoff accumulation. [10]

El Bosque Dam

El Bosque dam is located at an altitude of 1741 meters above sea level; it has a total capacity of 248 hm^3 and a useful storage capacity of 202.4 hm^3. The maximum depth of the dam is approximately 40 m, with a width of 4 km and a length 6 km. The main uses are the agricultural irrigation in the neighbouring towns to the south, drinking water supply and electricity generation. Zitácuaro River or San Juan Viejo, San Isidro River and part of the Tuxpan River through tunnels and channels, as well as runoff and intermittent streams [6], supplies it. It was determined that the contribution of this dam is 6.2 m^3/s on average, which represents 39 % of the system.

3. Methodology

An historical review of the operation of the dams El Bosque, Valle de Bravo and Villa Victoria in a period from 1994 to 2011 was carried out. The system operation was accomplished with the continuity equation [13], in case of a three parallel dam system (the analysis was made by separate basins) is the following:

$$S_{j,i+1} = S_{j,i} + I_{j,i} - O_{j,i} \tag{1}$$

Where: *i* is the time interval considered (in this case months), *j* is the subscript corresponding to each dam, $S_{j,\,i+1}$ is the volume of final storage, $S_{j,i}$ is the volume of initial storage, $I_{j,i}$ are the inputs to the reservoir and O_j the total output obtained by the following equation:

$$O_i = Evni + Vei \tag{2}$$

Where *Evni* is the net evaporation obtained from the historical values of precipitation minus evaporation; *Vei* is the monthly volume of extraction obtained from the operation policy (herein curve Z) as shown in Figure 2 and the extractions percentages for each dam. In this study a monthly extraction percentage for each dam was considered equal to 1/12.
The Z curve shows the range of values of extraction and storage depending on the characteristics of each reservoir.
Thus the slope formed between the minimum points and maximum meet a range of optimal, i.e. values, at operation under these conditions is simulated, all values of extraction and storage below the slope ensure optimal operation in the system.

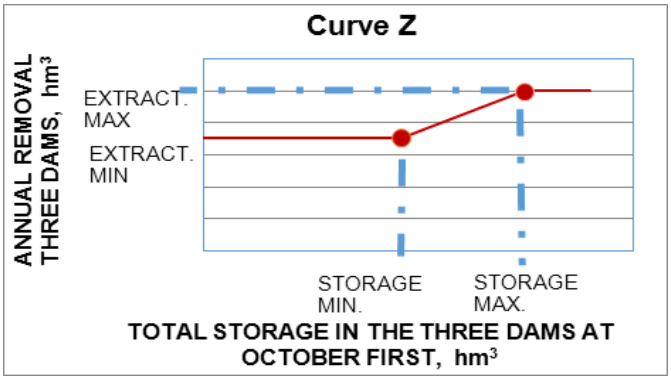

Fig. 2. Curve Z

3.1 Input data

The inflow volume for each dam recorded from 1994 to 2011 was considered for the simulation of the system operation. Figure 3 shows the inflow volumes of El Bosque dam, (similar results were determined for the other two dams, Valle de Bravo and Villa Victoria).

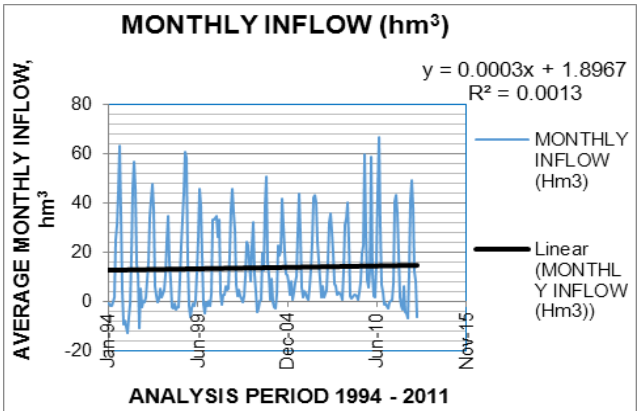

Fig. 3. Inflow El Bosque dam

The elevation was set as a function of the storage volume, as shown in Figure 4 that represents the values of the El Bosque dam; in the same way the expressions of the other two dams were obtained.

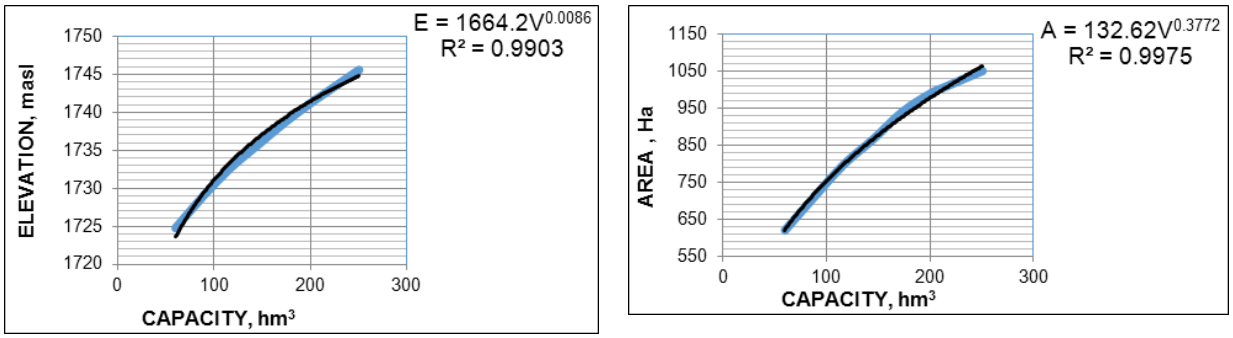

Fig. 4. Curve Elevation – Capacity – Area

In this way the analysis of the total extractions was then carried out, they were obtained from the annual historical percentages from the period 1994 to 2011 and with them the curve Z of historic extractions was built as the basis for the study of optimization. Table 2 shows the values that define the curve Z of Figure 5.

TABLE 2: Values of Total Storage and extraction curve Z for historical data

Total Storage 3 dams (hm^3)	Total Annual Extract. (hm^3)
0.00	352.65
459.80	352.65
747.20	500.00
900.00	500.00

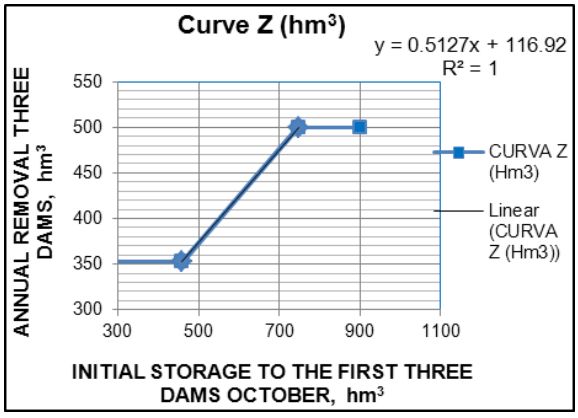

Fig. 5. Curve Z. Historical analysis

Table 3 shows the percentages of the historical total extraction for each dam.
The results of the operation for the three dams with the assumption of constant monthly extraction are shown in Table 4.

TABLE 3: Historical percentage of extraction

Dam	% ANNUAL
Villa Victoria	0.1825
Valle de Bravo	0.4265
El Bosque	0.3910
Total Annual	**1.0000**

TABLE 4: Historical operation (3 dams)

Concept	(hm^3)
Total extraction	8 011.11
Total spill	541.42
Total deficit	195.05

Based on the information obtained in the historical review, we proposed getting policies which allow obtaining the optimum extraction for the three dams of the system; helped with genetic algorithms and the simulation of the system operation.

3.2 Genetic Algorithm

Genetic algorithms had been used for optimization purposes since the middle of the eighties of the twentieth century, recent applications in hydrology and hydraulic stresses in the work of Huang [13], Zhang [14], Dominguez [15], among others.

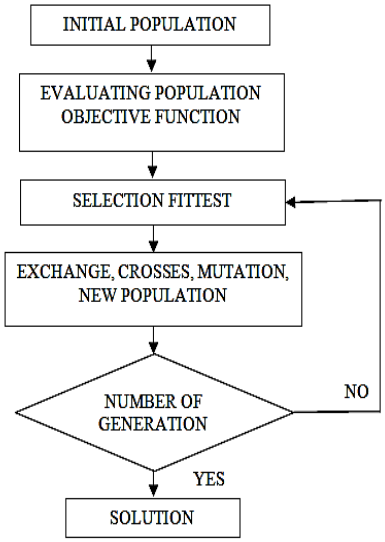

Fig. 6. Block diagram of an AG

Genetic Algorithms (GA) are adaptive methods, commonly used in problems of searching and optimization of parameters, based on sexual reproduction and on the principle of survival of the fittest." [16]. The fundamental characteristic of the GA is the use of an operator of recombination or crossing, as the primary mechanism of search, and a rendering algorithm by proportional to the performance, it is represented in a general way that the operators used on its application are the selection, the exchange or crosses and mutation, the structure of a simple genetic algorithm is presented in Figure 6 [17]. The selection can be done by the method of the roulette wheel or the stochastic universal or tournament [18]. The exchange is made at the level of binary code but can also be done at the level of real numbers; the mutation may or may not be considered and it allows new individuals appear in a generation.

In the present study, individuals correspond to sets of four parameters that make up the points on the curve of annual water extractions of the system of dams analyzed (call curve Z) the curve shows the total annual extractions as a function of the total storage for the three dams measured on October the first, tests with several parameters were carried out to analyze the behavior of the system. In a first analysis, three trials were performed where the fixed annual percentage of extraction a priori on the basis of the historic operation for each dam, leaving as variables the four points of the curve Z. In the trials 1 to 3, the objective function (OF) was to maximize the extractions by imposing penalties in case of spill and deficit conditions in the system, this is:

$$OF = Max\left\{c_e * V_e \quad - c_{der} V_{derr} \quad - c_{def} V_{def}\right\}... \tag{3}$$

Where, for the simulation period of n years, V_e is the total storage of extractions for three dams, V_{derr} is the total storage of spills for the three dams, V_{def} is the total storage of deficits for the three dams; C_e is a heavy coefficient for the extraction, C_{der} is a penalty coefficient in spill case, C_{def} is a penalty coefficient for deficit event.

In a second analysis we also considered in addition to these parameters, the percentages of annual extraction that must be assigned to each dam, i.e., the algorithm requires that the sum of the percentages of extraction be equal to 100 % of the entire system. Therefore these four tests will have 7 unknowns (3 more variables considering the extraction percentage assigned to each of the three dams). The aim of this problem is to optimize the extractions for each dam decreasing the spills and avoiding deficits that may present and identify which is the annual extraction percentage that accomplish the above assertions. Due to the fact that in trials 4 to 7 the extraction percentages of each dam were left free, we add to the OF the restriction that the sum of the percentages of annual extractions of the three dams should be 1, for this the difference was penalized respect to one of the sum of the percentages of annual extraction, and thus the equation for the OF in the following way:

$$OF = Max\left\{c_e * V_e \quad - c_{der} V_{derr} \quad - c_{def} V_{def} \quad - c_{err} Err\right\}... \tag{4}$$

Where $Err = 1 - (\sum_{i=1}^{3} pi)$; *pi* is the annual percentage assigned to the dam *i*, *i=1, 2, 3*; C_{err} is a penalty factor to minimize the value of *Err*. The program for the simulation of the system was coded in Fortran and the executable program is called by the genetic algorithm to evaluate the objective function with each individual in each generation [19]. To perform the tests with the genetic algorithm is taken into account 200 individuals and 500 generations.

TABLE 5: Parameters of lower bounds

hm³	**Lower Limit (hm³)**			
	Initial Storage Vol.	**Initial Extract.**	**Final Storage Vol.**	**Final Extract.**
Test 1	100	100	400	200
Test 2 to 7	100	250	400	350

TABLE 6: Parameters of upper bounds

hm^3	Upper Limit (hm^3)			
	Initial Storage Vol.	Initial Extract.	Final Storage Vol.	Final Extract.
Test 1	459.8	352.7	747.2	500
Test 2 to 7	459.8	352.7	747.2	500

The penalty coefficients help the genetic algorithm to find the optimal values that comply with the assertions of such equation. These penalty coefficients are shown in Tables 7 and 8.

TABLE 7: Penalty Coefficients first analysis

	Test 1	Test 2	Test 3
C_e (extract)	1	1	1
C_{derr}	10	10	100
C_{def}	1 000	1 000	1 000

TABLE 8: Penalty Coefficients second analysis

	Test 4	Test 5	Test 6	Test 7
C_e (extract)	1	1	1	1
C_{derr}	100	100	100	1 000
C_{def}	1 000	1 000	1 000	1 000
C_{err}	1 000	10 000	100 000	100 000

The test was processed by trial and depending on the results for each parameter, such as the penalty coefficients or the upper and lower limits to adjust the curve Z, in order to cover the largest values depending extraction-modified storage. [20]

4. Results and discussion

Once historical percentages of each extraction were determined, they are simulated using various genetic algorithms operating policies, for this study, seven tests that meet the requirements of water extraction were performed. Table 9 shows the results obtained and Figure 7 shows the Curve Z feature of each test.

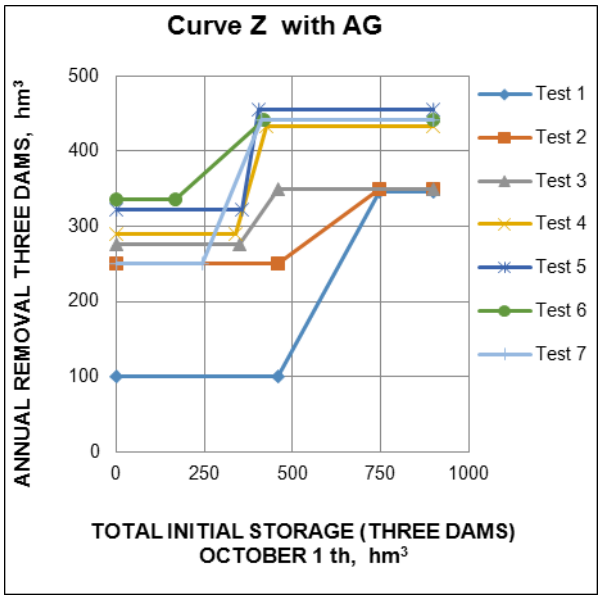

Fig. 7. Curve Z. Calculated in 7 trials

Table 9 shows that the objective function of equation 1, for the tests 1 to 3 the extraction, is below the historical (8 011.11 hm^3), although it is clear that increases with each test. However for the trials 4 and 5, the extractions are the best, but the goal is to accomplish an extraction rate of 1.

TABLE 9: Total result of the system for the seven trials

hm^3	Three Dam Total		
	Extraction (hm^3)	Spill (hm^3)	Deficit (hm^3)
Test 1	6 135.20	2 009.37	0.00
Test 2	6 238.09	1 919.46	8.68
Test 3	6 300.22	1 862.54	12.89
Test 4	8 075.30	478.31	51.55
Test 5	8 518.30	398.60	366.56
Test 6	7 399.80	924.40	0.00
Test 7	7 597.80	759.71	0.00

Tables 10 and 11 show the extraction percentages of the 7 tests, it is appreciate that the values of the tests 6 and 7 are close to 1, in fact, until the moment the Test 6 is the best option; with the intention to adjust as much as possible to the unit, two other tests were realized increasing the penalty coefficients.

TABLE 10: Extraction percentage, first analysis

Dams	Test 1	Test 2	Test 3
%P1 (EB)	0.39	0.39	0.39
%P2 (VB)	0.43	0.43	0.43
%P3 (VV)	0.18	0.18	0.18

TABLE 11: Extraction percentage, second analysis

Dams	Test 4	Test 5	Test 6	Test 7
%P1 (EB)	0.37	0.34	0.35	0.37
%P2 (VB)	0.48	0.44	0.45	0.45
%P3 (VV)	0.22	0.21	0.21	0.21
SUM	**1.0758**	**0.9854**	**1.0085**	**1.0324**

It is then analyzed which was the maximum historical total storage of October the first and this was 782.52 hm^3, this value is found in the year 1994, when it was assumed that reservoirs were at NAMO, this means that the three dams were at their highest levels. Therefore there were a couple of trials where values are adjusted to the Final Storage Volume in the lower and upper limits, see tables 12 and 13. In addition to modify the penalties; ensuring minor spills and deficits in this new essay, see Table 14.

TABLE 12: New parameters lower limits

hm^3	Lower Limit (hm^3)			
	Initial Storage Vol.	Initial Extract.	Final Storage Vol	Final Extract
Test 8	100	250	**783**	350
Test 9	100	250	**783**	350

TABLE 13: New parameters upper limits

hm^3	Lower Limit (hm^3)			
	Initial Storage Vol.	Initial Extract.	Final Storage Vol	Final Extract
Test 8	100	250	**783**	350
Test 9	100	250	**783**	350

TABLE 14: New penalty coefficients

	Test 8	Test 9
C_r (extract)	1	1
C_{derr}	10 000	100
C_{def}	1 000	1 000
C_{err}	100 000	100 000

Values that can be found with these new parameters are shown in the Table 15, where the results found are the best compared with the historical and they have the best behavior; in the percentages that correspond to each dam was found overexploitation of 27 % for the Test 8 as shown in Table 16, therefore for the test 9 is adjusted this extraction percentage almost the value of 1 using the best coefficients discussed above.

TABLE 15: Total Result last two trials

hm^3	Total		
	Extraction (hm^3)	Spill (hm^3)	Deficit (hm^3)
Test 8	8 219.90	421.91	94.86
Test 9	8 219.90	421.91	94.86

TABLE 16: Extraction percentages improvement

Dams	Test 8	Test 9
%P1 (EB)	0.43	0.35
%P2 (VB)	0.61	0.44
%P3 (VV)	0.24	0.21
SUM	**1.2772**	**1.0011**

The graph in Figure 8, shows the curve Z from these two trials, it is worth to mention that the Test 9 will be considered as optimal.

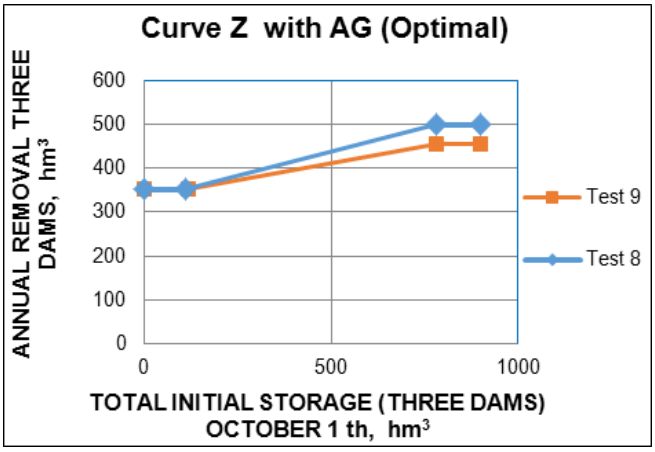

Fig. 8. Curve Z with the last two trials

Therefore, the extraction percentage associated with each dams in the Cutzamala System is shown in Table 17 and compared with the historical values for its best analysis:

TABLE 17: Comparative extraction percentages of each dam

Dams	Historical	Test 9
%P1 (EB)	0.39	0.35
%P2 (VB)	0.43	0.44
%P3 (VV)	0.18	0.21
SUM	1.0000	**1.0011**

TABLE 18: Total Historical Comparative against Test 9

	Historical (hm^3)	Test 9 (hm^3)	(%)
Total Extraction	8 011.11	8 219.90	102.61 %
Total Spill	541.42	421.91	77.93 %
Total Deficit	195.05	94.86	48.63 %

In the table above it can be concluded that El Bosque dam reduces the extraction in an 11.19 %; in Valle de Bravo dam is increased by a 3.43 % and, for the Villa Victoria dam also increases the extraction in a 16.54 % compared with what is currently being done in the system.
Table 18 gives a comparison of the total the historic operation against the total test 9 to analyze in which proportion the situation was improve in the Cutzamala System.
Finally, Figure 9 shows a graphical comparison of the extracting behavior of El Bosque dam with simulation of Test 9 against the historical one.

Should be remembered that the historical data are in Tables 2, 3 and 4 where it shows the curve Z, extraction percentages and the historical operation, respectively; Operating results of analysis with measured data.

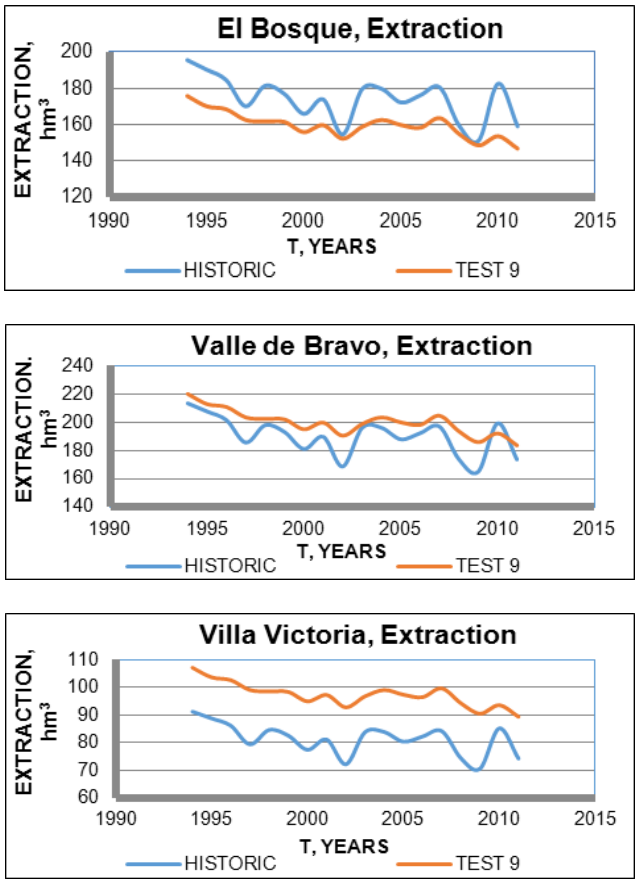

Fig. 9. Extraction. El Bosque, Valle de Bravo and Villa Victoria Dam

We must remember that with the historical review of the operation, with a period of 17 years, total withdraws of 8 011.11 million m^3 were found in the system, total spills of 541.42 million m^3 and a total deficit of 195.05 million m^3, if we have used the extraction policy 9, it would have been a more appropriate operation, with its extraction is slightly higher (8 219.90 million m^3) spills decline (421.91 million m^3) and the deficit is reduced almost half (94.86 million m^3). In this way the values that form the optimal curve Z are shown in the Table 19 and plotted in Figure 10.

TABLE 19: Optimal values Curve Z

Test 9	
Storage (hm^3)	**Extraction (hm^3)**
0.00	351.61
117.71	351.61
782.77	456.22
900.00	456.22

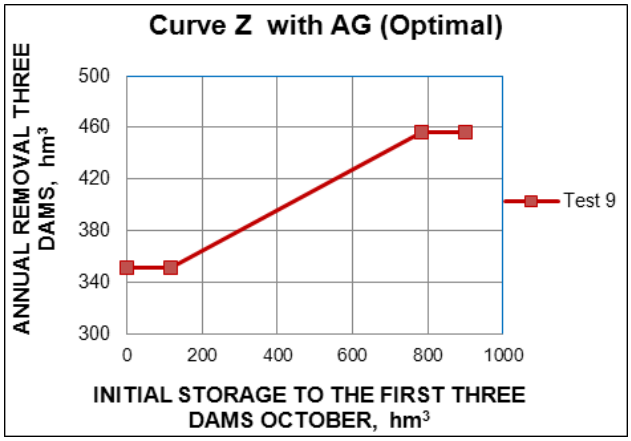

Fig. 10. Curve Z with optimal values (Test 9)

5. Conclusions

The Cutzamala System is the most important work of hydraulic infrastructure in the central region of Mexico; its main objective is to supply at least 16 m^3/s of water to the capital of the country since 1982. The system is formed by Tuxpan and El Bosque dams, located in the state of Michoacan, as well as the Ixtapan del Oro, Villa Victoria, Valle de Bravo, Chilesdo and Colorines, in the State of Mexico; each one is part of the system of Cutzamala River.

In this study were obtained annual operation policies to know the increasing demand of drinking water using three of the most important dams of the system: El Bosque, Valle de Bravo and Villa Victoria, assuming that it operates as a parallel system, this is because the information about diversion dams is not known . One hypothesis considered in the operation of the reservoirs was to assume a constant monthly extraction at each year for the three dams. Used Evolutionary Algorithms, in particular genetic algorithms, to evaluate an objective function in which it seeks to maximize the extractions and minimize, imposing penalties, the presence of spills and deficit in the main dams of the system. The operation of the assembly with the rules of operation, as well as defined was simulated using the historical record of income volumes in the year 1994 to 2011. The optimal policy found succeeded in reconciling the objectives successfully.

Once analyzed the historical data on the basis of a operation of reservoirs found the total extraction of the system that was 8 011.11 million m^3, with total spill of 541.42 million m^3 and a total deficit of 195.05 million m^3, that compared with the result of the Test 9 provides that the total annual extraction of a year (it is considered a year for the total of the system, the storage accumulated in the first October), met with a most appropriate extraction, which is greater with 8 219.90 million m^3, spills diminish significantly to 421.91 million m^3, while the deficit is reduced almost to the half with 94.86 million m^3.

In this way it is determined that the dam El Bosque must be extract a 35 % of the total annual extraction, to Valle de Bravo a 44 % and Villa Victoria must comply with 21 %. While it is a policy that the extraction is greater in a 2.61 % compared with the total extraction historic, met the objective of obtaining the lowest possible spill and same with the deficit, which is able to almost half to the three dams Cutzamala System.

The results obtained here assume the three dams analyzed work in parallel, in other words, they are independent and supply to the water treatment plant water Los Berros, this is a hypothetical case due to the fact that actually the Tuxpan dam connects with El Bosque that in turn overflowed to Valle de Bravo along with the of Ixtapan del Oro and Colorines diversion dams, while Villa Victoria and Chilesdo if fed directly to the water treatment plant.

References

[1] International Commission on Large Dams IGBC / ICOLD, "Dams and water in the world. A book about the role of dams in water management", Spain, Madrid;

[2] G. Popov, A. Krasteva, B. Kostov, D. Ivanova, Kl. Klimentov, "Optimization of the energy consumption of a pump system used for industrial water supply", Annals of faculty engineering Hunedoara – international journal of engineering, Tome XII ISSN: 1584-2665, Romania, 2014;

[3] J. Legorreta, MC. Contreras, MA. Flores, N. Jimenez, "External Basins", Ecologica - Water. Manualplaneta.com, Exploring Ecotourism, 1997;

[4] C. Tortajada, E. Castelán, "Water Management for a Megacity: Mexico City Metropolitan Area", Article AMBIO: A Journal of the Human Environment, 32 (2):124-129. 2003;

[5] INE, National Institute of Ecology, "Prioritization and recommendations for conservation actions in the Cutzamala basins System", Address of Integrated Watershed Management", Directorate general for research of ecological management and conservation of ecosystems with water, 2009;

[6] White Book, "Sustainability of the System Cutzamala", National Water Commission, pp. 93-95, 2012;

[7] O. Escolero, S. Martinez, S. Kralisch, M. Perevochtchikova, "Vulnerability of the sources of drinking water supply for the City of Mexico in the context of climate change", Mexico City, Center of Atmospheric Science, UNAM, 2009;

[8] C. Cristescu, C. Dumitrescu, G. Vrânceanu, L. Dumitrescu, "Considerations on Energy Losses in Hydraulic Drive Systems", "Hidraulica" (No. 1/2016) Magazine of Hydraulics, Pneumatics, Tribology, Ecology, Sensorics, Mechatronics, ISSN 1453 – 7303, pp. 36-46, 2016;

[9] C. Tortajada, "Environmental Sustainability of Water Management in Mexico", Third World Center for Water Management, Mexico, 155 p., 1999;
[10] CNA-SEMARNAT, "Cutzamala System. Water for millions of Mexicans", Working paper of the Regional Management of waters of the Valley of Mexico and Cutzamala System, Mexico, pp. 3-31, 2005;
[11] V. Bunge, J. Martinez, K. Ruiz-Bedolla, "Scenarios of the hydric dynamics in the region of input from the Cutzamala system", Working Document of the Directorate General for ecological management and conservation of ecosystems, National Institute of Ecology and Climate Change, Mexico, 2012;
[12] F. Aparicio, "The fundamentals of surface hydrology", Mexico, 1992;
[13] Wen-Cheng Huang, Lun-Chin Yuan, Chi-Ming Lee, "Linking genetic algorithms with stochastic dynamic programming to the long-term operation of a multireservoir system Water Resources Research", 38, pp. 401-409, 2002;
[14] X. Zhang, R . Srinivasan, D. Bosch, "Calibration and uncertainty analysis of the SWAT model using Genetic Algorithms and Bayesian Model Averaging", Journal of Hydrology, Volume 374, issues 3-4, pp. 307-317, 2009;
[15] M. R. Dominguez, J. M. L. Arganis, "Validation of methods to estimate design discharge flow rates for dam spillways with large regulating capacity", Hydrological Sciences Journal 57 (3), pp. 460-478, 2012;
[16] M. Gestal, D. Rivero, J.R. Rabuñal, A. Pazos, "Introduction to genetic algorithms and genetic programming", La Coruña, pp. 11-18, 2010;
[17] J. Holland, Adaptation in Natural and artificial systems, MIT Press, 1975;
[18] D. E. Goldberg, "Genetic algorithms in search, optimization and machine learning", Boston, MA. Addison-Wesley, 1989;
[19] R. Mendoza, "Program Manual: SIMEPPAR.FOR", Morelia, Mich., Institute of Engineering, UNAM, 2013;
[20] MATLAB Reference Guide. The MathWorks, Inc., 1992.

Energy Use in Hydraulic Drive Systems Equipped with Fixed Displacement Pumps

PhD.eng. **Petrin DRUMEA**[1], PhD.eng. **Catalin DUMITRESCU**[1],
Dipl.eng. **Alexandru HRISTEA**[1], Res. Assist. **Ana-Maria POPESCU**[1]

[1]Hydraulics and Pneumatics Research Institute INOE 2000-IHP, Bucharest, Romania

Abstract: *Using hydraulic drives has begun a long time ago, but in the 20th century they witnessed an outstanding expansion. Penetration of such systems in the field of complex equipment requiring high forces and speeds, provided with pumping units of 5 ÷ 500 KW, has represented an outstanding progress of hydraulics technology. Rather great progress, still not enough, has been done to reduce energy losses during use of fixed displacement pump systems. This paper is only the first part of a larger material which explores the evolution of energy efficiency increase over time.*

Keywords: *hydraulic drives, fixed displacement pump, energy consumption, energy loss, energy efficiency*

1. Introduction

One of the most important technical and scientific activities of recent years is related to the proper management of energy use. It is difficult to understand why mankind has come to waste significant percentage of the amount of energy produced (tens of percents) for subjective reasons. In this line, it should be pointed out that none of mechanical, electrical, hydraulic or pneumatic drives has not aimed since the beginning at lining up the amount of energy involved spent in performing a work-cycle phase with the amount of energy required, usable (output) energy.
In the field of hydraulics things started from providing for each working phase the energy required, there being no real interest in analyzing the usage of extra power, which has not been used in certain work-cycle phases. Thus, fixed displacement pump hydraulic systems have been for long time enough and satisfying.
Starting from the idea that power consumption is a function of flow and pressure and since pressure in the system is given by load, technical and scientific efforts targeted methods of varying the flow rate delivered, and therefore we witnessed the occurrence of adjustable pumps. From this moment the evolution of pumping groups consisted of creating the best devices for pump adjustment, which shall seek to equalize energy (or power) consumption to usable (output) energy in every moment of performing the work cycle of the machine.

2. Power use when driving a single actuator (hydraulic cylinder)

We will analyze hereinafter a common situation, where a branch of the machine requires a single actuator which will be controlled by a single directional valve from a single fixed displacement pump.
From the beginning it is established that delivery rate will be constantly at maximum (rated flow) Qn, and pressure limited by a safety valve to $p_{max.}$
In Figure 1 operation of cylinder C is ensured by starting the pump P and selecting the circuit **1** or **2** by means of hydraulic directional valve D, whose positions are selected according to system requirement by using electromagnets E_1 and E_2.

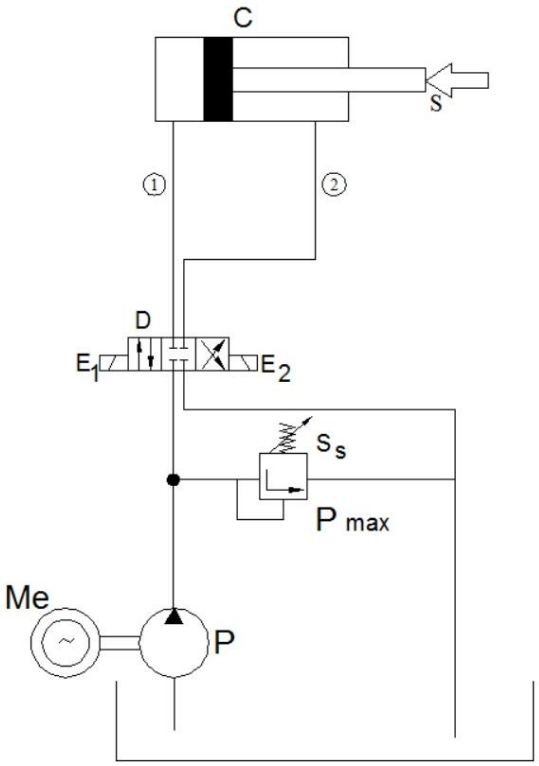

Fig. 1. Hydraulic diagram for driving a single actuator

For this simple configuration there can 4 working versions: a, b, c, d, assessed in the following lines depending on the pressure and flow requirements. For each of the working versions the next notations will be used:
N_u = usable (output) power;
N_e = excess power (power installed but unused);
N_p = lost power, converted into heat;
N_i = installed power.
Figure 2 graphically presents those 4 cases of energy (power) consumption.

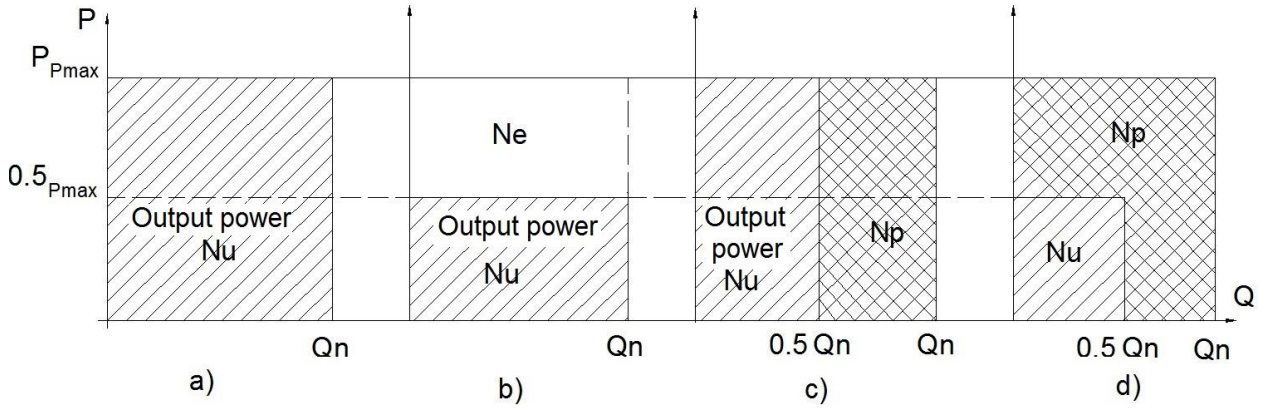

Fig. 2. Power graphs of energy consumption

a) The actuator needs all pump flow $Q_a = Q_n$ to achieve speed V_1.
To overcome load (S_a) pressure in actuator must reach the value $p_a = p_{max}$. In this case:

$$N_{ua} = \frac{p_a \cdot Q_a}{600\ \eta} = \frac{p_{max} \cdot Q_n}{600\ \eta} = N_c \qquad (1)$$

b) The actuator needs all flow $Q_b = Q_n = Q_1$ to achieve speed V_1.
This time load (S_b) is smaller than load S_a.

$S_b = 0.5\ S_a$, hence it results that pressure p_b is: $p_b = 0.5 \quad p_a = 0.5\ p_{max}$

Since all the flow delivered by the pump is used, output power is:

$$N_{ub} = \frac{p_b \cdot Q_b}{600\ \eta} = \frac{0.5\ p_{max} \cdot Q_n}{600\ \eta} = 0.5\ N_c \tag{2}$$

The remaining power (0.5 N_c), although installed, is not used, and therefore $N_{eb} = 0.5\ N_c$, there being no losses and warming.
c) The actuator needs half of the flow $Q_c = 0.5\ Q_n$ to achieve speed V_c, and it must work at pressure value $p_c = p_{max}$ to be able to overcome load S_c.
In this case half of the pump flow will be discharged via general valve of the system, so lost power:

$$N_p = \frac{p_{max} \cdot 0.5\ Q_n}{600\ \eta} = 0.5\ N_C \tag{3}$$

The actuator needs half of the rated flow to achieve speed V_d, and it must work at half of the maximum pressure so that to be able to overcome load (S_d) $p_d = 0.5\ p_{max}$, and $Q_d = 0.5\ Q_n$.

In this case output power $N_{ud} = \frac{p_d \cdot Q_d}{600\ \eta} = \frac{0.5\ p_{max} \cdot 0.5\ Q_n}{600\ \eta} = 0.25\ N_c$ (4)

Mostly of energy is turned into heat.
$N_{pd} = 0.75\ N_c$

3. Power use in a hydraulic system with 2 actuators and 2 active phases

A hydraulic system which is common in industrial practice has the diagram showed in Figure 3. Analysis of energy loss is done for one phase only per each cylinder.

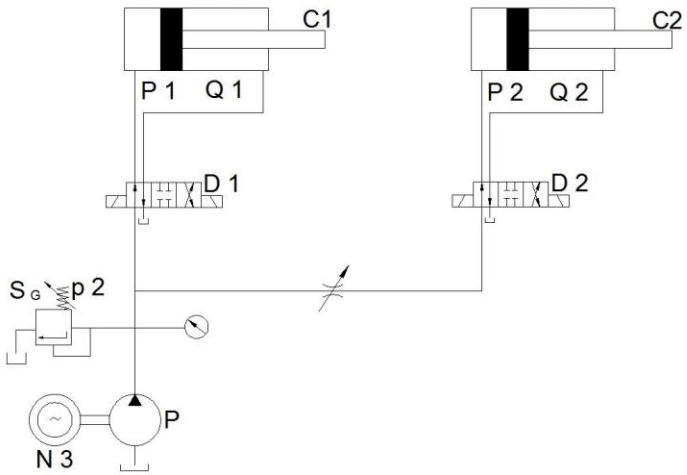

Fig. 3. Hydraulic diagram of a system with 2 actuators

In the first phase, pump flow is conveyed via directional valve D_1 to cylinder C_1 whose rod must overcome load S_1, and as a result pressure p_1 installs in the cylinder.
In the second phase, pump flow is conveyed via directional valve D_2 to cylinder C_2 whose rod must overcome load S_2, and as a result pressure p_2 installs in the cylinder.

Admitting that $p_2 = 3\ p_1$ and $Q_1 = 2\ Q_2$ it is roughly determined that $N_i = N_3 = \frac{p_2 \cdot Q_1}{600\ \eta}$, since the pump flow and valve control are constant, but at their maximum value.

In phase 2 usable power consumption is $N_2 = \frac{p_2 \cdot Q_2}{600\ \eta}$.

As one can see in the graph presented in Figure 4, usable power consumption for the 2 phases is NOT the same, but installed power N_i is the same.

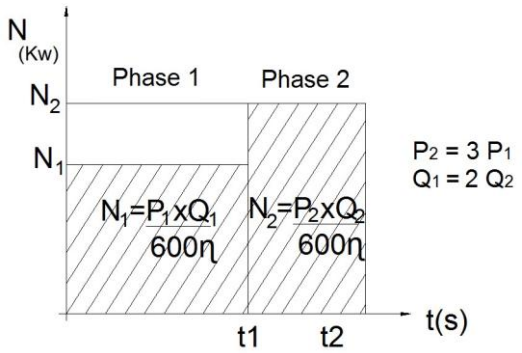

Fig. 4. Graph of usable powers consumption

Returning to the (rough) relationship - η includes all losses and yields –

$$N_2 = \frac{p_2 \cdot Q_1}{600\,\eta} = 2\ \frac{p_2 \cdot Q_2}{600\,\eta} = 2N_2 = 3\ = \frac{1 \cdot Q_1}{600\,\eta} = 3\,N_1, \tag{5}$$

if we relate to consumption utility, as one can also see in Figure 5, we obtain:

$$N_1 = \frac{N_3}{3}; \qquad N_2 = \frac{N_3}{2}; \qquad N_1 = \frac{2}{3}\,N_2 \tag{6}$$

It is very clear that power consumption is not at an optimum level in any of the phases, losses due to heating being extremely high.

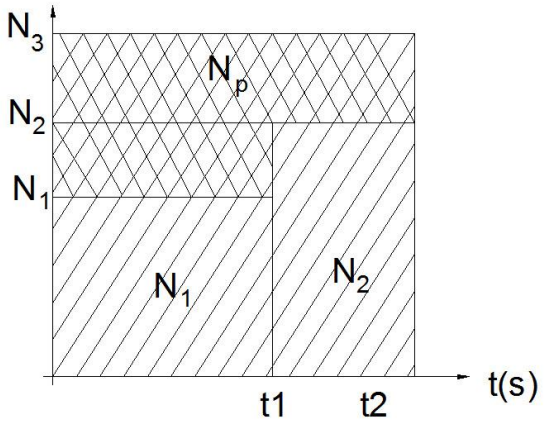

Fig. 5. Total energy consumption

4. Power use in systems in which each circuit has pressure control

To improve power use in circuits with two cylinders (Figure 3) it is possible to use the circuit in Figure 6, in which phases 1 and 2 are selected by directional valves D_1 and D_2 and controlled as to the pressure level by means of relief valves S_1 and S_2.
This simple modification of the diagram indicates lower power loss, even though the installed power is quite high. As one can see in Figure 7, excess power (power installed but unused) N_e increases in size at the expense of lost power N_p.

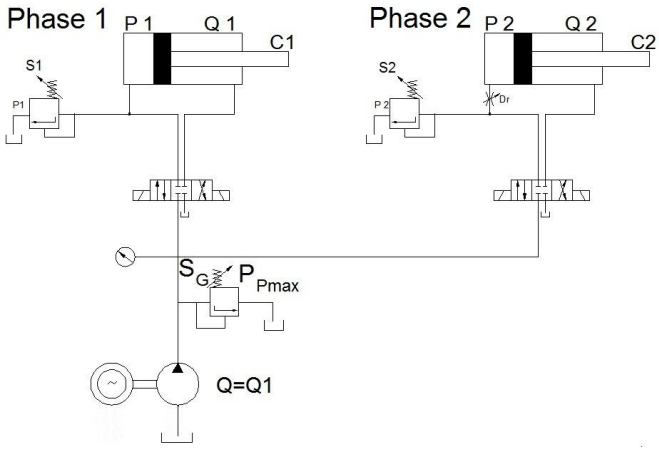

Fig. 6. Driving diagram with safety valves on each circuit

The graph in Figure 7 shows that in first phase in which all the flow $Q_1 = Q_n$ is used, but not at maximum pressure, only at a value $p_1 = \frac{1}{3} p_2$, a large portion of power remains unused (N_{e1}) and only a small portion is lost (N_{p1}).

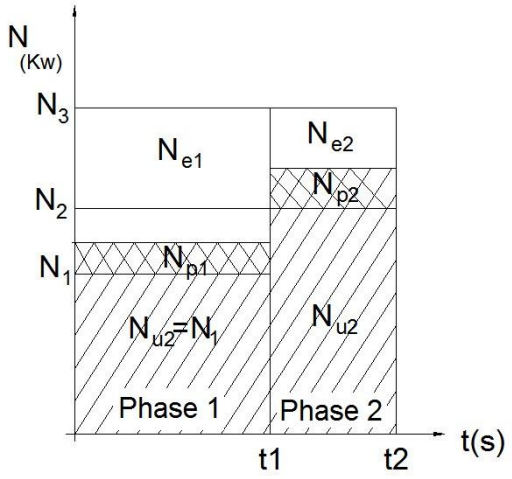

Fig. 7. Graph of level of the losses

In the second phase one can notice that losses are low; in this case as well a small portion of the installed power appears as unused power.
Nevertheless, the graph in Figure 6 shows better energy use compared to that shown in the graph in Figure 5.
Starting from the case in which: $p_2 = 3p_1$; $Q_1 + 2\,Q_2$ and $p_{max} \cong 1.25\, p_2$;

$$p_{max} = 1.25\, p_2 = 1.25 \cdot 3\ \ p_1 = 3.75\, p_1 \tag{7}$$

it results that installed power is:

$$N_i = N_3 = \frac{Q_1 \cdot p_{max}}{600\,\eta} \tag{8}$$

In phase 1

$$N_{u1} = \frac{p_1 \cdot Q_1}{600\,\eta} = \frac{2Q_2 \cdot 1/3p_2}{600\,\eta} = \frac{2}{3}\,\frac{Q_2 \cdot P_2}{600\,\eta} = \frac{2}{3}\,N_{u2} \tag{9}$$

It can be noticed that much of the power is not used

$$N_{e1} = N_3 - N_{u1} - N_{p1,} \tag{10}$$

and if we admit that $N_{p1} = 0$

$$N_{e1} = \frac{Q_1 \cdot p_{max}}{600\,\eta} - \frac{Q_1 \cdot p_1}{600\,\eta} = \frac{Q_1 \cdot 2.75\, p_1}{600\,\eta} = 2.75\, N_{u1} \tag{11}$$

It turns out that there is a poor use of installed power, but at least with reduced energy losses.
In phase 2

$$N_{u2}\,\frac{Q_2 \cdot p_2}{600\,\eta} \tag{12}$$

This time energy loss is:

$$N_{p2} = \frac{(Q_1 - Q_2)p_2}{600\,\eta} = \frac{Q_2 \cdot p_2}{600\,\eta} = N_{u2} \tag{13}$$

and it is quite close to the loss in Figure 3.
By introducing this type of valve the losses in the first phase has been turned into unused energy, so with no consumption and no heating, although this power is installed.
Concluding:

$$N_3 = N_{u1} + N_{p1} + N_{e1} = N_{u2} + N_{p2} + N_{e2}. \tag{14}$$

5. Using multiple pumps

5.1. Improving energy balance when using double pumps

One of the traditional solutions adopted to reduce energy losses in systems in which the phases are difficult to select is that with two coaxial pumps, as in the diagram in Figure 8.

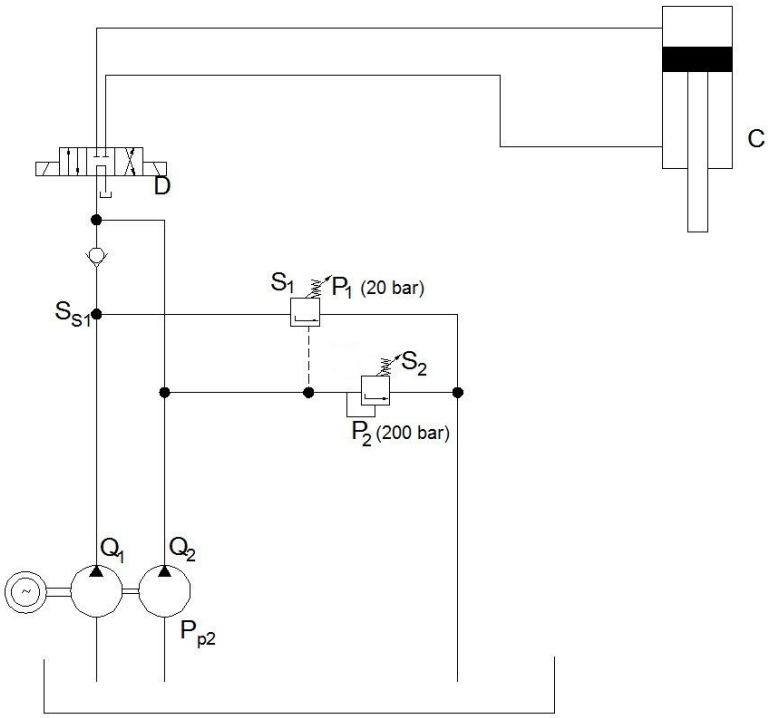

Fig. 8. Double pump hydraulic system

This solution is most often used in hydraulic systems of presses in which necessarily there are at least 3 standard phases.

The standard phases of the press are:

1. Rapid approach phase. Requires maximum flow and low pressure (Q_1; Q_2 and $p_1 \cong 0.1\, p_2$).
2. Full pressure phase. Requires low flow (for low speed) and maximum pressure ($Q_2 \cong 0.1\, Q_n$ and $p_2 = p_{max}$).
3. Rapid retract phase. Requires high flow and low pressure. Load is determined by the weight of the movable element plus friction forces.

Solving the problem with only one pump would lead to the situation in which in the second phase, the pressing phase, power losses would be as in Figure 2, C variant, where the flow lost through the valve would be approximately 90%.
By using the hydraulic system in Figure 8 with rough guide values set for each phase, energy losses look like in the graphs in Figure 9.

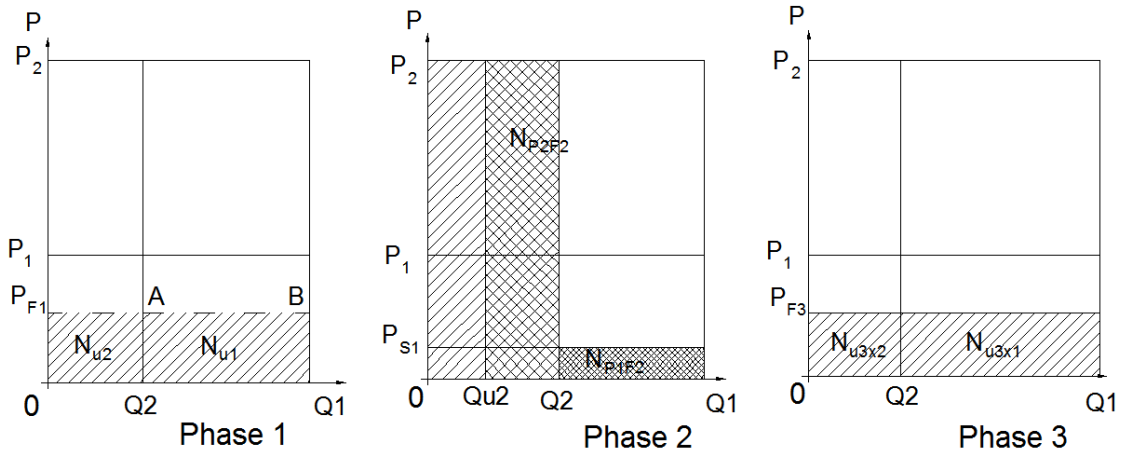

Fig. 9. Energy consumption at double pump systems

● **In phase 1** – Output power – $N_{uF1} = N_{u1} + N_{u2} = \frac{P_{F1} \cdot Q_{F1}}{600\,\eta}$ (15)

$Q_{F1} = Q_1 + Q_2$, and the pressure is established by the load and it s $p_{F1} < p_1 < p_2$

Power consumption $N_{cF1} \cong N_{uF1}$

N_{u1} – it is represented by the rectangle O – p_{F1} – B – Q_1, and

N_{u2} – it is represented by the rectangle O – p_{F1} – A – Q_2

● **In phase 2** – as a result of pressure increase in the system above p_1, valve S_1 opens and check valve S_{S1} is locked; thus, the whole flow Q_1 goes to the tank at minimum pressure set by valve S_1 (p_{S1}). This lost power has the value $N_{p1F2} = \frac{Q_1 \cdot p_{S1}}{600\,\eta}$, (16)

where p_{S1} is about 3 ÷ 6 bar, hence $p_{S1} < p_1$.
In this phase it is possible that part of the flow Q_2 is also discharged through pressure valve S_2 at pressure p_2, and only Q_{u2} is used.

$$N_{p2F2} = \frac{KQ_2 \cdot p_2}{600\,\eta}, \quad (17)$$

where K < 1 depending on the working speed in phase 2.

$$N_{pF2} = N_{p1F2} + N_{p2F2} \cong N_{p2F2} \quad (18)$$

$$N_{u2} = \frac{p_2 \cdot Q_{u2}}{600\,\eta} \quad (19)$$

● **In phase 3** –rapid retract phase- the whole pump flow p_{p1} is used at pressure resulting from weight and friction. Pressure is established on the circuits of both pumps.

5.2. Improving energy balance when using triple pumps or 3 coaxial pumps

Hydraulic systems which used pumping units with 3 coaxial pumps (Figure 10) or 3 pumps driven by independent electric (or heat) motor were actually the first steps towards digital hydraulics. Each pump has its own flow (Q_1, Q_2, Q_3) of which we can select for the system one, two or even all three, getting the flow rates Q_1; Q_2; Q_3; $Q_1 + Q_2$; $Q_1 + Q_3$; $Q_2 + Q_3$ or $Q_1 + Q_2 + Q_3$.

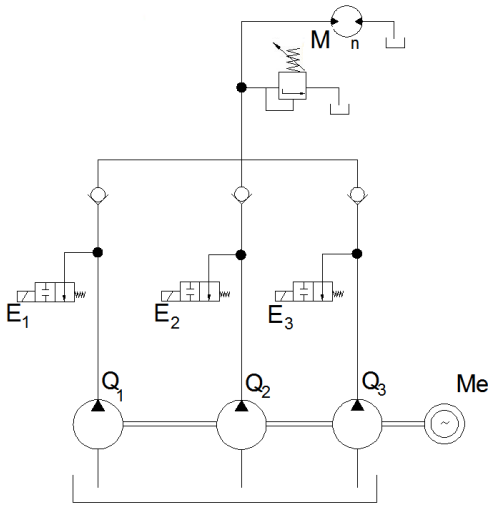

Fig. 10. Hydraulic system with 3 fixed displacement pumps

Using the electric automation system there is selected one of the seven variants of flow, which can provide one of the seven different speeds for the hydraulic motor M.

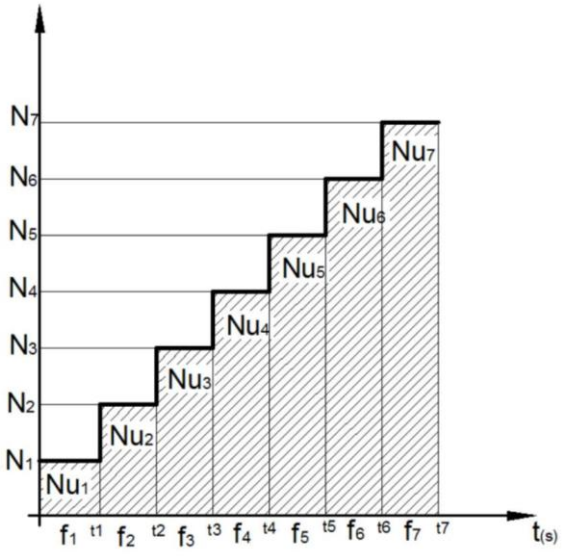

Fig. 11. Graph of installed power use

Output power is:

$$N_i \cong \frac{P_S \cdot (Q_1 + Q_2 + Q_3)}{600\,\eta}, \qquad (20)$$

where $Q_2 = 2Q_1$; $Q_3 = 4Q_1$

Depending on flow requirements, one or more pumps will be selected.

$$N_{u1} = \frac{P_S \cdot Q_1}{600\eta} \quad (21)$$

$$N_{u2} = \frac{P_S \cdot Q_2}{600\eta} = 2 = \frac{P_S \cdot Q_1}{600\eta} = 2\,N_{u1} \quad (22)$$

$$N_{u3} = \frac{P_S\,(Q_1+Q_2)}{600\eta} = 3\ \frac{P_S \cdot Q_1}{600\eta} = 3\,N_{u1} \quad (22)$$

$$N_{u4} = \frac{P_S \cdot Q_3}{600\eta} = 4 = \frac{P_S \cdot Q_1}{600\eta} = 4\,N_{u1} \quad (23)$$

$$N_{u5} = \frac{P_S\,(Q_1+Q_3)}{600\eta} = 5\ \frac{P_S \cdot Q_1}{600\eta} = 5\,N_{u1} \quad (24)$$

$$N_{u6} = \frac{P_S\,(Q_2+Q_3)}{600\eta} = 6\ \frac{P_S \cdot Q_1}{600\eta} = 6\,N_{u1} \quad (25)$$

$$N_{u6} = \frac{P_S\,(Q_2+Q_3)}{600\eta} = 6\ \frac{P_S \cdot Q_1}{600\eta} = 6\,N_{u1} \quad (26)$$

$$N_{u7} = \frac{P_S\,(Q_1+Q_2+Q_3)}{600\eta} = 7\ \frac{P_S \cdot Q_1}{600\eta} = 7\,N_{u1} \quad (27)$$

For each of the seven phases, besides output power Nu there is also power installed in excess, that will not be consumed; there will be lost only the part of this power which ensures oil recirculation through the pumps that are not actively involved in that particular phase, plus normal losses caused by operation of the pumping system. The amount of power that is lost is small compared to the amount of useful power consumption. The great advantage of this solution is that besides economical use of power the system allows simple automation, flow accuracy up to 12.5% and also functional structure quite simple and inexpensive.

6. Conclusions

This material only refers to fixed displacement pump hydraulic systems, and it highlights certain aspects such as:

- Although fixed displacement pump hydraulic systems have wasteful behaviour in terms of energy, there are a lot of cases in which they can be kept within reasonable limits;
- Complex high power systems lead to extremely significant energy losses, and therefore hydraulics technology has made considerable progress by using adjustable pumps and, more recently, by using Load Sensing and digital hydraulics.

Acknowledgment

This paper has been developed in INOE 2000-IHP, with financial support of ANCSI, under the Research Programme *–NUCLEU 2016,* project title: *Physics of processes for reducing energy losses and developing renewable energy resources by use of high-performance equipment,* project no. PN 16.40.03.01, financial agreement no. 5N/2016.

References

[1] G. Matache, St. Alexandrescu, A. G. Pantiru, Gh. Sovaiala, M. Petrache, "The analysis of flow losses through dynamic seals of hydraulic cylinders", HIDRAULICA no. 1, pp. 52-60, ISSN 1453 – 7303, 2013;
[2] C. Cristescu, L. M. Micu, I. C. Dumitrescu, P. Krevey, "Using Load Sensing control systems to increase energy efficiency of hydrostatic transmissions", HIDRAULICA no. 4, pp. 71-77, ISSN 1453 – 7303, 2015;
[3] C**.** Cristescu**,** P. Drumea, D. Ion Guta, C. Dumitrescu, "Theoretical research and laboratory experimental tests regarding the dynamic behavior of hydraulic system for energy recovery at the braking of motor vehicle", in: Proc. of *The 8-th International Fluid Power Conference-IFK 2012 "Fluid Power Drives!"*, March 26-28, 2012, Dresden, Germany, pp. 435 - 446, (www.ifk2012.com);

[4] I. Nita, C. Cristescu, Al. L. Visan, Al. Marinescu, "Increasing the energetic efficiency of pet bundling press using hidrostatic energy recovering systems**"**, in Proc. of HERVEX 2012, pp. 235 - 241, ISSN 1454 – 8003;
[5] M. Petrache, S. Anghel, A. I. Popescu, **"**Hydraulics for mobile vehicles. New drive schemes", in Proc. of HERVEX 2012, pp. 185 - 190, ISSN 1454 – 8003;
[6] P. Drumea, C. Cristescu, O. Heipl, *"*Experimental researches for determining the friction forces in the piston seals of the hydraulic cylinders / Experimentelle untersuchungen zur bestimmung der reibkräfte in kolbendichtungen von hydraulikzylindern*"*, in: Proc. of the 17-th International Sealing Conference ISC-2012, pp. 473-48, Sept. 13-14, 2012, Stuttgart, Germany*;*
[7] H. Theissen, "Fluid Power for sustainability", Proc. of International Salon of Hydraulics and Pneumatics HERVEX 2011, November 9-11, Calimanesti-Caciulata, Romania, pp. 137-157, ISSN 1454 – 8003, 2011;
[8] *** "Hydraulics in Industrial and Mobile Applications" *(Assofluid)*, Publishing House: Grafiche Parole Nuove s.r.l., Brugherio (Milano), Italy, September 2007, pp.174-175;
[9] P. Drumea, C. Dumitrescu, Al. Hristea, A. Mirea, "Energy loss reduction in hydraulic systems with fixed pump in agricultural machinery", Proc. of. 5th International Conference on Thermal Equipment, Renewable Energy and Rural Development TE-RE-RD 2016, pp. 249-254;
[10] V. Marin, R. Moscovici, D. Teneslav, "Sisteme hidraulice de acţionare şi reglare automată"/ "Hydraulic automatic drive and control systems", Technical Publishing House, Bucharest, 1981.

Electrical Analogy of Liquid Piston Stirling Engines

Aman GUPTA[1], Sunny NARAYAN[2]

[1] Indus University, bharadwaj1717@gmail.com

[2] Indus University, rarekv@gmail.com

Abstract: *The use of fossils for of heat and power generation is a cause of concern due to emissions which are a great threat to human life. Solar and geothermal energy can be harnessed as renewable sources. According to second law of thermodynamics, theoretically maximum thermal efficiency is of Carnot cycle. However there are other cycles having advantages which includes liquid piston engine. This device is able to convert low-grade heat into hydraulic work. The basic principle of a Fluidyne is similar to a Stirling engine. This work deals with the dynamic modeling of liquid piston engines which is type of Stirling engine. Similarities between this device and an RLC electric circuit were considered. Pressure oscillations in engine were analyzed analogous to charging and discharging of a RLC circuit.*

Keywords*: Engines, Pumps*

1. Introduction

Use of fossil fuels is a concern due to emissions which are a great threat to human life. Solar and geothermal energy can be harnessed as renewable sources [1]. According to second law of thermodynamics, theoretically maximum thermal efficiency is of Carnot cycle [2]. However there are other cycles having advantages which includes liquid piston engine. This device is able to convert low-grade heat into hydraulic work. The basic principle of a Fluidyne is similar to a Stirling engine.
A gas when heated expands and if its expansion is confined, its temperature rises. This can be understood more easily by following operations [3]:

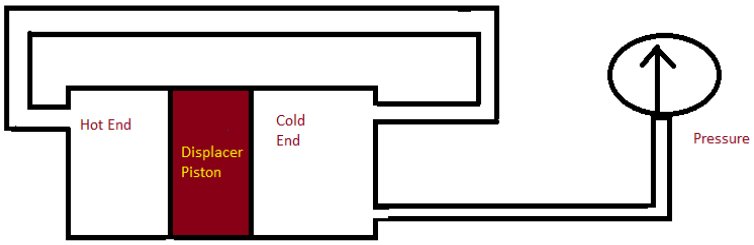

Fig. 1. Motion of a displacer piston in cylinder

A thermal engine is a device which converts heat energy into mechanical energy. The operation of a heat engine can be described by a simple thermodynamic cycle as follows:
Initially the displacer piston is at centre, with half of the gas in hot side and other half of gas in cold side of cylinder. The pressure gauge is neutral.

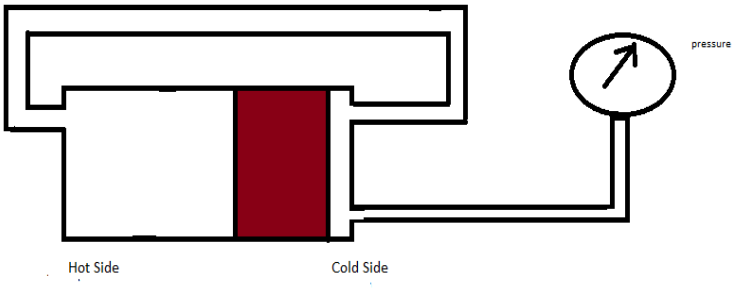

Fig. 2. Motion of displacer piston towards cold side

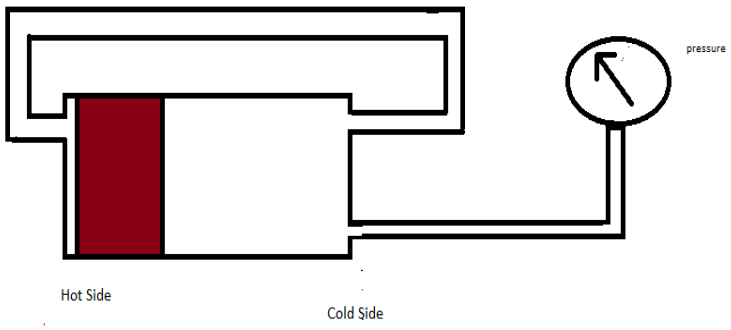

Fig. 3. Motion of displacer piston towards hot side

As the displacer piston moves towards the cold end, the gas is displaced towards the hot end by the connecting tube, its temperature and hence pressure goes up as indicated by the gauge.
As the piston moves towards the hot side, the gas is displaced towards the cold end, its temperature and hence pressure falls. The changes in the displacer pressure can be used to drive another piston known as the power piston. When the gas pressure is high, the power piston moves towards the open end of cylinder, hence doing some work which can be used to pump water or rotate a crankshaft.
Pumps are the most important mechanical devices that play an important role in our daily lives. They have been used in the form of Persian wheels or water wheels since ancient times for irrigation purposes. They cause displacement of the working fluid by adding energy to it.

2. Pumping setups

There are several available setups wherein pressure variations can be used for pumping water. Commonly used pumping configuration involves a T piece at the end of output tube and two non-return valves. On the outward stroke, the fluid is forced through the upper valve whereas during the inward stroke, the fluid is drawn through the lower non return valve. However this setup has some drawbacks.
Above a certain pumping head, the work needed to pump the fluid becomes greater than the volume change in the engine.
Another configuration uses the pressure variations in the working gas. When the pressure of gas is low, the fluid is drawn up from lower valve and as it rises, the fluid is expelled.

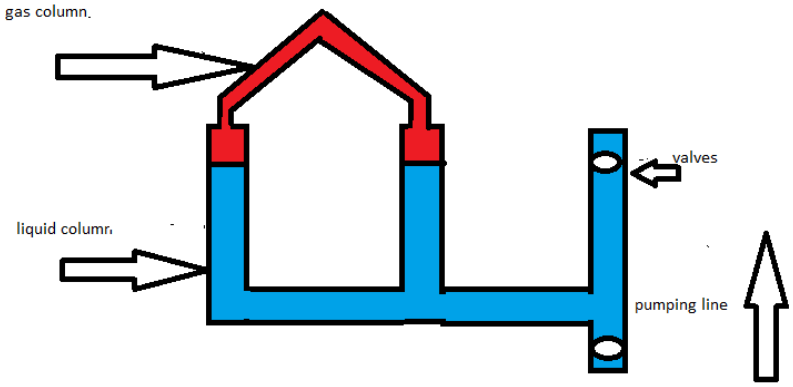

Fig. 4. Pumping configurations (a)

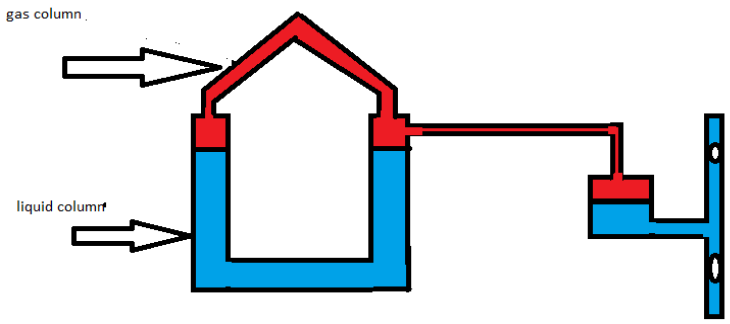

Fig. 5. Pumping configurations (b)

3. Electrical analogy

The modeling methodology of this device is explained in [4– 8]. Each component of Fluidyne is represented by a RLC circuit wherein resistors are attributed to heat transfer and viscous/form drag effects, capacitors denote gravitational/hydrostatic and vapor compressibility effects and inductors describe the effects of inertia.
Pressure (*Pi*) difference across a physical device component in the fluid domain is represented by a voltage (Ei) difference across an equivalent analogous electrical component. Volumetric flow rate V'(t) is represented by the current (I) flowing through the corresponding electrical component. In the thermal analysis a temperature (T) difference across is represented by a voltage (V) drop and the resulting entropy flow rate (S) may be represented by an analogous current (I) flowing through the electrical component.

The operation of Fluidyne engine can be represented in terms of following two operations similar to charging of an electrical circuit:

During the suction phase which is analogous to charging of RLC circuit we have:

$$ZI + \frac{q}{C} = V_{in} \tag{1}$$

Differentiating on both sides we have:

$$ZC\frac{\delta^2 q}{\delta^2 t} + \frac{\delta q}{\delta t} = 0 \tag{2}$$

Electrical analogous equations for this phase may be written as:

$$ZC\frac{\delta^2 V}{\delta^2 t} + \frac{\delta V}{\delta t} = 0 \tag{3}$$

Applying Laplace on both sides we have:

$$ZC(D^2V') + DV' = 0 \tag{4}$$

$$ZC[S^2F(S)] + [SF(S) - V'(0)] = 0 \tag{5}$$

$$F(S) = V'(0)\left[\frac{1}{S} + \frac{1}{S + \frac{1}{ZC}}\right] \tag{6}$$

Taking inverse Laplace we have:

$$V'(t) = V'(0)[1 - e^{\frac{-t}{ZC}}] \tag{7}$$

$$V'(t) = V'(0)[1 - e^{\frac{-t}{\zeta}}] \tag{8}$$

Where ζ=ZC
When t=ζ we have

$$V'(t) = V'(0)[1 - e^{-1}] = 0.63\,V'(0) \tag{9}$$

Hence this phase may be represented graphically as:

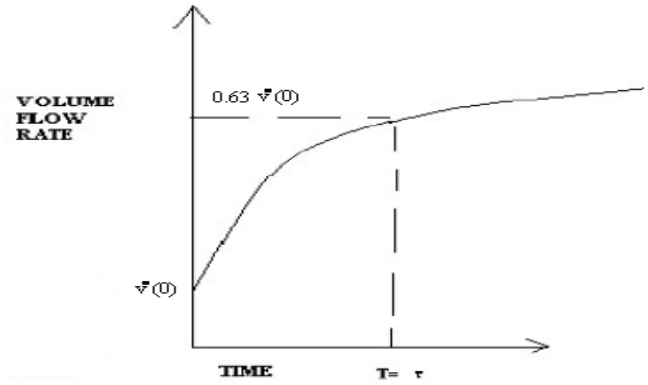

Fig. 6. Suction phase

During the discharge phase which is analogous to charging of RLC circuit we have:

$$ZI+\frac{q}{C}=V_{in} \tag{10}$$

Differentiating on both sides we have:

$$Z\frac{\delta q}{\delta t}+\frac{q}{C}=0 \tag{11}$$

Electrical analogous equations for this phase may be written as:

$$Z\frac{\delta V'}{\delta t}+\frac{V'}{C}=0 \tag{12}$$

Applying Laplace we have:

$$ZC[SF(S)-V'(0)+F(S)]=0 \tag{13}$$

$$F(S)=\frac{V'(0)}{S+\frac{1}{ZC}} \tag{14}$$

$$V'(t)=V'(0)[e^{\frac{-t}{\zeta}}] \tag{15}$$

Where ζ=ZC
When t=ζ we have

$$V'(t)=V'(0)[e^{-1}] = 0.36\,V'(0) \tag{16}$$

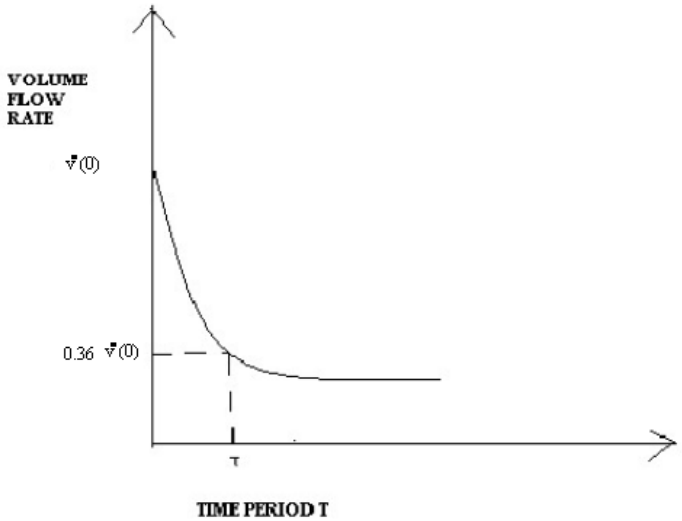

Fig. 7. Discharge phase

When suction volume equals discharge volume we have:

$$V'(t)=V'(0)[1-e^{\frac{-t}{ZC}}]=V'(0)[e^{\frac{-t}{\zeta}}] \quad (17)$$

$$\frac{t}{\zeta}=0.693 \quad (18)$$

Hence t=0.693ζ

$$V'(t)=0.5\,V'(0) \quad (19)$$

This may be represented graphiclaly as:

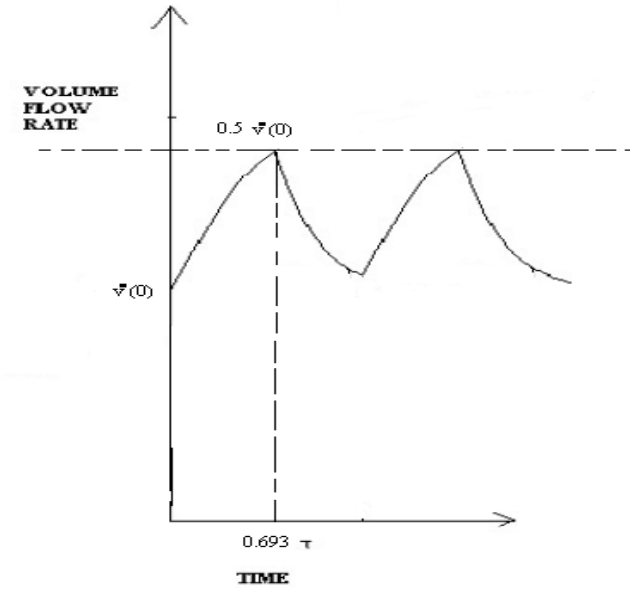

Fig. 8. Neural phase

4. Conclusions

In this work motion of a liquid piston engine has been analyzed. An electrical analogy was designed for the physical device in which both suction and discharge phase were studied similar to a RLC circuit [9-15]. Further improvements in this device may be done by use of regenerator or bigger tubes to improve heat transfer rate.

Nomenclature
V Voltage
t Time
S Stroke length
ρ Fluid density
Q,V' Fluid Flow rate
C Capacitance
Z Impedance
q Charge flow rate
I Current

References

[1] A. W. Crook, "Profiting From Low-Grade Heat: Thermodynamic Cycles for Low-Temperature Heat Sources", Institution of Electrical Engineers, London, UK, 1994;

[2] Y. Dai, J. Wang, and L. Gao, "Parametric Optimization and Comparative Study of Organic Rankine Cycle (ORC) for Low-Grade Heat Recovery", *Energy Conversion and Management*, vol. 50, no. 3, pp. 576–582, 2009;
[3] T. C. B. Smith, "Thermally Driven Oscillations in Dynamic Applications", Ph.D. Thesis, University of Cambridge, Cambridge, UK, 2006;
[4] C.N. Markides, and T. C. B. Smith, "A Dynamic Model for the Efficiency Optimization of an Oscillatory Low Grade Heat Engine", *Energy*, vol. 36, no. 12, pp. 6967–6980, 2011;
[5] R. Solanki, A. Galindo, and C. N. Markides, "Dynamic Modelling of a Two-Phase Thermo fluidic Oscillator for Efficient Low Grade Heat Utilization: Effect of Fluid Inertia", *Applied Energy*, vol. 89, pp. 156–163, 2012;
[6] R. Solanki, A. Galindo, and C. N. Markides, "The Role of Heat Exchange on the Behavior of an Oscillatory Two- Phase Low-Grade Heat Engine", *Applied Thermal Engineering*, vol. 53, pp. 197–209, 2013;
[7] R. Solanki, R. Mathie, A. Galindo, and C. N. Markides, "Modelling of a Two-Phase Thermo fluidic Oscillator for Low-Grade Heat Utilization: Accounting for Irreversible Thermal Losses", *Applied Energy*, vol. 106, pp. 337–354, 2013;
[8] C. N. Markides, A. Osuolale, R. Solanki, and G.-B. V. Stan, "Nonlinear Heat Transfer Processes in a Two- Phase Thermo fluidic Oscillator", *Applied Energy*, vol. 104, pp. 958–977, 2013, page 5 of 6;
[9] S. Narayan, 2015, ''Designing of Liquid Piston Fluidyne Engines'', Hidraulica no 2 2/2015, (ISSN 1453-7303), http://hidraulica.fluidas.ro/2015/nr2/18-26.pdf;
[10] S. Narayan, 2015, ''A Review of Design of Stirling Engines'', Hidraulica no 3/2015, (ISSN 1453-7303), http://hidraulica.fluidas.ro/2015/nr3/18-26.pdf;
[11] V. Gupta, R. Singh, S. Narayan, 2015, **''**Motion analysis of Fluidyne engines'', TEHNIČKI GLASNIK, vol-9, no 3, September, 2015, http://hrcak.srce.hr/index.php?show=clanak&id_clanak_jezik=215219;
[12] A. Gupta, S. Narayan, 2015, "A Review of Design of Stirling Engines'', Hidraulica no 3/2015, (ISSN 1453-7303), http://hidraulica.fluidas.ro/2016/nr1/18-26.pdf;
[13] A. Gupta, R. Singh, S. Narayan, ''Designing, construction and working of novel thermal pumps'', LAP LAMBERT Academic Publishing, ISBN 978-3-659-71500-6;
[14] S. Narayan, 2015, ''Efficiency analysis of liquid piston engine system'', International Conference BULTRIB '15;
[14] S. Narayan, 2015, ''Review of Stirling engine system'', International Conference BULTRIB '15.

CFD Analysis of a Wind Turbine Assembly Model

Teaching assistant **Fănel Dorel ȘCHEAUA**[1]

[1]"Dunărea de Jos" University of Galați, fanel.scheaua@ugal.ro

Abstract: *The need for energy is growing worldwide today and hydrocarbon reserves are limited resources that are exploited at full capacity at this moment. Also noxious products released into the atmosphere due to the burning of hydrocarbons have harmful effects on the environment. Therefore the research activities and development of solutions for obtaining energy from renewable sources are fully supported in most countries with a high level of economic development. Such solutions are including the solar power, wave energy or wind force. Wind force generated by the movement of air masses between areas with pressure differential is an inexhaustible resource that can easily be converted into electricity in an environmentally friendly manner without the need of fuels combustion. To harness the energy produced by the movement of air currents many wind farms were developed, composed of many wind turbines that by rotational movement are generating electricity. Around the world there are areas where wind is acting with a constant velocity in time being considered as ideal locations of installing wind turbines through which wind power is converted into electricity. In this paper is described a wind turbine assembly for which was conducted a three-dimensional model with Solid Edge V20 CAD program. A CFD analysis was carried out for the wind turbine model using ANSYS CFX in order to highlight the working process of the turbine when describing the rotational movement of the propeller within the fluid region represented by air which is describing a translational movement with imposed velocity.*

Keywords*: wind turbine, 3D modelling, computational fluid dynamics (CFD)*

1. Introduction

The increase of energy needs at present is inevitable on the background of continuous growth of the number of inhabitants and their living standards. As alternatives to conventional energy production processes are methods based on capturing solar energy, wind or wave power. All these methods are considered as environmentally friendly processes that have a huge potential for exploitation, which is currently insufficiently exploited.
Among the methods presented the process of obtaining energy using wind power is one with great potential for development worldwide. From the earliest times of antiquity they were used applications that were based on wind power and in the Middle Ages many windmills were built. Nowadays modern wind turbines are built on continental areas with constant strong winds as well as on the sea, near the coast.
The winds, as a result of the dissipation of solar radiation into the atmosphere and the earth rotational motion, are generated due to the movement of atmospheric air masses due to activity of the sun that heats unevenly the ground. Due to this fact air masses are found having different temperatures, which leads to the movements occurrences.
The warm air being lighter and with lower pressure tends towards for ascending movement, while cold air is denser, weighty and having a greater pressure. Such an imbalance is created that generates thermal and baric air movement in areas with higher pressure to lower pressure areas tending towards the achievement of uniformity value of pressure at equilibrium. Thereby the winds arise, that as a result of the earth rotation and the occurrence of inertial forces have trajectories that change in different ways, proportional to the height at which they are located above the ground.
The air movement at high velocity and approximately constant over time is capable of forming significant pressure forces on propeller blades surface of a wind turbine which determine its rotational movement.

Calculations were carried out whose result shows that about 25% of solar energy that reaches the earth's atmosphere is converted into wind energy which is a huge source of energy for mankind. The total wind energy that is available and can be taken at this time exceeds more than 4 times the energy needs of humanity.
The share of energy production based on wind force has increased by approximately five times between 1999 and 2006 reaching, in some countries, the share of wind energy in total energy consumption to be quite important. For example for European countries bordering the sea or ocean the wind energy share of total energy production is approximately 23% in Denmark, 8% in Spain and 6% in Germany.

2. Wind turbine assembly model

The wind energy can be captured using special construction plants, equipped with turbine, capable to take over wind force and convert it into mechanical energy (direct mechanical work) or electricity through a generator.
A three-dimensional model for a wind turbine assembly was made using Solid Edge software in a simplified manner which is presented in 0.

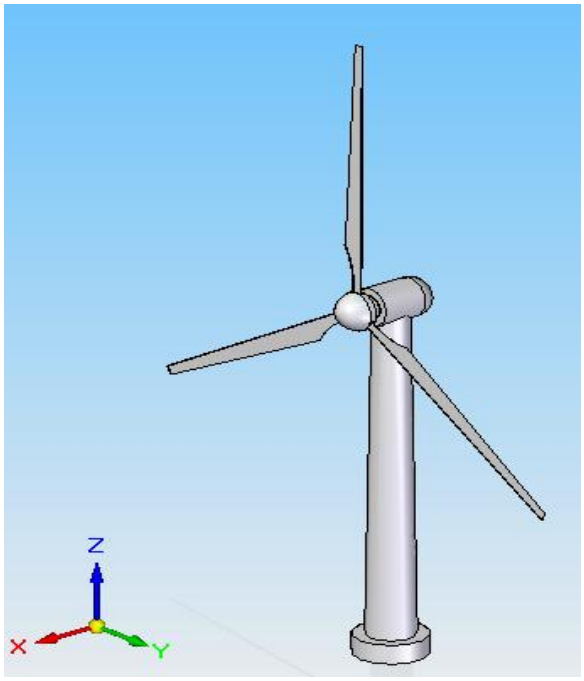

Fig. 1. Wind turbine three-dimensional model assembly

The turbine assembly performs the process of converting wind energy into mechanical energy through the interaction forces between the airflow and blade surface. The blades are constructed with an aerodynamic profile and are usually made of fibreglass or polymeric material. In order to achieve an efficient capture process the turbine has to be oriented so that the plane of blades rotation to be oriented perpendicular to the wind direction. The heights of a wind tower have different values (60 to 130 m) and the total height at which wind turbines have been constructed was up to 200 m. [7]
The wind brings the amount of kinetic energy which is converted into mechanical energy through the turbine. Wind energy is considered as transiting air energy through an area at a given moment of time. The wind power can be evaluated by the relationship: [6]

$$P_w = \frac{1}{2}\rho_a A_p v_w^3 \quad (1)$$

Where:

- P_w - wind power;
- ρ_a - air density;
- A_p - propeller covered surface;
- v_w - air velocity.

Under normal conditions of pressure and temperature can not be captured the total power amount due to the friction forces that prevent the air exhaust that already performed the mechanical work on the turbine blades. It is necessary to introduce an adjustment coefficient value to be used in the power calculation relationship that describes the turbine total power efficiency. Thus the equation that describes the wind turbine real power amount can be evaluated as: [6]

$$P_{wt} = \frac{1}{2}c_p \rho_a A_p v_w^3 \quad (2)$$

The adjustment coefficient of power provided by the wind turbine, *(c_p)*, is expressed as the ratio between the turbine mechanical power of and the total power that can be captured. Based on the analysis of the power factor it was determined that a wind turbine is more energy efficient as the number of blades is lower. A turbine with a smaller number of blades develops a lower resistant moment and finally will have a higher rotational speed. The highest value of efficiency factor is recorded at three-bladed wind turbines.

It was established the theoretical value for the wind turbines power coefficient at approximate value of 55% from total wind energy. In reality the power coefficient of wind turbine models currently used is 30 - 40% of wind energy. [6]

Currently, there are several types of wind turbines made with different models and values for the propeller blades, coverage area and tower heights. In Table 1 are presented some calculation values for the turbine diameter, area covered and mechanical power at the turbine shaft depending on the wind velocity.

TABLE 1: Calculation specific parameter values for wind turbine

Wind velocity (m/s)	Turbine diameter (m)	Turbine area (m^2)	Turbine power (kW)
12	5	19.63	6.85
13	15	176.70	78.47
14	25	490.85	272.24
15	35	962.08	656.30
16	45	1590.38	1316.68
17	55	2375.75	2359.22
18	65	3318.20	3911.48
19	75	4417.73	6124.63
20	85	5674.33	9175.39
21	95	7088.00	13267.90
22	105	8658.75	18635.62
23	115	10386.58	25543.26
24	125	12271.48	34288.69
25	135	14313.45	45204.81

They were calculated the appropriate amount values for the mechanical power obtained at the turbine shaft by using the turbine covered area, wind velocity, air density and the adjustment coefficient of 33%.
A diagram is shown in Figure 2 in order to emphasize the numerical results for the total power at the turbine shaft function of the turbine blades covered area during the rotation movement.
In the calculation the wind velocity was considered within the range of *12-25 m/s* and the air density of $1.225\,kg/m^3$ at temperature of $15^{\circ}C$.

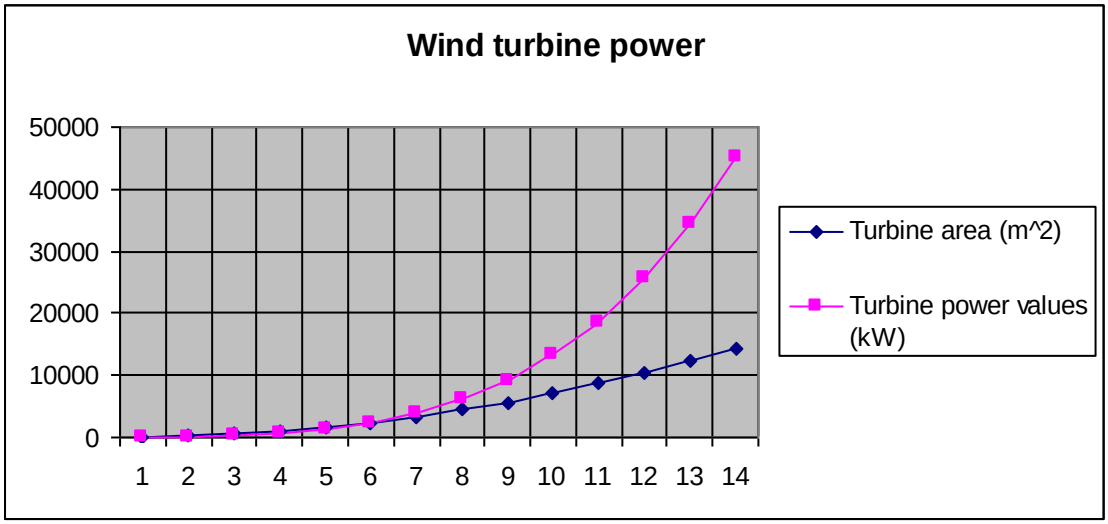

Fig. 2. Wind turbine power for different covered area values

The calculated values for the mechanical power at the turbine shaft depending on wind velocity values acting on the turbine propeller blades are shown in Figure 3. The wind speed is the key parameter in the operation of wind turbines but the optimum operation relies on wind constant action over time. At very high wind velocities can be compromised the integrity of the turbine and in this situation by using special braking devices the turbine can be slow down ensuring in this way a safe operation during strong wind conditions.

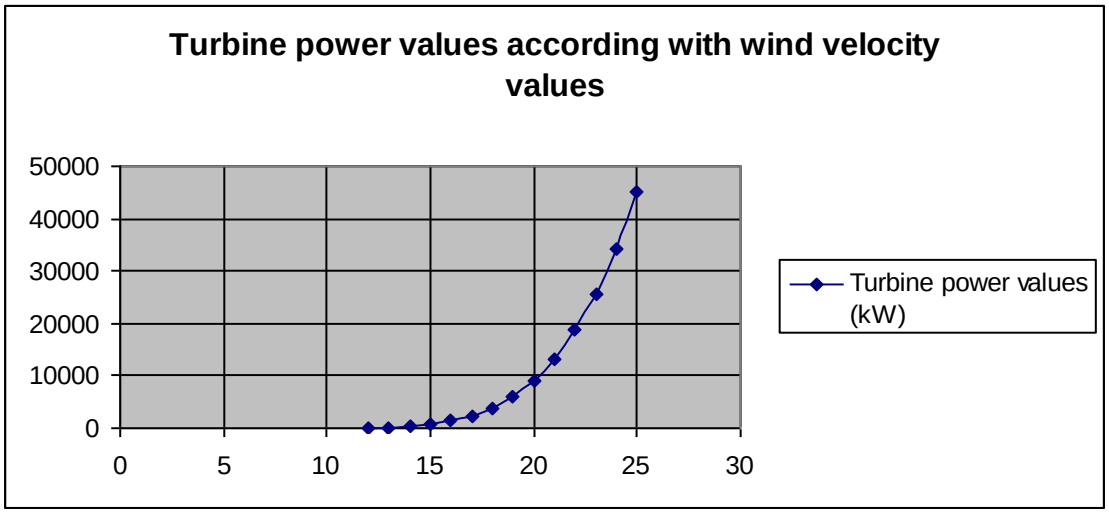

Fig. 3. Wind turbine power for different wind velocity values

3. Computation fluid dynamics analysis for the wind turbine assembly model

In order to achieve a numerical analysis using ANSYS CFX software the three-dimensional model of the wind turbine has been imported into Design Modeler where it was declared the fluid region as a turbine enclosure, as shown in Fig. 4.

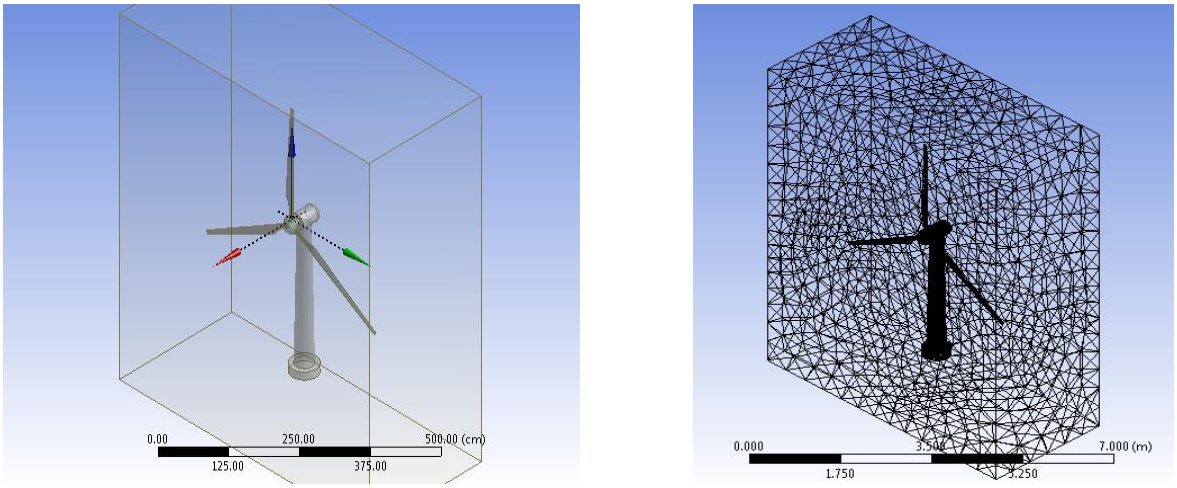

Fig. 4. The wind turbine assembly model imported in ANSYS Design Modeler and Mesh

It was then performed finite element mesh network of triangular shape with a number of 55453 nodes and 301293 elements using CFX Mesh. Defining the proper analysis was performed with CFX Setup, where they were declared initial data necessary for starting the calculation process. After the calculation they were achieved results regarding the working fluid flow (air) inside the analyzed fluid region and how the turbine rotational movement occurs within the fluid region creating specific turbulences. The results are presented in terms of air velocity and pressure in the turbine propeller blades plane.
The values obtained for the fluid velocity and total pressure for the analyzed case are presented in 0.

TABLE 2: Result values obtained for total pressure and fluid velocity

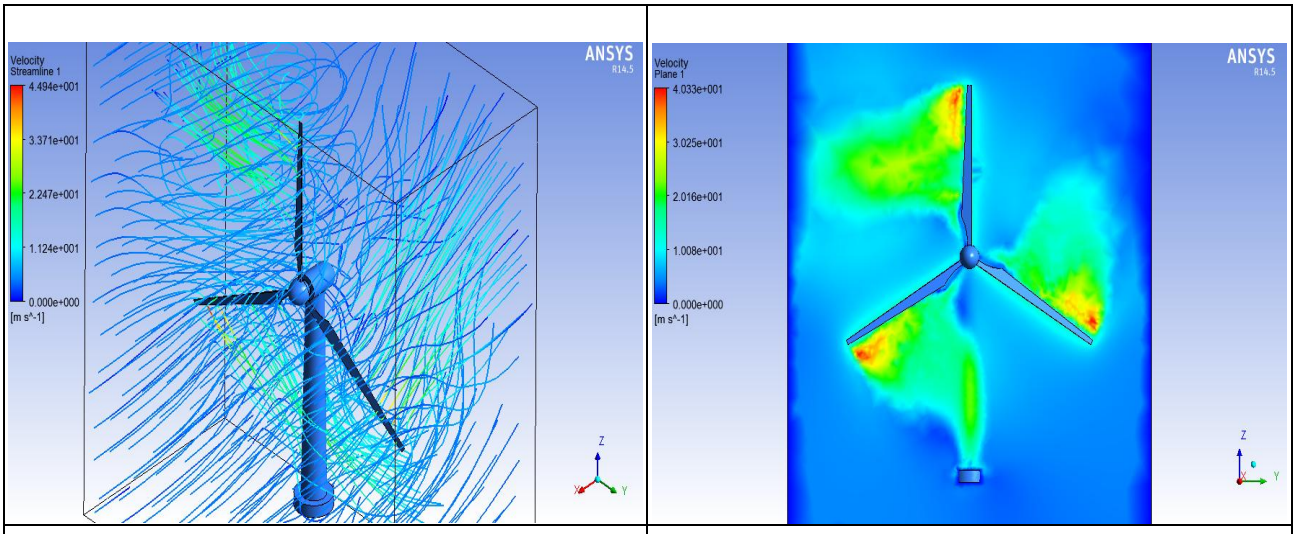

a) Velocity streamlines | b) Velocity values in YZ plane

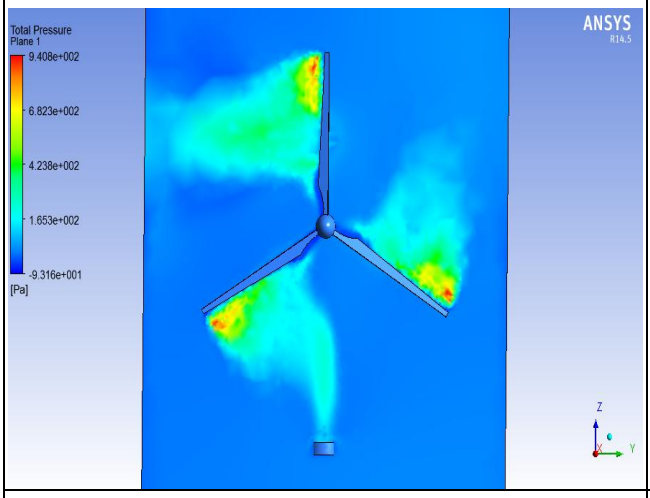

c) Pressure values on YZ plane

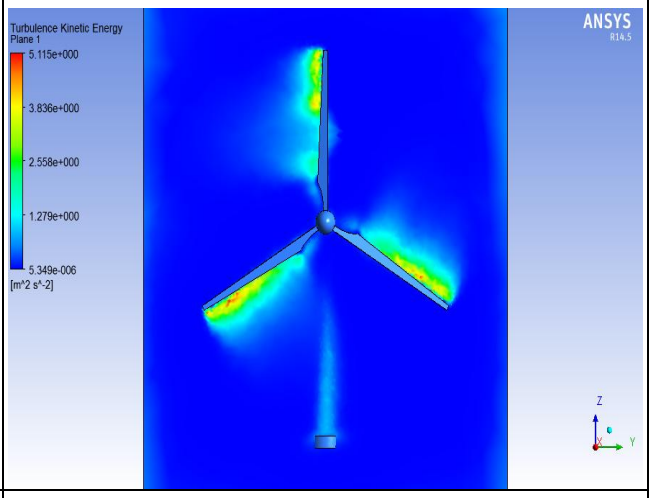

d) Turbulence kinetic energy values on YZ plane

4. Conclusions

A wind turbine model was built and analyzed in terms of the operating principle in this paper. The computational fluid dynamics (CFD) analysis was performed using ANSYS CFX and the results are presented in terms of velocity and pressure of the working fluid represented by air. It was calculated the mechanical power at the turbine shaft depending on the area covered by the propeller blades taking into consideration the wind velocity values acting directly on the turbine.
The wind power is an inexhaustible resource of energy that can be captured easily using wind turbines. It is a viable alternative to burning fossil fuels for electricity and is getting used increasingly more in favorable areas where the winds act with a constant force in time.
Currently, there are regions with entire parks of installed wind turbines generating electricity in an environmentally friendly manner and energy production per turbine is around of 1.5 - 7.5 MW. These wind plants have considerable dimensions with overall height range of 100 to 200 m, with a rotational velocity ranging between 10 to 20 rev / min and working safely at wind speeds between 12 and 15 m / s. [7]

References

[1] G. Axinti, A. S. Axinti, "Acționări hidraulice și pneumatice", Vol III, Publishing House: Tehnica-Info, Chișinău, 2009;
[2] F. D. Scheaua, "Seismic protection of structures using hydraulic damper devices", Annals of the University Dunarea de Jos of Galati, Fascicle XIV, Mechanical Engineering, 14, 2010;
[3] F. D. Scheaua, A. S. Axinti, G. Axinti, "Mathematical model analysis on hydraulic energy dissipation devices", Hidraulica Magazine, 2012;
[4] http://dta.eu/hydraulics/hydraulic-valves/, accessed at 2016-06-01
[5] https://www.google.ro/energie eoliana, accessed at 2016-06-01
[6] https://www.Curs energie eoliana, accessed at 2016-06-01
[7] http://www.aweo.org/windmodels.html , accessed at 2016-06-01
[8] http://www.alternative-energy-news.info/technology/wind-power/wind-turbines/, accessed at 2016-06-01

Increasing the Efficiency of Wood Biomass Gasification Boilers

PhD.eng. **Gabriela MATACHE**[1], Tech. **Ioan PAVEL**[1],
Dipl.eng. **Adrian PANTIRU**[2], Dipl.eng. **Marius CICIU**[2]

[1] Hydraulics and Pneumatics Research Institute INOE 2000-IHP, Bucharest, fluidas@fluidas.ro

[2] S.C. Ferroli Romania S.R.L., Bucharest

Abstract: *Increasing efficiency in combustion processes is set as a goal in all the research and innovation, energy and environment strategies. Gasification boilers work under nominal conditions while maintaining a temperature of about 200 °C along the smoke flue in order to avoid the deposition of coal tar.*
This paper presents some solutions to increase efficiency of wood gasification boilers by recovering heat from the gas exhausted at the smoke flue (which otherwise would be lost to the atmosphere) and re-introducing it in the gasification or combustion air circuit. The energy thus re-introduced into the combustion process can increase efficiency of gasification boilers by a few percentage points, which means that significant amounts of biomass are saved and the process of global warming slows down.

Keywords: *Gasification, combustion, boiler, wood biomass, pyrolysis, efficiency.*

1. Introduction

(One of the most important sources of fuel for humankind was represented by wood. Essential for using this type of fuel is that energy can be recovered in a sustainable manner (being renewable). Worldwide there is a potential big enough for the use of wood for energy purposes. Many of Europe's forests can be used for energy purposes without compromising existing natural ecosystems. Harvesting and processing wood for energy purposes other than those involving large quantities of waste, often remain untapped. Thus, wood chips or sawdust, which can produce the so-called pellets or briquettes are a valuable fuel. A big advantage of wood is that it retains the energy content in time, even in the first two to three years there is a relative increase, which is the period when drying occurs. This feature is important because if you do not have a properly degree of drying all wood humidity will be eliminated in the boilers causing a drop of the caloric power. Another disadvantage is that the burning time of the wet wood decreases the combustion temperature, which leads to imperfect oxidation of all the combustible ingredients, appearance of smoke, clogging of the flue gases ducts and reducing the boiler lifetime.
Gasification is the conversion of solid fuels into gaseous fuels, produced by partial oxidation using oxygen, air, water vapor or mixtures thereof in special equipment (gas-generators). The entire process takes place by partial combustion and heating of biomass with heat generated during combustion. The mixture of emerging gases has a high energy value which can be used, like other gaseous fuels, to produce heat or electricity.

2. Methodology

Wood boilers with gasification run on the process of wood distillation by pyrolysis. When the air is limited, the wood turns into charcoal as it burns. At the same time there appears the "wood gas", which is directed into the burner nozzle to be burned at the bottom of the boiler. This method of wood burning allows the effective use of wood as fuel.
Combustion is a three-step process in every region of the boiler:

- Region 1 – wood drying and gasification,
- Region 2 - wood gas burning when the secondary air enters the preheating nozzle,
- Region 3 - lower combustion in un-cooled combustion chamber.

Thus, the controlled combustion system ensures high efficiency - often up to 90%. Taking this into account, the boiler performance is continuously variable from 40% to 100%. Burning space typically includes the nozzles made of special refractory materials. The control of boiler operation is made by use of an electronic controller, depending on the working temperature.

In the gasification process the inputs are the biomass and the air, and the outputs - fuel gas and ash with a neutral CO_2 balance.
The fuel gas containing CO, H_2, CO_2, N_2 and tar can be used as follows:

- for burning in a specialized burner, from which there result flue gases with high enthalpy containing, in very low concentrations, PM and CO, hot gas that is used to:
  - processes of heating water, steam or air,
  - in internal combustion engines to produce electrical energy.
- the content of tar and PM is filtered and then it is used in internal combustion engines to produce electrical energy.

Figure 1 presents a block diagram of the procedure of biomass energy recovery by thermochemical gasification.

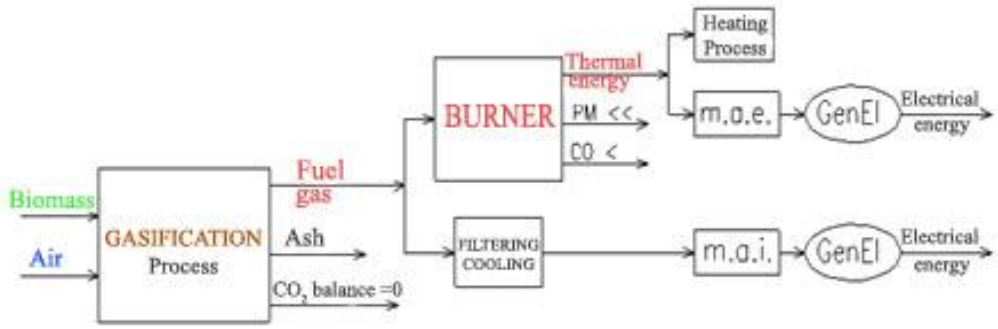

Fig. 1. Block diagram of the biomass energy recovery by gasification

Given the high degree of automation of the gasification boilers, operation of such devices poses only minimum requirements. The content of the fuel compartment is sufficient for at least 4-10 hours of operation on medium power. The boilers are designed for installation in systems with forced or gravitational circulation.
Gasification boilers can burn dry wood mass, natural wood waste in a variety of forms, from chips to logs with lengths up to 80 cm and a diameter up to 30 cm, briquettes or pellets.

3. Energy module with TLUD micro-gasification process

Functional diagram of a TLUD generator with coupled burner is shown in Figure 2. The micro gasification process is supplied with air from a variable speed fan. Figure 3 presents a functional diagram of a TLUD generator at which the gasgen burner is separated from the gas generator. "Gasgen" (gas generator product) is a combustible gas with low calorific power and for efficient combustion there are used specialized burners, FLOX type [1, 5, 9, 10].
Biomass is introduced into the reactor and rests on a grate through which the gasification air passes bottom-up. Process initialization is made from the free top of biomass layer.
The heat energy is obtained by burning the hot gasgen resulted in pyrolysis phase; this is mixed with the preheated combustion air introduced into the combustion zone through ports arranged at the top of the reactor. The mixture with high turbulence burns with flame at the upper orifice of the generator with temperatures of 900-1000 ºC. To adjust the thermal capacity required the air flow rate for gasification D_{ag} and the one for combustion D_{ard} are varied with two flaps, coupled mechanically or by varying the fan speed. The TLUD process is with a fixed bed of biomass, and therefore the generator operates under rechargeable batch.
The gasification process is done with a light intensity with specific consumption per hour of 80 – 150 $kg._{bm}/m^2h$ which leads to reduced specific power for the reactor: 250 – 350 kW/m^2. The slow process maintains a superficial velocity of the gasgen produced at very low values $v_{sup} \leq 0.06$ m/s, resulting in reduced entrainment of free ash and concentration of $PM_{2.5}$ at the burner output of maximum 5 mg/MJ_{bm}, value of at least five times smaller than current standards imposed for thermal generators with solid fuel. [3, 5, 7,9, 10]

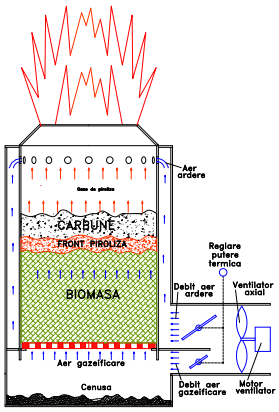

Fig. 2. Functional diagram of the TLUD generator with coupled burner

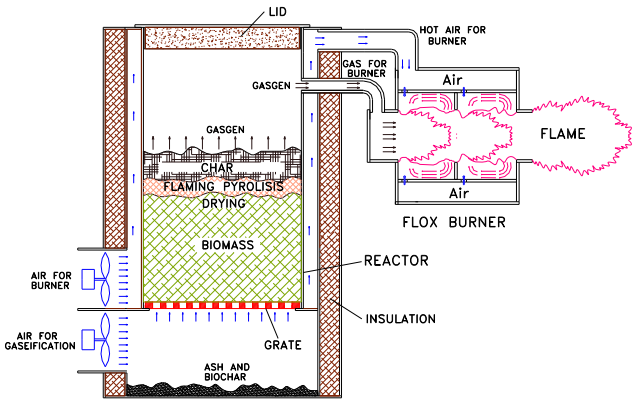

Fig. 3. Functional diagram of the TLUD generator with FLOX burner

Because it provides a very good mixing of gasgen with burning air at an optimum excess of 1.4 - 1.5, in the flue gases the CO concentration is less than 2%, or 0.8 g/MJ$_{bm}$, value below the currently required standards. These aspects make the TLUD heat generator the less polluting compared to other systems of the heat generation from solid fuel.

This type of heat generator has been developed and used in stoves for preparing food in remote areas, operating very well with a wide variety of local biomass. An outstanding example in terms of environmental and energy performance is the portable stove produced by PHILIPS, in which the fan is powered by electricity produced by a heat-generating with semiconductors, mounted under the grate, being a typical thermal generator with energy independence.

Figure 4 presents a block diagram of a TLUD energy module. The inputs of this energy module are:

- biomass consumption C_{bm};
- air needed for gasification D_{ag} and for combustion D_{ard};
- thermal load control parameter u_{Pt}.

The outputs of the energy module are:

- biochar D_{ch} produced by pyrolysis and partly reduced;
- thermal power P_{th} of the flue gas at the burner output;
- concentration of C_{CO} in the combustion gases;
- concentration of solid particles PM in the combustion gases.

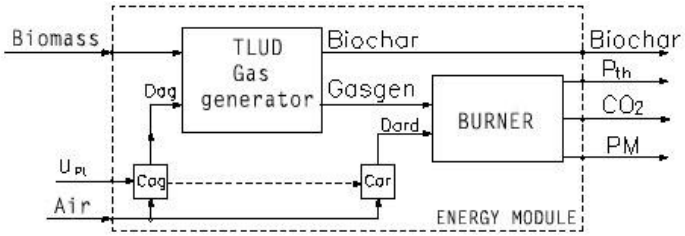

Fig. 4. Block diagram of the TLUD energy module

The inputs of the TLUD generator are biomass, gasification and combustion air and electricity. The electric energy consumption is no more than 0.3% of the thermal energy produced, which recommends the use of TLUD thermal generators in heating systems in remote areas.

From the experiments carried out with TLUD modules it has been found that the conversion efficiency of the biomass entirely gasified into gasgen is in the range 92-95%. [1, 2, 4, 6, 8].

To achieve thermal and functional performance currently required by industrial consumers of thermal energy, an automatic control device type PLC can be attached to the TLUD heat generator.

Energy recovery is a topic addressed by most of the local, national and global development strategies, and this is the basis of sustainable development.

The effects of energy recovery consist in:
- lower wood consumption for heating premises, so lower maintenance costs,
- resource preservation,
- the natural environment is more stable,
- saved trees bring satisfaction, wellness and relaxation to people.

In a research project supported by the Financial Agreement no. 67/2014 there have been developed versions of TLUD gasifiers that aim to recover energy in the chimney (150- 200º C), thus preventing condensation and tar deposition. So the proposed solutions focus on keeping constant the temperature imposed at the chimney and recovery of the heat energy in this area, which can be partly reintroduced in the combustion process or can be converted into electrical energy (e.g. for charging a battery by means of Peltier modules).

A first version is shown in Figure 5, where the energy recovery system is done using Peltier modules. This turns the heat lost at the chimney into electricity. By using this solution one can charge a battery that can provide energy independence of a hot air generator and this one can be used in locations with no other sources of energy.

Peltier modules convert the temperature difference of the outside surfaces of the module into electricity. They are mounted in the energy recovery chamber with "the warm" face towards the chimney (which has 150-200º C) at a distance of about 100 mm, and "the cold" face towards outside (to ambient temperature). From this mounting we aim to achieve a difference in temperature of the Peltier module faces of max. 68ºC, at a working temperature of max. 138ºC. From the proposed mounting according to the technical sheet there results working voltage of max. 16.2V and working current of max. 30.7A.

Power consumption of hot air generator (240W; 20A) is provided by a 12V battery which is charged by 4-6 Peltier modules which operate at nominal capacity in the described terms of installation.

Another version proposed in the project is shown in Figure 6. Recovery of energy from the exhaust gases from the chimney is based on preheating the gasification and combustion air, maintaining constant temperature of the flue gases outlet. Temperature of gases exhausted through the chimney is maintained in the range 150-200ºC to prevent condensation and deposition of tar, by use of an air flap driven by the control module. The recovery system analyzed is designed to take the heat around the chimney (that would have been lost) and introduce it in the combustion and gasification air supply circuit.

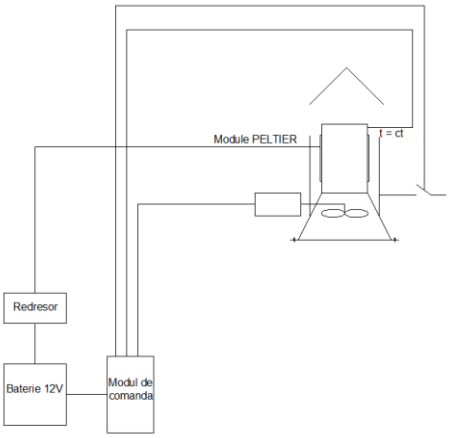

Fig. 5. Diagram of a TLUD gasifier -1st version (with Peltier module)

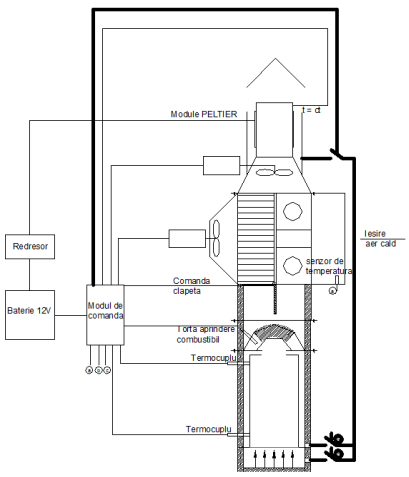

Fig. 6. Diagram of a TLUD gasifier -2nd version

Figure 7 shows a version of a system which recovers energy from the exhaust gases from the chimney by preheating the gasification and combustion air, maintaining a constant temperature at the flue gas outlet by adjusting the rotational speed of the forced draft fan.

Maintaining constant the temperature of the exhaust gases (to prevent energy losses) can be done by adjusting the forced draft fan speed, having a negative effect in reducing the power of the hot air generator.

One last version, Figure 8, shows a system for recovering energy from the exhaust gases from the chimney with a preheating of the gasification and combustion air and maintaining a constant temperature on the exhaust system by adjusting rotational speed of the warm air fan.

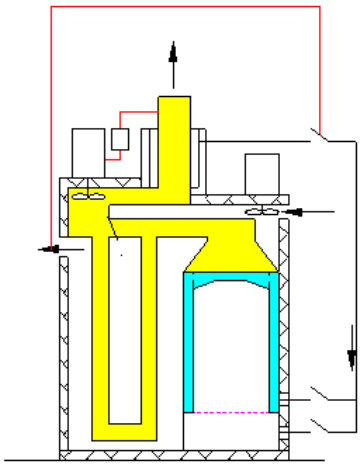

Fig. 7. Diagram of a TLUD gasifier -3rd version

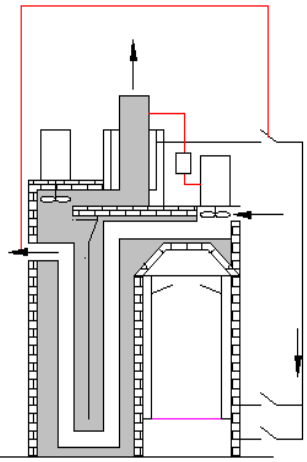

Fig. 8. Diagram of a TLUD gasifier -4th version

Maintaining constant the temperature of the exhaust gases can also be done by adjusting the rotational speed of the warm air fan and keeping the exhaust gas temperature constant in conditions of raising the hot air flow provided. A combination of both solutions of avoiding energy loss at the chimney by adjusting the forced draft fan speed or the warm air fan speed could optimize the overall efficiency of the generator.

4. Conclusions

The advantages of applying energy recovery and increased efficiency solutions to the gasification boilers are:

- superior recovery of the flue gases heat so their input temperature in the chimney is lower, about 170...200°C compared to the 250°C at the existing boilers;
- complete combustion of gasgen that leads to diminishing the specific loss by incomplete combustion;
- reducing the risk of carbon monoxide poisoning;
- the use of wood fuel with a greater moisture content, about 20%, as the primary combustion air has a higher temperature;
- increasing the actual efficiency of the boiler from 81 ... 86% to 90%;
- wood fuel saving for the same energy produced by other boilers.

Besides energy recovery of wastes, it is also aimed at:

- replacing fossil fuels such as black oil, fuel gas and coke (conservation / protection of resources);
- reducing the impact of CO_2 emissions on climate (climate protection);
- reducing the dependence of global energy markets connected with cutting costs;
- increasing the degree of flexibility of waste management by reducing the amount of residual waste.

Arguments in support of biomass use:

- it diversifies the energy supply sources;
- it replaces high CO_2 emission conventional fuels;
- it contributes to the waste recycling;
- it protects and creates jobs in rural areas;
- it gives the possibility of adjusting, automation and control of the system depending on the actual requirements or the heated premises.

Acknowledgement

Research presented in this paper has been developed with financial support of UEFISCDI (Executive Unit for Financing Higher Education, Research, Development and Innovation) under PCCA 2013 Programme, Financial Agreement no. 67/2014.

References

[1] P. Basu, "Biomass Gasification and Pyrolysis: Practical Design and Theory", Academic Press, 2010;
[2] A. Belonio, "Rice husk gas stove handbook", College of Agriculture, Central Philippine University, 2005;
[3] A. Belonio, "Dual- reactor rice husk gasifier for 6-ton capacity recirculating-type paddy dryer", Central Philippine University, Iloilo City, Philippines;
[4] H.A.M. Knoef, *Editor*, "Handbook Biomass Gasification Second Edition", BTG Biomass Technologies Group, Nederlandes, 2012;
[5] H. Mukunda, et al., "Gasifier stoves – science, technology and field outreach", CURRENT SCIENCE, vol. 98, no. 5, 10 March 2010;
[6] E. Murad, "Optimisation of biomass gasification load regime", International Conference ENERGIE - MEDIU CIEM 2005, UPB, Bucharest, October 2005;
[7] E. Murad, A. Culamet, G. Zamfiroiu, "Biochar- Economically and ecologically efficient technology for carbon fixing", Conference HERVEX 2011, November 9-11, Călimăneşti , ISSN 1454-8003;
[8] E. Murad, Gh. Achim, C. Rusănescu, "Valorificarea energetică şi ecologică a biomasei tăierilor din livezi", ICEDIMPH-HORTING Scientific Session, September 20, 2012;
[9] J. Porteiro, D. Patino, et al., "Experimental analysis of the ignition front propagation of several biomass fuels in fixed-bed combustor", FUEL 89, 2010, pp. 26-35;
[10] S. Varunkunar, "Packed bed gasification-combustion in biomass domestic stove and combustion systems", PhD Thesis, Department of Aerospace Engineering Indian Institute of Science, Bangalore, India, Feb. 2012.

The Nuntași Riverbed Hydraulic Distribution Vector Speed

Prof. PhD.eng. **Mariana PANAITESCU**[1], Prof. PhD.eng**. Fanel-Viorel PANAITESCU**[2]

[1] Constanta Maritime University,marianapan@yahoo.com

[2] Constanta Maritime University,viopanaitescu@yahoo.ro

Abstract: *In Romania, the current legislation provides normatives for knowledge, rational use, protection of water resources, and also organizes specific activities of defence against floods and supervises the quality of groundwater resources through prevention and control measures in case of accidental pollution.*
These things we pursue in this paper which aims the assessing and hydraulic modeling of surface water environmental risk.
All abstractions of groundwater in South Dobrudja must be protected against pollution by setting up hydro and sanitary protection zones, in order to ensure a better exploitation of groundwater resources. The most accurate method of determining protection zones is represented by mathematical modeling. Modelling gives a qualitative, sufficiently complete image of the free surface flows, as well as a satisfactory quantitative assessment. The paper present the modeling of the riverbed with environmental eroding risk in Dobrudja area with applicability on the lake basin Nuntasi using MIKE and ArcGis software.

Keywords: *riverbed, surface water, hydraulic modeling, environment, risk, lake*

1. Introduction

In Romania, the current legislation provides normatives for knowledge, rational use, protection of water resources, and also organizes specific activities of defence against floods and supervises the quality of groundwater resources through prevention and control measures in case of accidental pollution.
Dobrudja is composed of three major structural blocks namely: Dobrudja South, Central Dobrudja and North Dobrudja separated by faults Capidava -Ovidiu and Peceneaga - Camena (Fig. 1). More than 80% of Dobrudja appears to be siliceous rocks [1]. Dobrudja catchment area is very poor in own surface resources. Basically, they consist of several major rivers surface (so far there is no use in rivers due to low water flow permanently) and in coastal lakes and related Danube [2].

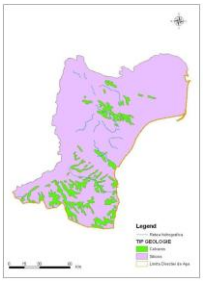

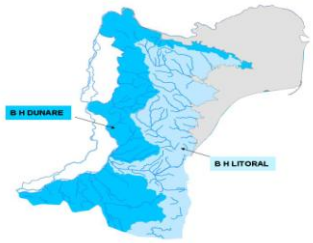

Fig. 1. Structure of Dobrudja bocks [1] **Fig.2.** DOBRUDJA hydrographic Basin [3]

The catchment area Dobrudja identifies 16 rivers with areas greater than 10 km², 18 natural lakes and four water storages that are larger than 0.5 km².
Dobrudja Basin consists of Seaside and streams tributary to the Danube River catchment area corresponding to Dobrudja (Figure 2) [3], [4].
To characterize a basin is necessary to know its characteristic elements-morphological variables of the watercourse system (Fig. 3). These can be divided into:

- Elements of hydrology and river network
- Geological features
- Features on vegetation.

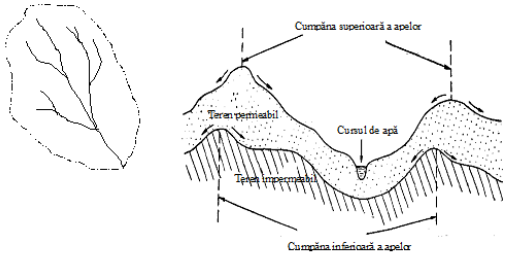

Fig.3. Hydrographic basin schema

Hydrogeologic basin represents the aquifer (underground), simple or complex, where the groundwater flows to surface to the same element drainage that can be a stream or a line of springs. Evaluation of the scheme of water flows is determined mainly by the knowledge of two categories of information: morphometry river system; hydrometric river system. Morphometric characteristics of the river system are expressed through: transversal profile of the riverbed; longitudinal profile of the riverbed; flashy stream.
Hydrometric data, obtained using methods and techniques is represented by the level of surface currents; surface currents speeds; surface currents flow. With these elements we represent the limnimetric key and the flow hydrograph.

2. Methods and research

Process modeling of flow and transport for free level aquifers involves the imposition of special conditions, especially due to variation in the free surface.
Basic equations of mathematical modeling of flow dynamics of non permanent surface water are based on the following physical principles: continuity equation (conservation of mass fluid respectively contaminant); equation of time (when fluid conservation, energy conservation (H. - J. Diersch, 2005) [5], [6]. General modeling assumptions are: incompressible fluid and homogeneous, two-dimensional flow, parallel throughout the riverbed slope small bed, small variations in the parameters of cross sections, the distribution date hydrostatic pressure [6].
Depending on the model attached flow modeling adds specific equations [6], [7].
Free level aquifers approach depends on the case - two-dimensional or three-dimensional. The usual method, preferred in hydraulic modeling, involves the calculation of free surface on a fixed network.
Solving numerical patterns of flow for whites erodible purpose engineering is based on the Finite Difference numerical integration of a system of algebraic equations, nonlinear rule.
Modeling the river bed with environmental eroding risk the following elements need to be studied:

- Data location and description of the catchment area, applicable to Nuntasi;
- Data on power sources aquifer basin, applicable to Nuntasi;
- Balance river flows in the Dobrudja area for 1999, 2004, 2007 and 2010;
- Reporting to the climatologically normal space Dobrudja basin [8].
- Hydrometeorological regime for Nuntasi catchment area reported to Constanta County [8].

The analysis will be done for the creek Nuntasi and not for Lake Nuntasi.
Balance flow to the hydrographic area Dobrudja for 1999, 2004, 2007 and 2010 is shown in Table 1.

TABLE 1: Balance flow to the hydrographic area Dobrudja

Year	**Balance flows**	**Inlet flow [m3 /s]**	**Outlet flow [m3 /s]**
1999*[27]*	North boundary West boundary South boundary Black Sea Surface supplementary flow	- - - - 91 367.34	5417.58 7 869.45 17 98.06 60 800.55 -

2004	North boundary West boundary South boundary Black Sea Surface supplementary flow	- - -175.33 - 98 452.89	5923.72 8104.57 1945.27 67845.13 -
2007	North boundary West boundary South boundary Black sea Surface supplementary flow	- - -189.37 - 99 321.23	6123.48 8765.41 2006.39 69929.16 -
2010	North boundary West boundary South boundary Black Sea Surface supplementary flow	- - 143.28 - 39 987.25	2 320.63 4 248.47 8 579.01 24 998.52 -
TOTAL		329 636.69	286675.83

Supply aquifer - is mainly from rainfall and the loss of irrigation water systems.
Nuntasi Lake River Basin lies between 28^0 37''30' NV and 28^0 45' N-E and also parallel 44° 30 'latitude and parallel 44° 35' (Fig. 4)[9].

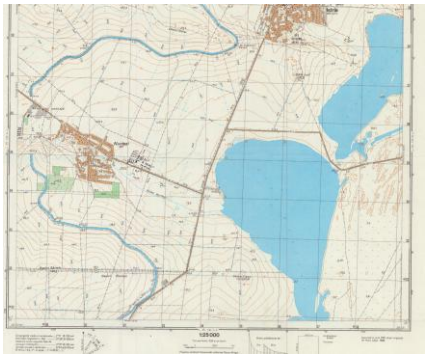

Fig. 4. Nuntasi River Basin [9]

Study of modeling assumptions are:
- flow-permanent, two-dimensional, parallel throughout the riverbed,
- incompressible fluid and homogeneous,
- slope small bed, small variations in the parameters of cross sections
- hydrostatic pressure distribution date [36].

The equations for the flow cross-section are the Saint-Venant equations (1), (2), (3), (4) and for along the riverbed flow, the turbulent flow equations, equation for turbulent kinetic energy (6), dissipation equation ε (7):

$$\rho \cdot Q \cdot dt - \rho \cdot (Q + \frac{\partial Q}{\partial x} dx)dt = \rho \cdot dA \cdot dx = \rho \cdot \frac{\partial A}{\partial t} dx \cdot dt \,; \quad (1)$$

where

$$\frac{\partial Q}{\partial x} = \frac{\partial A}{\partial t}, \quad (2)$$

$$\frac{\partial Q}{\partial x} - B \cdot \frac{\partial h}{\partial t} = 0 \,; \quad (3)$$

and conservation of momentum equation (4)

$$\frac{\Delta M}{\Delta t} = \frac{\Delta(M \cdot U)}{\Delta x} + \frac{\Delta p}{\Delta x} - \frac{F_f}{\Delta x} + \frac{F_g}{\Delta x}; \tag{4}$$

where

M- total momentum; Δ(M.U) - momentum of flow debt; $\frac{\Delta p}{\Delta x}$ - hydrostatic pressure distribution; $\frac{F_f}{\Delta x}$ - variation of frictional force with riverbed; $\frac{F_g}{\Delta x}$ - contribution of gravity force on Ox axis.
The differential equation of flow is (5):

$$\frac{\partial Q}{\partial t} + \frac{\partial(\alpha \frac{Q^2}{A})}{\partial x} + g \cdot A \cdot \frac{\partial h}{\partial x} + \frac{gQ|Q|}{C^2 A \cdot R} = 0, \tag{5}$$

where
Q- fluid flow [m^3 /s]; h-depth of water in riverbed [m]; C- Chézy coefficient (C=1.R1/6/n); n- Manning coefficient, roughness; A-cross area [m^2]; R-hydraulic radius [m].
The equation for turbulent kinetic energy (6) and dissipation equation ε (7) are

$$\frac{\partial}{\partial t}(\rho_m k) + \nabla \cdot (\rho_m \bar{v}_m k) = \nabla \cdot \left(\frac{\mu_{t,m}}{\sigma_k} \nabla k \right) + G_{k,m} - \rho_m \varepsilon; \tag{6}$$

$$\frac{\partial}{\partial t}(\rho_m \varepsilon) + \nabla \cdot (\rho_m \bar{v}_m \varepsilon) = \nabla \cdot \left(\frac{\mu_{t,m}}{\sigma_\varepsilon} \nabla \varepsilon \right) + \frac{\varepsilon}{k}(C_{l\varepsilon} G_{k,m} - C_{2\varepsilon} \rho \varepsilon); \tag{7}$$

where mixture density ρ_m consist of several phases (α_i..... α_N), with density ρ_i (8), speed vector $\bar{v}_m$ (9), component concentration z, $C_{l\varepsilon}$, k- permeability tensor, μ-cinematic viscosity, ε -phases volume fraction α (10)

$$\rho_m = \sum_{i=1}^{N} \alpha_i \rho_i; \tag{8}$$

$$\bar{v}_m = \frac{\sum_{i=1}^{N} \alpha_i \rho_i \bar{v}_i}{\sum_{i=1}^{N} \alpha_i \rho_i}; \tag{9}$$

$$\mu_{t,m} = \rho_m C_\mu \frac{k^2}{\varepsilon} \tag{10}$$

Turbulent kinetic energy generated on speed gradient will be done by formula (11):

$$G_{k,m} = \mu_{t,m} \left(\nabla \bar{v}_m + \left(\nabla \bar{v}_m \right)^T \right) : \nabla \bar{v}_m \quad . \tag{11}$$

Mixture density will be (12)

$$\rho_m = \sum_{i=1}^{N} (\alpha_i \cdot \rho_i) \quad . \tag{12}$$

Mixture speed will be (13)

$$\bar{v}_m = \frac{\sum_{i=1}^{N}(\alpha_i \cdot \rho_i \cdot \vec{v}_i)}{\sum_{i=1}^{N}(\alpha_i \cdot \rho_i)}. \quad (13)$$

Turbulent viscosity is done by formula (14)

$$\mu_{t,m} = \rho_m \cdot C_\mu \cdot \frac{k^2}{\varepsilon}, \quad (14)$$

where C_μ is a constant.
So, turbulent kinetic energy which is generated on speed gradient will be (15)

$$G_{k,m} = \mu_{t,m}\left(\nabla\vec{v}_m + (\nabla\vec{v}_m)^T\right) : \nabla\vec{v}_m. \quad (15)$$

For the flow modeling we select a sector and we will note the geometric and hydraulic parameters and related to this sector, the settling flow diagram by hydraulic modeling [10]. In our case, the modeling will be done by using software MIKE 11 [11].
Flow stability is required for the convergence of the solution achieved by modeling, given the initial conditions and the approximation by finite differences that need to be consistent.
Explicitly provided stability is the number Courant (16) [10], where Cr <1.

$$Cr = (\sqrt{g \cdot D} + v) \cdot \frac{\Delta t}{\Delta x} \quad . \quad (16)$$

Boundary conditions of the flow are:

- discharge flow upstream of the control section, downstream
- tributaries flow
- condition for convergence solution-end flow, Q = 0
- water depth, h (1 ÷ 2.3) m
- weather-wind, currents
- conditions for Q / h downstream flow (never upstream).

There was used information provided by operating with ArcGis software (Fig. 5), software MIKE Zero (Fig. 6) and Nuntasi topographic map of the basin (Fig. 4).

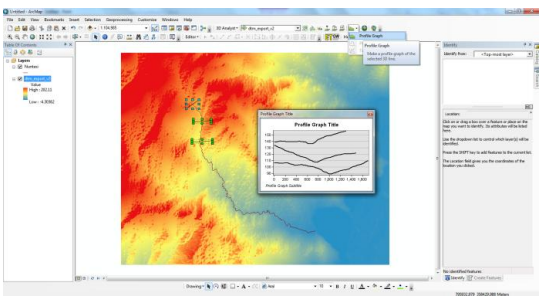

Fig. 5. Location Nuntasi River Basin on ArcGis [35]

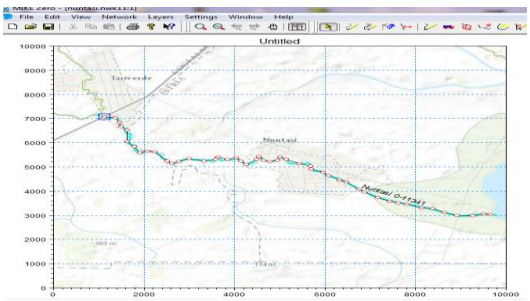

Fig. 6. Nuntasi basin topographic map-MIKE [36]

Based on topographic data, initial hydraulic data and data obtained by graphic-analytical and also the limnimetric key of Nuntasi riverbed using MIKE 11 software was simulated a flow specific to a situation of flood in 2007 and compared to the level of 1999 (Fig. 7).

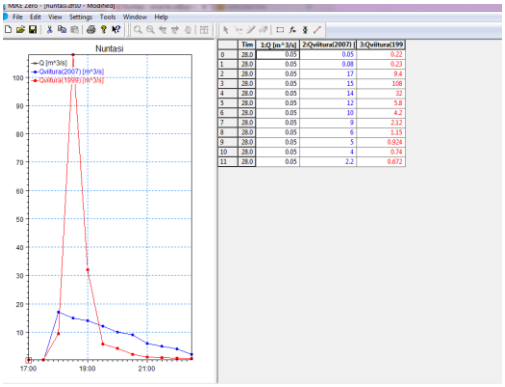

Fig. 7. Flow simulation for two discharge flow (flood in 1999 and 2007).

3. Results and interpretations

Varying flow was analyzed from downstream to upstream along the length of 14 km of the river course. We used first the ArcMap program's related information to determine files of the Nuntasi river's spatial route (Fig. 8).

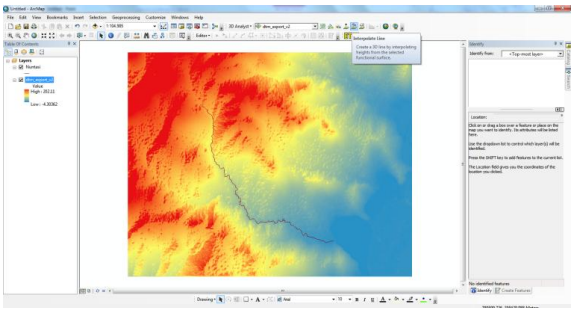

Fig. 8. Shapefile with the plan river route of Nuntasi

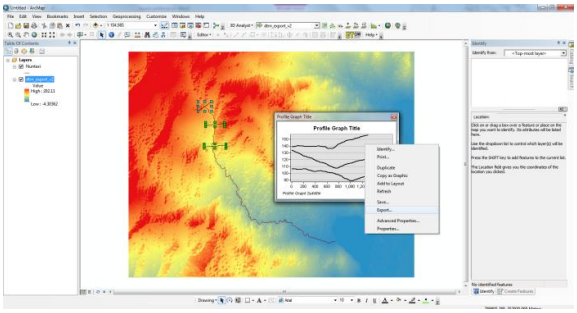

Fig. 9. Digital Terrain Model for framing Nuntasi river

With this information was passed to achieve digital terrain model to fit Nuntasi River (Fig. 9). Subsequently, was used ArcGIS software to extract cross sections of the course of the river. With this information entered into the program MIKE 11 resulted files giving details of the actual flow section of the river wedding party. The final results of modeling with MIKE 11 program are plotting and maximum rates for the flood of 2007 (Fig. 10) and flow profile along the riverbed Nuntasi (Fig. 11).

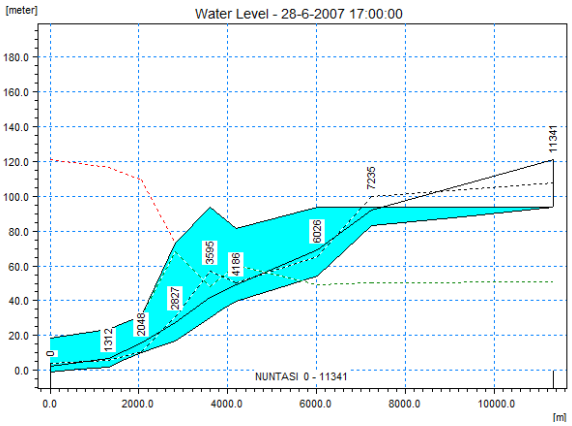

Fig. 10. Shares riverbed for flood in 2007.

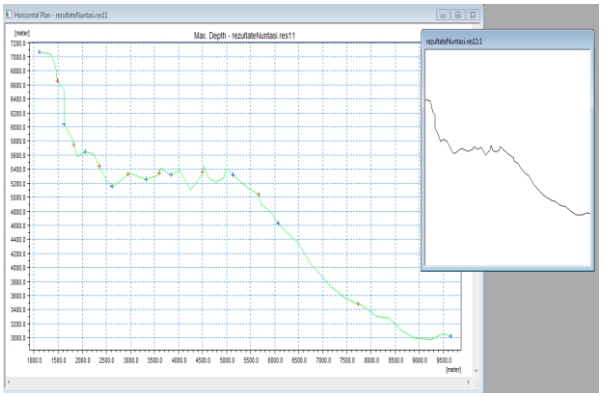

Fig. 11. The final flow speed along the riverbed

On the length of Nuntasi river was represented the allowance variation of the riverbed, the distribution of the velocity vector for related shares initially introduced in the program.

4. Conclusions

One of the risk factors is represented by the floods. For studying the flow in the Nuntasi riverbed eroded with environmental risk were analyzed elements: location and description of the hydrographic area, data sources feeding the aquifer basin data sources feeding the aquifer basin balance flows to the hydrographic area Dobrudja for 1999, 2004, 2007 and 2010, reporting to the climatologically normal catchment area Dobrudja; hydro meteorological regime for the guests catchment area reported at Constanta County; morphological and morphometric elements of the bed of the guests; Nuntasi riverbed proper flow modeling.
Building the model accordingly to Nuntasi basin riverbed assumed the existence of a stage modeling that was done with the program MIKE 11 situation of 2007, to a forecast of rainfall for a period of 14 hours, the hydrograph basin Nuntasi, based on rainfall intensity curve; then there is simulated the flow along the river, indicating the distribution of speeds of flood related natural hydrograph.

Acknowledgement

Thank you for supporting Romania DHI Company using ArcGis and MIKE 11, especially Mrs. Director Maria Cheveresan and Mr. Mihai Valentin Stancu, Hydro technician engineer.

References

[1] M. Ielenicz, I. Săndulache, "Romania - Platteaus and Hills" (România - podişuri şi dealuri), University Publishing House, Bucharest, 2008;
[2] D. Scradeanu, A. Gheorghe, "General Hidrogeology", chapter "Natural factors supply and underground waters regime" (Hidrologie generala, cap. Factori naturali ai alimentarii si regimului apelor subterane", Technical Publishing House, Bucharest, pp. 1-42, 2014;
[3] http://www.rowater.ro/daDobrudja/, "Planul pentru prevenirea, protecţia şi diminuarea efectelor inundaţiilor în spaţiul hidrografic Dobrudja-Litoral", slides, sl.9, 2012;
[4] M. Panaitescu, F.V. Panaitescu, "Hydraulics. Theory and applications", Nautica Publishing House, Constanta, 2011;
[5] I. Mircea, "Modelarea curgerii apei subterane prin acviferul cantonat în calcarele sarmaţiene din DOBROGEA DE SUD" (Modeling of groundwater flow through aquifer garrisoned in the sarmathian calcars in SOUTHERN DOBRUJA), Bulletin AGIR, nr. 3, pp.113-116, 2013;
[6] *** Hydro-Informatics, Modelling tools MIKE 11, Part 1-Introduction, IHE 2001-2003;
[7] *** "Bulletin on risk assessment: Risk assessment as an aid to dam safety management", I.C.O.L.D., 102 p., 1999;
[8], http://www.isuDobrudja.ro/wp-content/uploads/2016/03/Planul-de-Analiz%C4%83-%C8%99i- Acoperire-a-Riscurilor-al-jude%C8%9Bului-CONSTAN%C5%A2A-2015.pdf, "Planul de analiză şi acoperire a riscurilor al judeţului Constanţa", pp.14-20/83, 2015;
[9] Archives of M.A.N., R.S.R., Military Topographic Directorate, 1981;
[10] I.A. Enache, "Modeling of flows components of the waters from Dobrudja – Seaside Hydrographyc Basin" (Modelarea componentelor scurgerii apelor din bazinul hidrografic Dobrogea-Litoral), Bachelor's thesis, Constanta, 2014;
[11] R. Courant, K.O. Friedrichs, H. Lewy, "On the partial difference equations of mathematical physics", Math. Ann. vol.100, 1928.

Environmental Awareness of Anthropogenic Impact

Carmen Otilia RUSĂNESCU[1], Gigel PARASCHIV [1], Sorin Ștefan BIRIȘ[1], Marin RUSĂNESCU[2]

[1] Polytechnic University of Bucharest, Faculty of Biotechnical Engineering

[2] Valplast Industry, Bucharest, Romania

Abstract: *This paper presents awareness of pollution problems displayed by students of the Faculty of Biotechnical Engineering, future environmental engineers.*
Survey was conducted using a questionnaire consisting of five questions. It was noted that for the final year students is very important to protect the environment, this due to deepening subjects in years of college.

Keywords: *environmental pollution, anthropogenic impact*

1. Introduction

Romania began its transition with some major environmental problems because legislation failed to deliver effective pollution controls. In addition, the slow-down in the economy helped to reduce the scale of environmental damage, although rising unemployment helped to breed a survival mentality which had made the public wary of supporting radical environmental programmes.
Before 1989, Bucharest was considered the largest and most complex industrial centre of Romania, gathering units with lower pollution potential, as the food industry, textile and so on, but as well units with higher pollution potential, such as those in energy production, chemical industries, metallurgy, construction, machinery and equipment manufacturing.
The industrialization phenomenon underwent differently in intensity and spatial expansion, depending largely on the political, historical and economic factors.
After the industrial landscape became a major economic and cultural presence in the urban landscape of Bucharest, a visible change is remarked in the landscape since 1989 by creating urban deserts and conversion of industrial to other functions, required by the continuously changing city, to be competitive at European and global level [4].
The environment represents the ensemble of natural and artificial elements in which life evolves or the sum of the factors exterior to the human body such as: the atmosphere, the light, as well as all the other beings. The water, air and soil, constituents of the biosphere are known under the name of environment factors. For the survival of the animal, vegetal and human kingdom the degree of pollution should be reduced for a cleaner and healthier environment. [2]
Knowing of the conditions of life within each medium has lead to an efficient protection. It is essential to have knowledge about the pollutant sources, especially the pollutants that could prejudice the development of live and then their impact upon the environment and upon life, generally.
In order to characterize and control the phenomena that are specific to some types of activities, and to know their impact upon the environment at a certain point, it is necessary for these things to be known through models of global appreciation upon the state of health or of polluting the environment. The first condition that imposes to the applied model is that of allowing for the comparison of the state of environment at a certain time with the possible state in the near future [2].
Determining the impact upon the environment can be considered a positive argument if the capitalization of the research results are taken into account [3].
Environmental education goes through various stages of formal and non formal education. It is based on social sciences and humanities, education programs must aimed the learning to conserve the nature and a better use of resources [1].

It aims to:
• Human awareness of the existence of natural and social environment;
• Empowering its proper understanding of the relation human-nature-community;
• Formatting an environmental conduct.
Achieving these major objectives it can be made only through complementary actions to all educational factors: school, family, society, and the complex extracurricular activities ensure the climate of these interactions with beneficial influence in shaping the personality of students.
In carrying out environmental education have to be respected the following principles:
- Addressing the environment in its totality: natural and artificial, technological and social, economic and political, cultural and historical.
- Considering environmental education as a continuous process, beginning at preschool and continuing through all formal and non-formal stages;
- Exploration of the major environmental problems from local perspective, regional, national and international, so that students to know the environmental factors also from other geographical regions;
- Focus on current and potential environmental problems, taking into account their trend in history;
- Promoting values and local needs, national and international to prevent and resolve environmental problems;
- To discover symptoms and real causes of environmental problems;
- Promoting cooperative learning.
Environmental Education puts students in direct contact with nature in order to develop love for all forms of life.
Presentations and analysis of environmental problems begin, usually, with a discussion of the causes of phenomena and ends with positive alternatives and possible ways of solution.
Obviously, for people to participate actively, intelligently and beneficial to the process of administration, development and environmental protection must be educated since the school banks to deal with environmental problems to be able to face the environmental problems in the current context.
Harsh reality and the problems of modern society require a redefinition of objectives in education and the education in science and the environment.
The contemporary education in the field of environment should be characterized by several important aspects:
To focus not only on the classical approach of the environment and its protection, but also on the human being in context of a healthy environment;
To change people's attitudes about environmental protection, meaning the state exceeded their declarations and training in order to effectively engage in such actions;
The school programs to be designed to lead to a passive knowledge to active interaction with the environment, to be translated theory into practice. [1]
The changes that should occur to education at all levels of education would mean restructuring the education content.

2. Results and discussion

To verify awareness of the impact of environmental pollution on the students use the following questionnaire, consisting of the following questions:
How aware are you of the environmental issues?
What rights do you think animals, birds and plants have compared to people?
Do you recycle selective? (Yes/ No)
Do you think that nonhuman species status is an indicator of the future for us humans?
Do you consider that your actions help solve the problems of the planet?

After processing the answers given by students the following results were obtained:

How aware are you of the environmental issues? (very aware / not interested).

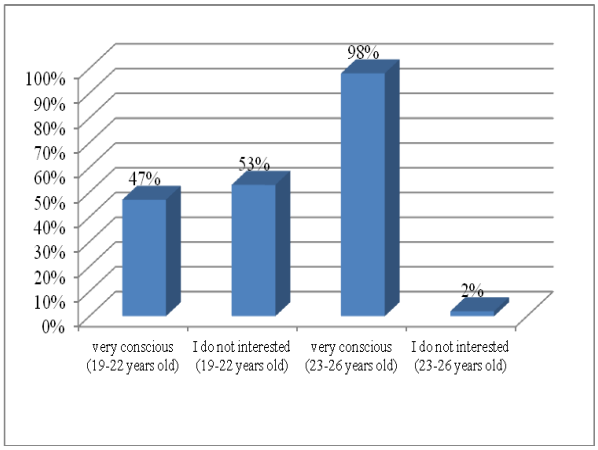

Fig. 1. Awareness to students aged 19-22 years, 23-26 years towards environmental issues

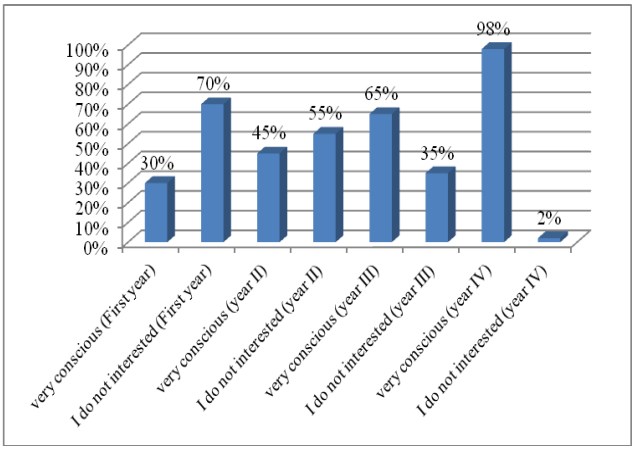

Fig. 2. Awareness of students by year of study towards environmental issues

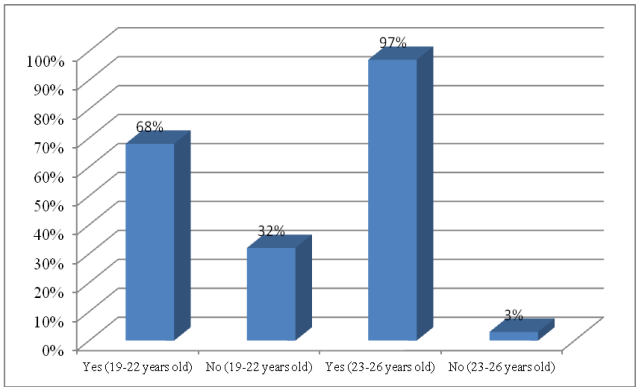

Fig. 3. The answer students aged 19-22 years old, 23-26 years old on selective recycling

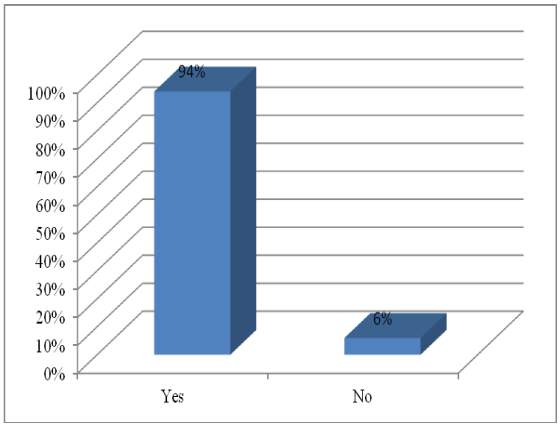

Fig. 4. If students answer animals, birds and plants living together have the same rights as men (Those living / No right)

Do you think that non-human species status is an indicator of the future for us humans? (Yes No).

Do you consider that your actions help solve the problems of the planet? (Yes No).

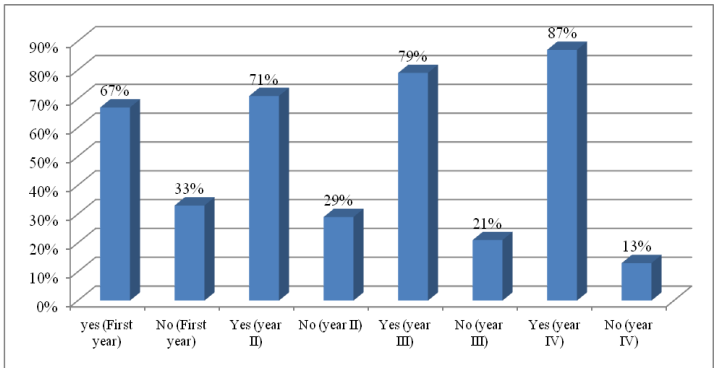

Fig. 5. Students' opinions on the state of non-human species that is an indicator of the future for people

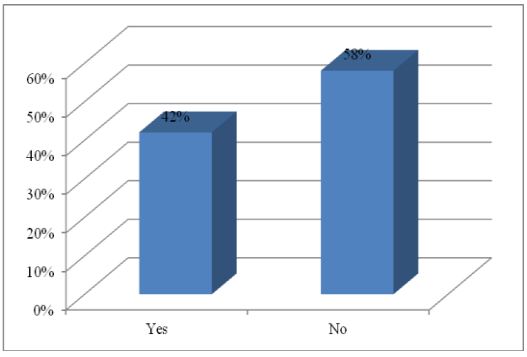

Fig. 6. Environmental actions help solve the problems of the planet

Conclusions

The conclusions were drawn, analyzed and plotted. They are:

When asked about their *awareness of environmental issues* it was observed that with advancement in the years of study the students became more aware of the environmental issues and this is due to the multitude of notions learned about pollution, remediation, environmental engineering. Of students aged 19-22 years only 47% were aware, compared to those aged 23 to 26 years- 98%.
Awareness of students by year of study towards environmental issues has been raised with the increase in years of study; in the first year of studies 30% of students were aware of problems concerning environmental pollution, in the second year 45%, in year III 65%, in the fourth year 98% of the students were aware of the problems of environmental pollution.
The answer of students *on selective recycling:* It was better amongst students aged 23-26 years (97%) than those aged 19-22 years (68%).
When asked *if animals, birds and plants living together have the same rights as humans* students' answer was 94% positive.
Students' answer *whether nonhuman species status is an indicator of the future for us humans* was 87% yes.
When asked *if their actions could help solve problems of the planet*, 42% of students agreed, 58% found we should all get involved to prevent environmental pollution.

- As time passes and with deepening in the faculty the environmental issues, students are becoming more aware of environmental issues.
- The multitude of news and documentaries presented in the media about the planet earth resources have made the students understand that the use of natural resources at will is a good thing for generations to come, and even for the present.
- Regarding the rights of birds, animals, plants, we found that students believe that they have any right to humans.
- The selective recycling - final year students are aware of the impact on the environment of selective recycling, and the lowest in years recycle at random, by recycling 68% and 97% of them selectively. Over the years of college, selective recycling will not have "secret" to the students and this will become the norm as eating, breathing, drinking water, etc.
- The status of non-human species is an indicator of the future for people, according to students who responded to the questionnaire.
- The problem of solving planet using students' actions - there is little difference between those who believe they can help and those who think they cannot help.

The main objectives of environmental education are to:

- Cultivate love for the Earth and all elements on it: water, plants, animals, etc.;
- Increase the desire to protect, respect and preserve nature by involving children in demonstration activities;
- Develop skills of research, exploration, environmental investigation;
- Know organisms and phenomena in the environment and their characteristics;
- Enrich the active vocabulary with words from the environment area;
- Acquire some conduct rules to ensure the balance between human health, society and the environment;
- Know the plants and animals protected by law;
- Investigate remediation methods of environmental status by using students in activities of waste recycling, sanitation of towns, etc.
- Increase awareness of the need to save water, electricity, wood, etc. (natural resources);
- Take negative attitudes on those who violate environmental rules and laws.

Unfortunately, when they return to where they came, forgetting that nature is all there, they continue receiving the same every time. If nature does not ever seem as generous as it is for us humans, we took what we gave.
It is time to relearn respect for nature. Once we realize that the only solution to all our problems. The best and safest way for nature conservation is a new consciousness. That fact is that nature does not need us, but we need nature.
It all comes back to us.
All other solutions will come by themselves, but the first and most important is the awareness of environmental pollution.

References

[1] H. M. Sabo, "Environmental education and sustainable development –general aspects", 2011 International Conference on Social Science and Humanity IPEDR vol.5 (2011);
[2] I. Ifrim, D. Ciobanu, G. Andrioai, "A preliminary impact study upon the environment factors in the case of depollution of wastewaters from the pulp industry with mixtures of phosphoric acid and diammonium phosphate", Scientific Study & Research ♦ Vol. VIII (2) ♦ 2007 ♦ ISSN 1582-540X 185;
[3] I. C. Ioj**ă, "**Metode şi tehnici de evaluare a calităţii mediului în aria metropolitană a municipiului Bucureşti", Editura Universităţii Bucureşti, 2008;
[4]. D. A. Mirea, C. M. Ciocanea, M. Patroescu, "Spatial and temporal dynamics projection of industrial landscape in the environmental state", Case study: 3RD District of Bucharest present environment and sustainable development, Vol. 7, no. 2, 2013;
[5] C. O. Rusănescu, I. N. Popescu, M. Rusanescu, L. David, "Analysis of variation in relative humidity in autumn 2009", Revista International Journal of Energy and Environment, Issue 4, Volume 4, 2010, pp. 113-121, ISSN: 1109-9577;
[6] C. O. Rusănescu, G. Paraschiv, Gh. Voicu, M. Rusănescu, "Comparative Analysis of Atmospheric Temperature Values, Relative Humidity in 2009 and 2010 in West Side of Bucharest City", Bulletin UASVM Agriculture, 68(2)/2011, Print ISSN 1843-5246; Electronic ISSN 1843-5386, pp. 130-138;
[7] C. O. Rusănescu, "Meteorologie si climatologie. Indrumar de laborator", Editura Matrix Rom, Bucureşti, 2013;
[8] C. O. Rusănescu, M. Rusănescu, "Elemente de dinamica poluării", Editura Cartea Studenţească, Bucureşti, 2007;
[9] C. O. Rusănescu, M. Rusănescu, "Some aspects regarding the global warming", Hidraulica (no. 4/2013).

Prediction of Turbulent Flow Using Upwind Discretization Scheme and k-ε Turbulence Model for Porous Heat Exchanger

assistant professor **Petre OPRIŢOIU***

*Technical University of Cluj-Napoca, Department of MTC, str. Observatorului, nr.72-74, 400363, Cluj-Napoca, Romania, E-mail: petre.opritoiu@mtc.utcluj.ro

Abstract: *The present investigation is concerned with the prediction of turbulent flow using upwind discretization scheme and k-ε turbulence model for porous heat exchanger application. Many modeling techniques exist for the analysis of porous foam. The Fluent porous media model employs a momentum equation which accounts for both viscous and inertial losses in the foam and includes an effective thermal conductivity in the energy equation calculated via volume-averaging the coolant and foam thermal conductivities. The FLUENT computational fluid dynamics (CFD) software v.6.0 is used for more detailed modeling of the porous heat exchanger.*

Keywords: *computational fluid dynamics, turbulence model, flow characteristics, heat transfer performance*

1. Introduction

Porous media can be used for modeling a wide variety of engineering applications. It is generally desirable to determine the pressure drop across the porous medium and to predict the flow field in order to optimize a given design. The general design strategy is to minimize the coolant flow path length in contact with the porous medium, and to minimize the friction factor in that zone while simultaneously maximizing the heat transfer coefficient.
The maximum heat flux that can be accommodated is limited by the heat transfer coefficient achievable with flowing air and the maximum allowable operating temperature of the structural materials. Porous metal heat exchangers have been studied in the past because of the large surface area they provide for heat transfer.
For a given particle dimension d_p, the pressure drop through a porous medium ΔP is highly dependent on the porosity ε, while the heat transfer coefficient tends to depend more on the specific surface area, σ. Such a porous foam would have high porosity (which governs the pressure drop) but with specific surface area (influencing the heat transfer) higher than those that a conventional packed bed of spheres can provide.

2. Model development

Most existing models for heat transfer through a porous medium seem to be based on a semi-empirical approach such as the following circuit-based model described in [1].

$$h_{eff} = \varepsilon h_p + \frac{1}{R_0 + \frac{1}{\sqrt{h_p k_p S_p}\tanh\sqrt{\frac{h_p S_p}{k_p}t}}} \tag{1}$$

where h_{eff} is the effective heat transfer coefficient, h_p is the local particle-to-fluid heat transfer coefficient, R_0 is the porous medium/wall interface resistance, k_p is the porous medium thermal conductivity and t is the porous medium thickness.
Such a model provides a quick and convenient means for estimating the overall heat transfer coefficient but is limited in its range of application, in particular to account for cases with large spatial variation of the microstructure characteristics (e.g. the porosity and directional thermal conductivity), for cases with high porosity, and/or for design configurations where entrance effects plays a major role.

It would be very useful to develop a more comprehensive and fundamental model which first calculates the velocity profile and then the corresponding temperature distribution in the porous region, with the capability to account for microstructure variation and to include potentially important processes such as the local heat transfer between solid and fluid and the effect of dispersion. This model would provide a much better tool to perform a more detailed assessment and optimization of porous media for high heat flux application.

3. Turbulent flow in open-cell aluminum foam heat exchanger - physical situation

The physical situation considered and coordinate system employed in the simulations are revealed in fig.1, with their appropriate physical quantities that characterize presented flow situation, implying a number of iterations cycles required by the computer code to attain a pre-specified level of convergence. In this case the physical situation considered corresponds to the experimental situation of [2].
The final overall dimensions of the compressed foam blocks used in pressure-drop and heat transfer simulations were 250mm×100mm×50mm, with the cross-sectional area normal to the flow direction measuring 250mm×100mm. To make them functional heat exchanger, each foam was brazed in a central position to an adjoining heat spreader plate made by solid aluminum.
A typical flow and heat transfer configuration is shown. A heat source is bonded or joined to a thin conductive substrate on which a block of open-cell aluminum foam of length L and thickness W is attached. The foam is then placed in a channel, and cooling fluid of velocity u_0 at a temperature T_∞ is pumped through the open celled material, thereby affecting heat transfer from the hot source to the cooling fluid [3,4].
Air enters the heat exchanger with a uniform velocity profile, and the flow of air develops along heat exchanger. In the inlet region, the free stream is completely surrounded by the growing boundary layer and accelerates as the thickness of the boundary layer increases.
In this work aluminum foam, with physical data: 40PPI porous density and porosity ε=0.927, acting as a heat exchanger, bonded to a heated wall set at 358K, with air initially at 295K and v=2.2m/s flowing through the foam. The coupled fluid flow-heat transfer calculation was then performed using SIMPLE algorithm and 2nd order upwind differencing on the momentum equation (fig. 2) [5].

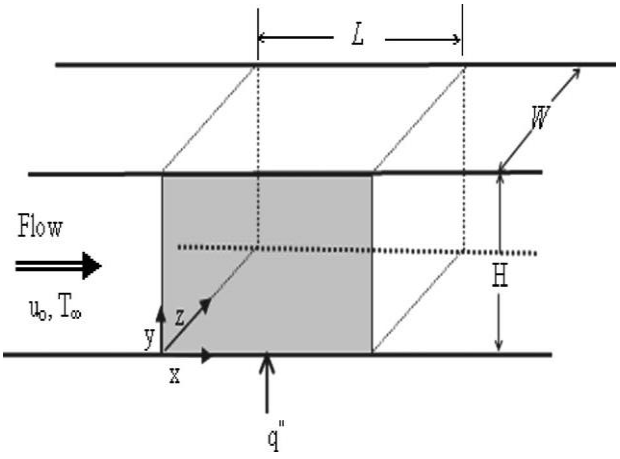

Fig. 1. Physical situations considered [5].

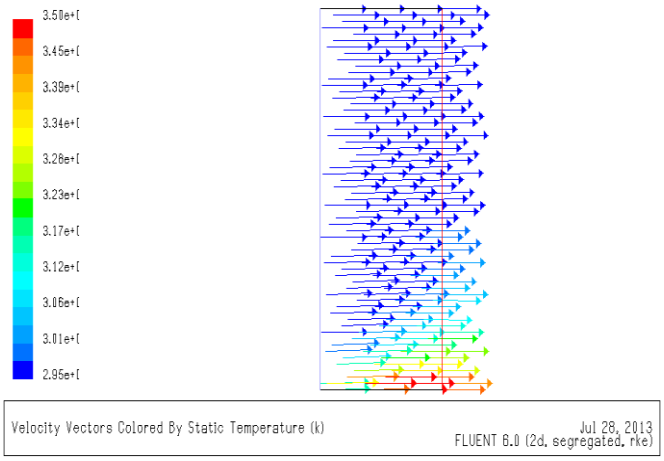

Fig. 2. Coupled fluid flow-heat transfer [5].

4. The finite difference discretization

In Fluent flow equation are solved, with their appropriate boundary conditions, by integrating them over finite–difference control volumes that form the physical integration domain considered, an example of the grid arrangement is depicted in fig. 3 where it is seen that the grid is staggered so that velocity components are situated mid-way between grid points [6].
The pressure, viscosity and any general scalar variable such as kinetic energy of turbulence, dissipation rate of turbulence kinetic energy are located at the grid points. The main advantage of

this arrangement is that the pressure difference between two adjacent grid points become the natural driving force for the velocity component located between these grid points.

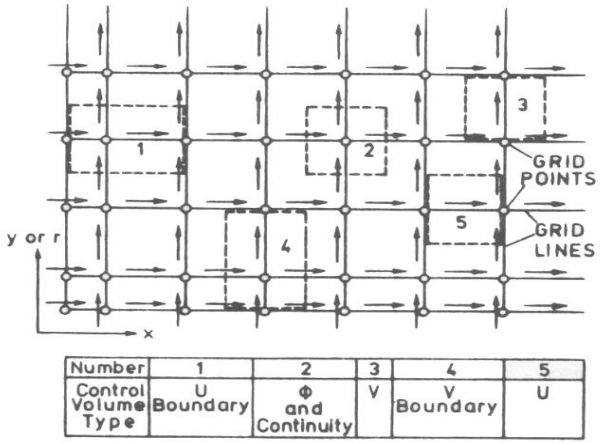

Number	1	2	3	4	5
Control Volume Type	U Boundary	Φ and Continuity	V	V Boundary	U

Fig. 3. Control volume specification [6].

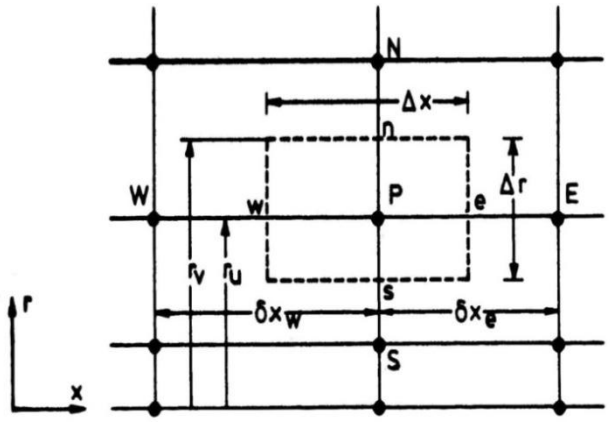

Fig. 4. Control volume for a scalar variable [6].

Now consider a single control volume for variable φ, as depicted in fig. 4, in which cell-face area at four points (e, w, n, s) is located mid-way between the grid points. The next step in the formulation of finite-difference equation is the assumption of the variation of φ between any two grid points. The diffusion terms are formulated using the central difference scheme. The schemes that are used to approximate the convection terms are only applied to the convected variable φ, the convecting velocity is discretized using the central-difference scheme.

In the ***central-difference scheme (CDS)*** the value of φ at an interface of the control volume is taken as the average value of the φ's at the grid points that lie on either side of the interface of the control volume. For velocities that are low enough, central-difference scheme is recommended, however it has been found that when the grid Peclet number is greater than 2, the coefficient matrix becomes non-diagonally dominant. As a consequence, a semi-implicit type numerical scheme, as normally used, becomes unstable.

The ***upwind-difference scheme (UDS)*** recognizes that the weak point in the CDS formulation is the assumption that the convected property φ at an interface is the average of the φ's at the grid points that lie on the either side of the interface, and it proposed a better resolution. That is, a piecewise-linear variation of φ between grid points is assumed for the diffusive flux, while for the convective flux the value of φ convected across an interface is taken to be the value of φ at the grid point on the upwind side of the face.

This approximation overcomes the stability problem associated with the use of the CDS. In the present study the upwind difference scheme is also employed for velocities that are low enough.

5. The wall functions

In the near-wall region, there is a steep variation in the fluid properties. To avoid the need for detailed calculations in these regions, algebraic relations are employed to relate the values of the dependent variables at a point on the wall to those at a point adjacent to the wall, a logarithmic layer is presumed to exist between these two points. FLUENT offers several discretization techniques for the convective terms of each governing equations. Using the segregated solver, the operator may choose to have either first or second order discretization of terms.

The first order method computes the solution at the center of each cell, while the second order method computes the solution at the center of each face. The first order discretization is generally acceptable for simple flow when the grid is aligned with the flow and a quadrilateral or hexagonal grid is in place.

A second order discretization method reduces errors over the first order methods, while generally increasing the difficulty of obtaining a convergent solution [7,8]. Reynolds number is used to determine y^+, a dimensionless distance from the wall. The implementation of wall functions is

necessary to overcome short falls in k-ε turbulence models. A criterion for the validity of wall functions exists. Acceptable range is $y^+ > 30$ (fig.5). Wall functions must also be implemented for the kinetic energy (k) and the turbulent dissipation rate (ε).

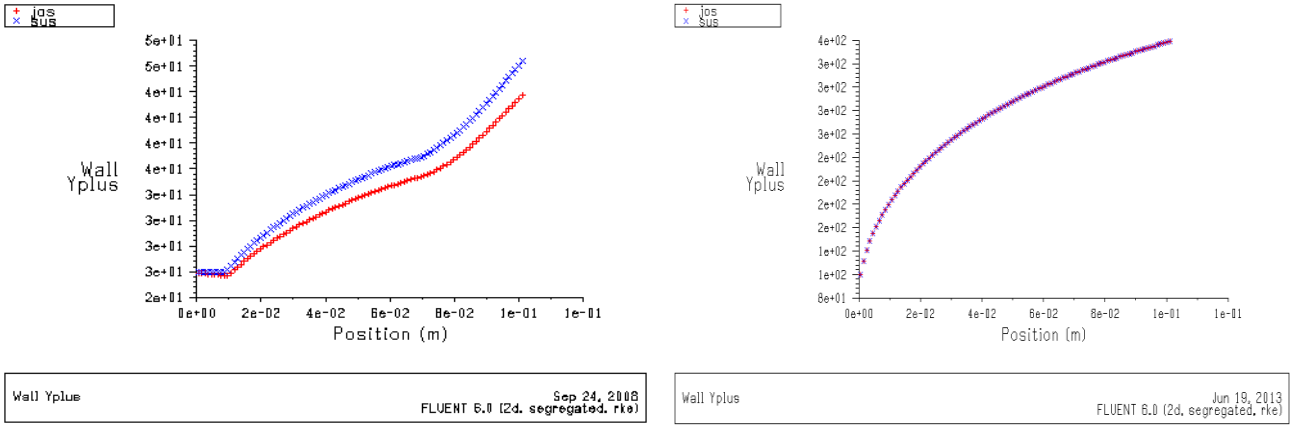

Fig. 5. Wall y plus function for open-cell aluminum foam heat exchanger: a. cooled by air, b. cooled by water [5].

6. Boundary conditions

In turbulent flow computations, additional boundary conditions for turbulence parameters need to be specified at inlet and outlet locations. This information can be supplied in the form of convenient, derived quantities such as turbulent intensity, length scale, viscosity ratio, hydraulic diameter, etc. It is important to review the default turbulent boundary condition (K=1.0, Epsilon=1.0). If these default settings are not representative for the flow field, error will be introduced into the solution.
The boundary condition set for the inlet is velocity. For this study, an inflow of mean velocity 2.2m/s was used. To generation turbulence an additional condition had to be applied. This involved turbulence intensity (I), which was calculated by eq. (2), [5,9].

$$I = 0.16\left(\mathrm{Re}_K\right)^{-1/8} \tag{2}$$

and the hydraulic diameter (D_h). The boundary condition set for the outlet is pressure. A viscous and an inertial resistance are applied in all directions. Porous media model is nothing more than an added momentum sink in governing momentum equations. Since the volume blockage that is present physically is represented in the model, FLUENT uses and reports a superficial velocity inside the porous medium, based on the volumetric flow rate, to ensure continuity of the following properties are required:
(a) Porosity (ε); (b) Viscous resistance (1/K), for aluminum foam:

$$\frac{1}{K} = \frac{32\pi}{\varepsilon \times d_p} \tag{3}$$

where K- permeability, [m^2] and d_p-pore diameter,[m]; (c) Inertial resistance (c_F):

$$c_F = \frac{2\left(\Delta P - \dfrac{\mathrm{v}L\mu}{K}\right)}{\mathrm{v}^2 \rho L} \tag{4}$$

The theoretical pressure drop per unit length for porous media was predicted following Forcheimer equation (1901):

$$\frac{\Delta P}{L} = \frac{\mu}{K} \cdot \mathrm{v} + \frac{c_F}{\sqrt{K}} \rho \cdot \mathrm{v}^2 \tag{5}$$

where Δp/L-pressure drop per unit length, [Pa/m], μ- fluid viscosity, [kg/m*s], ρ- fluid density, [kg/m^3], v-velocity, [m/s]. The hydraulic diameter is determined based on the size of the compressed porous cell, of the metal filament's diameter and the porous density. Boundary layers play an important role for heat transfer. The shape of the crossing section is determined by the metal filaments and it is meant to grow the local turbulence of fluid and heat transfer when it flows into the porous metal. Turbulence intensity values and resistance coefficients of viscous and inertial type, required for running the FLUENT software for a porous medium were obtained using MATHCAD program, starting from equations specific to Brinkman's porous environment [10].

7. Some computational details

A mesh which provides accurate results at laminar flow conditions may not be acceptable for turbulent flow situations. The turbulent boundary layer can be subdivided into several regions. Based on the region that needs to be resolved, the location of first cell adjacent to the wall is determined. When flow characteristics in the viscous sub-layer need to be captured,
Enhanced wall treatment should be used. Standard wall functions can be employed when the flow resolution starts from the log-layer region. Depending on the choice of near wall treatment, some constrains on the placement of the first cell from the wall are imposed, as prescribed in the following table.
When generating the mesh, care should be taken such that the first cell adjacent to the wall doesn't fall in buffer layer. Cell height calculations are based upon the cell centroid location. Enhanced wall treatment is recommended for the accurate prediction of frictional drag, pressure drop, separation, etc. Even here the mesh quality is acceptable, and no significant numerical issues have been encountered in solving the problem with a converged solution talking slightly over 200 iteration (fig.6a and b).

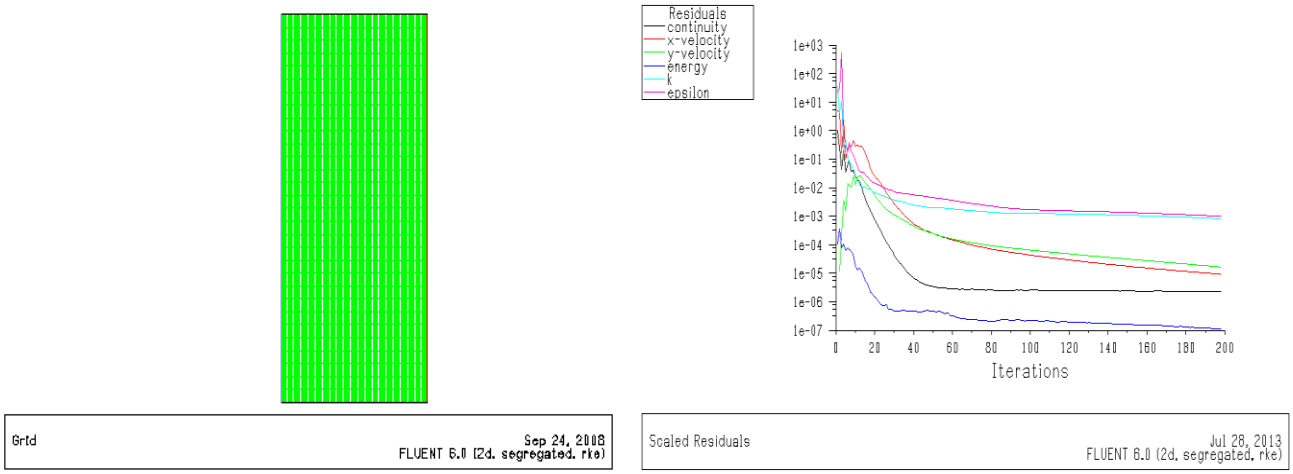

Fig. 6. Mesh (a) and plot of residuals (b) [4].

It is elegant and efficient to create mesh in one process. This also is more robust when topologically complex problems such as the open-cell metallic foam are being investigated. This means that the mesh generated required no intervention or correction so that solution is, as in flow/heat transfer presented here straightforward [4].

8. The turbulence model

The turbulence model employed in the present calculation is the k-ε model [5,7], and it necessitates the solution of two equation of transport for two turbulence quantities namely

turbulence kinetic energy k, and its rate of dissipation ε (fig. 7). Knowledge of the local values of k and ε allows the evaluation of a local effective viscosity from each the turbulent shear stresses are calculated.
A comparison of turbulence models was conducted. The principle underlying this was to compare the models and thus confirm their validity. k-ω Standard and k-ω SST models are not adequate for this case. Turbulence models offered similar results of simulation, with exception of Spalart-Allmaras model (S-A), Laminar model and Reynold Stress Model (RSM) [5]. The realizable model provides the best performance of all the k-ε model versions for several validations of separated flows and flows with complex secondary flow features (fig. 8).

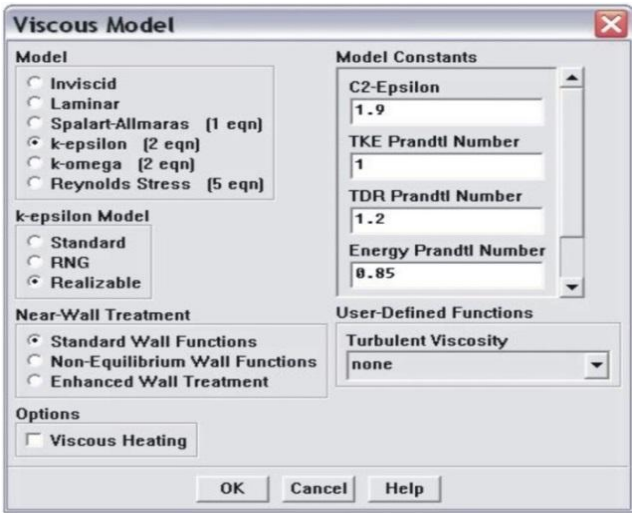

Fig. 7. k-ε realizable turbulence model [5].

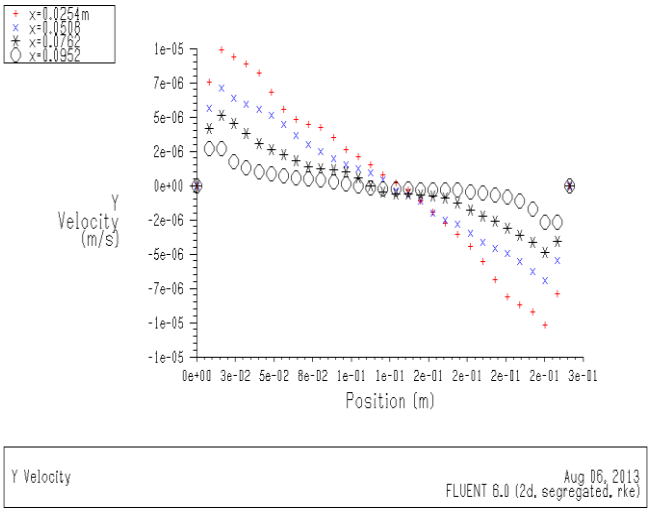

Fig. 8. k-ε realizable Model [5].

Developing turbulent heat exchanger flow is basically a transition from a boundary layer type flow at the entrance to a fully developed flow downstream. The free stream in the inlet region is completely surrounded by the boundary layer, which by diffusion of momentum through laminar and turbulent mechanisms grows in thickness as the distance from the inlet increases. The growing boundary layer accelerates the free stream which eventually losses its identity as the boundary layer merges with itself. Following the disappearance of free stream, further changes occur in the velocity distribution and turbulence structure until the flow attains fully developed state.

9. Numerical solution procedure

The numerical solution procedure employed to solve the finite-difference equations was the well know SIMPLE algorithm. This algorithm was embodied in the general two–dimensional computer code FLUENT [7]. In this computer code the flow variables are calculated in a semi-implicit line-by-line fashion over a staggered finite-difference grid system. Owing to the semi-implicit nature of the code, under relaxation factors are used. The first order discretization was used for all simulation in this study.
Pressure and velocity were coupled with the Semi-Implicit Method for Pressure Linked Equations (SIMPLE) algorithm. SIMPLE uses a relationship between velocity and pressure corrections to obtain mass conservation and a pressure field. The pressure discretization scheme was the default value standard. Solutions control under-relaxation factors for porous media: Pressure 0.3, Density 0.95, Body forces 0.95, Momentum 0.7, TKE 0.6, TDR 0.6, Turbulent viscosity 0.6, Energy 1 (fig. 9).
The flow field of axisymmetric expansion in a porous heat exchanger is a complicated phenomenon characterized by flow separation, flow recirculation and flow reattachment. As illustrated in the fig.10 such a flow field may be divided by a dividing surface into two main regions, one being the region of recirculation flow, the other being the region of main flow.

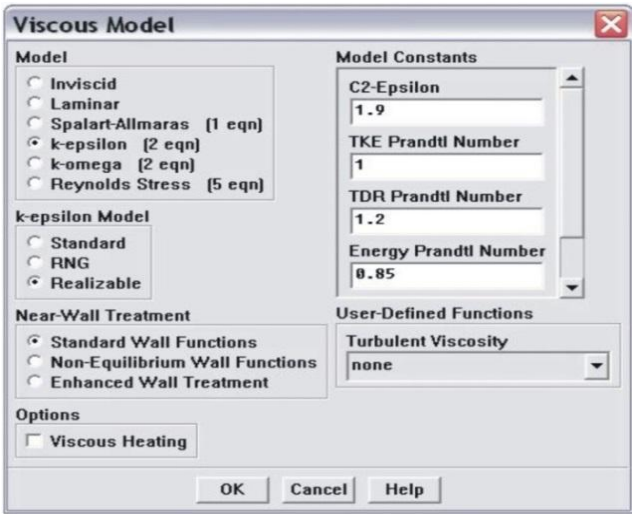

Fig. 9. Constants used in the k-ε turbulence model [5].

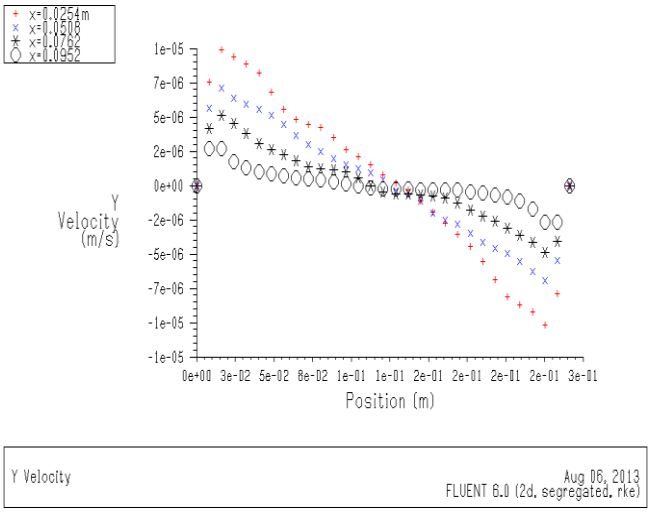

Fig. 10. Contours of velocity vectors vs turbulence intensity [5].

The point at which the dividing surface strikes the wall is called the reattachment point. In the recirculation zone, the high adverse pressure gradient results in reverse flow and promote turbulence. Eddies generated in the recirculation zone and in the vicinity of the reattachment point can be considered as highly concentrated source of turbulence. The subsequent convection, diffusion, and decay of turbulent eddies have a dominant influence on the characteristic of mean flow.

10. Model validation

The working method used, numerical simulation using Fluent software, for predicting turbulent porous heat exchanger flow was verified by comparison with experimental data reported in the literature [11]. The experimental work of [2,12] forms the basis for comparison.
One of the primary reasons to study forced convection in metal foams is to provide information necessary for the possible applications of these materials in electronic cooling and other thermal systems. The fibers of these materials could be thought of as a network of complex extended surfaces giving the advantage of increasing the interfacial area. In addition to the increased interfacial area the formation of eddies or fluid mixing promotes the heat transfer enhancement.
Validation of the flow is achieved through comparative research conducted on the distribution of pressure drop. Flow parameters are also validated, so the pressure drop calculated by simulation has a deviation of 1.31 – 8.27%, the relative error grows if the porosity has low values.

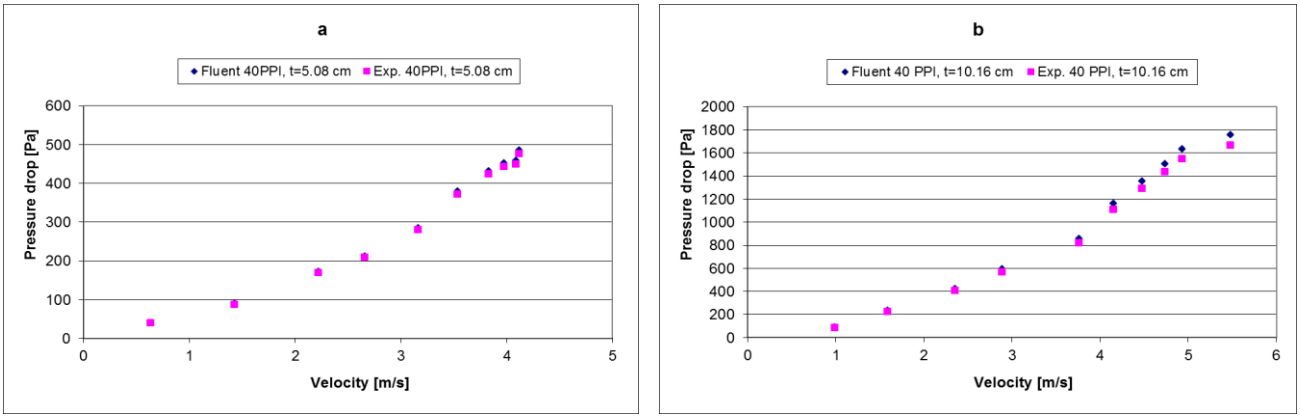

Fig. 11. Comparison between simulation and experimental pressure drop data at different velocities, for 40 PPI porous density, porosity ε=0.927 and heat exchanger thickness t= 5.08(a) and 10.16(b) [11].

The pressure drop is also influenced by the porosity, the density of porosity and the fluid velocity and thickness. At the same porous density and porosity the pressure drop is influenced by the flow rate of working agent and thickness. Relative error increased with thickness (fig. 11) [11].
Thermal convection coefficient values determined by simulation with FLUENT are also experimentally confirmed, the relative error between them is 0.54 ─ 10.23%. They depend on the flow rate, the nature of the agent flow (air or water), porosity, pore density and thickness of the heat exchanger.
The convective heat transfer is more intense near the limit surface between the solid aluminum heated board and the porous aluminum heated board, due to thermal contact resistance and low porosity in that area.
It is noticed that at the same porosity, the thermal convection coefficient is higher if the porosity density is higher, the difference between them increases with decreasing speed. Relative error is bigger if porous density decreased (fig. 12) [11].

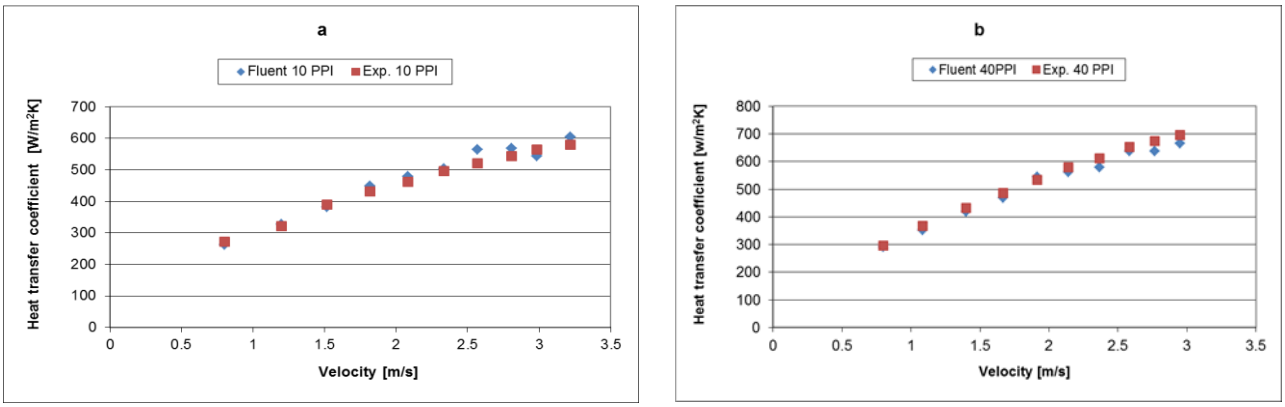

Fig. 12. Comparison between simulation and experimental heat transfer coefficient data at different velocities,for 10 and 40 porous densities and porosities ε=0.927(a) and ε=0.921(b) [11].

Comparing the values obtained by simulation with the experimental ones, relative errors resulted that were less than 5%, for most of the parameters studied, leading to the validation of simulation model developed in FLUENT by the experimental data.

11. Presentation and discussion of results

However, in our case with flow through a porous medium, researchers have shown that the localized heat transfer coefficient will vary with velocity, even at local Reynolds number less than 50.

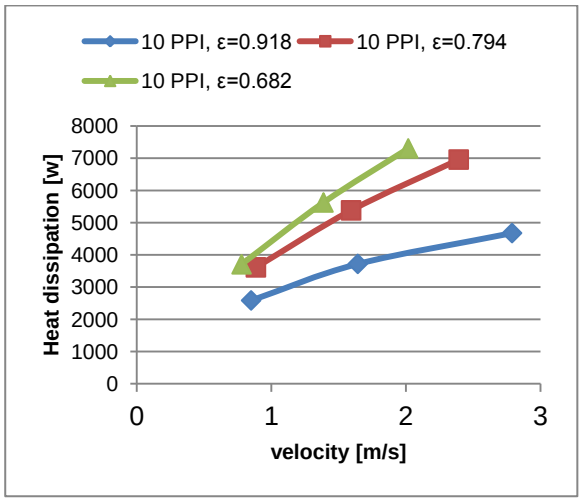

Fig. 13. Heat flux dissipation vs flow velocity [13]

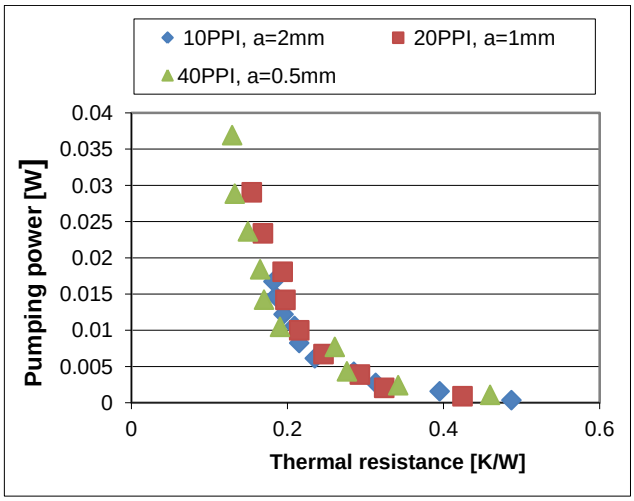

Fig. 14. Pumping power vs thermal resistance [13].

The heat transfer from the foam to the fluid will increase as either the porosity decreased (thus increasing surface area for heat transfer) or as the relative density (ρ) increases (thus increasing heat conduction through the ligaments) or as the velocity of the fluid increases (fig.13) [13].
However, all of these methods to increase heat transfer will result in increased pressure drop through the system. Thus, a delicate balancing act must be performed so as to maximize the ratio of heat output to pumping power[14,15]. In any heat exchanger design, the heat convection performance of the heat exchanger must be weighed against the energy required to operate the system, which is the pumping power in this configuration. In fig. 14 the optimal design is that which minimize the distance from the point to the origin of the plot. The simulated results of both pressure drop and heat transfer were compared with two of the best commercially available heat sinks with similar dimension to demonstrate both the advantages in thermal resistance and disadvantages of pressure drop increment with the use of highly porous media. In fig. 15 it could be seen that the metal foam heat sinks provide less thermal resistance than the best heat sink available from Thermaflo (Heat sink 1 and 2).

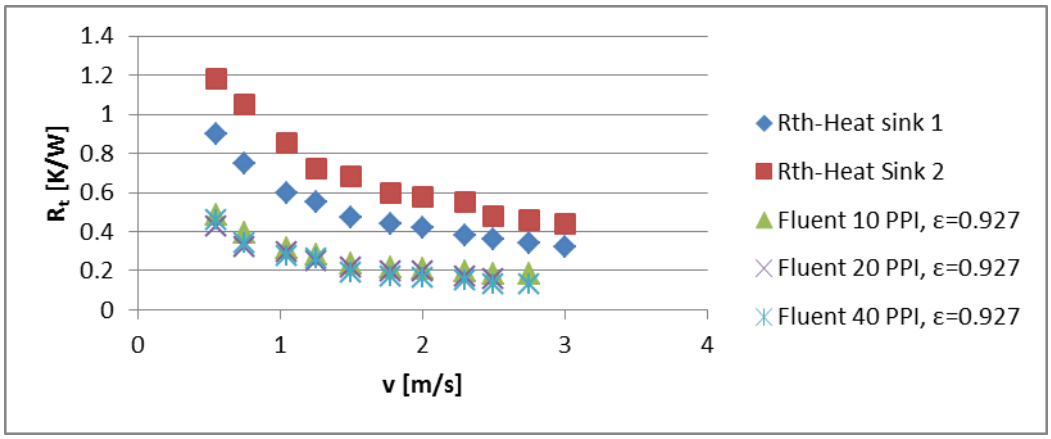

Fig. 15. Thermal resistance comparison plot.

Although there is a pressure drop increase for the use of porous materials as heat sinks. This pressure drop could be compensated by the increase in heat dissipation that the metal foams offer.

12. Conclusions

This model assumed heat transfer was dominated by the heat transfer of the fluid in the pores of the foam, rather than in the ligaments. In other words, since the foam is extremely conductive, the largest thermal resistance is at the local surfaces, rather than transmitting the heat through the foams. This model demonstrates several guiding principles of designing heat transfer devices utilizing cooling fluids and foams.

1. The highest conductivity ligaments are needed to transport the heat from the heat source rapidly into the foam so that it can then be transferred more uniformly to the cooling fluid.
2. While a turbulent fluid flow is desired to facilitate better mixing and high local heat transfer coefficients from the solid surfaces (ligaments) into the fluid, the effects of surface area are dominating as the surface area increases with the square of the change in pore diameter and the Reynolds number (turbulence) decreases monotonically with the change in diameter.
3. A low pressure-drop of the fluid through the foam is desired so that the required pumping power does not become overwhelming. Hence, low fluid viscosities are desired.
4. It is necessary to model the heat transfer of a system with a parametric study to optimize the various variables on the heat transfer. It was shown that there is a maximum pore diameter to optimize the ratio of dimensionless heat flux to pumping power. It was also shown that proper use of models could help optimize foam-based heat exchangers through parametric studies. For example, it was shown how the model could predict the effects of a geometric change in the system on reducing pressure while maintaining high heat transfer.

This type of model should be very useful in developing revolutionary new and exciting heat transfer devices. This work focused on developing an improved phenomenological thermo-fluid model in order to assess and optimize such porous heat transfer media with the intent of guiding the direction of future modelling, material and experimental.

References

[1] J. H. Rosenfeld, J. E. Toth, and A. L. Phillips, "Emerging applications for porous media heat exchangers", Proc. Int. Conf. on Porous Media and their Applications in Science, Kona, Hawaii, June 1996;
[2] E. Cruz, "Modeling of heat transfer in open cell metal foams', University of Puerto Rico, Mechanical Engineering Departament, 2004;
[3] P. Opritoiu, "Rans simulation of turbulent flow through porous media", Acta Tehnica Napocensis, nr.49., 2006;
[4] P. Opritoiu, "Fluid flow and pressure drop simulation in aluminium foam heat exchanger", Acta Tehnica Napocensis, nr.50, 2007;
[5] P. Opritoiu, "Modelling turbulence in open cell aluminum foam heat exchanger", Acta Tehnica Napocensis, nr.56, 2013;
[6] K. Tahir., "Predictions of some turbulent flows using upwind and hybrid discretisation schemes and two-equation turbulence model", Particulate phenomena and multiphase transport, vol. 5, Springer-Verlag, 1988;
[7] FLUENT v. 5/6, *Users manual,* Fluent inc.;
[8] Ajay Parihar, Shane Moeykens, *Flow through porous media*, Fluent inc., 2006;
[9] Michael Paul Scott, *Computational fluid dynamics study of flow through a shell and tube heat exchanger header with inlet modifiers*, Undergraduated thesis, University of Queensland, Australia, 2001;
[10] H. C. Brinkman, "On the permeability of media consisting of closely packed porous particles", Apl. Sci. Res., A1, pp.27-34, 1948;
[11] P. Opritoiu, "Validation of porous heat exchanger simulation model", Hidraulica, Magazine of Hydraulics, Pneumatics, Tribology, Ecology, Sensorics, Mechatronics, 2014;
[12] H. Alvarez, "Combined flow and heat transfer characterization of open cell aluminium foams', University of Puerto Rico, Mayaguez Campus, 2005;
[13] P. Opritoiu, "Heat transfer performance analysis in porous heat exchanger", Hidraulica, Magazine of Hydraulics, Pneumatics, Tribology, Ecology, Sensorics, Mechatronics, 2015;
[14] D. Opruţa, L. Vaida , A. Pleşa, "The simulation of fluid flow through a hydraulic resistance", Annals of DAAAM & Proceedings, 2008;
[15] D. Opruţa, L. Vaida, L. Naşcuţiu, A. Pleşa, "Coandă effect in oil flow through hydraulic command resistances", Conference: Annals of DAAAM and Proceedings of the International DAAAM Symposium, 2007.